THE UNIVERSITY OF CALGARY

A Theoretical Investigation of the Structure and Function of MAO

(Methylaluminoxane)

by

Eva Zurek

A THESIS SUBMITTED TO THE FACULTY OF GRADUATE STUDIES IN

PARTIAL FULFILLMENT OF THE REQUIREMENTS FOR THE DEGREE OF

MASTER OF SCIENCE

DEPARTMENT OF CHEMISTRY

CALGARY, ALBERTA

AUGUST, 2002

i

UNIVERSITY OF CALGARY

FACULTY OF GRADUATE STUDIES

The undersigned certify that they have read, and recommend to the Faculty of Graduate Studies for acceptance, a thesis entitled "A Theoretical Investigation of the Structure and Function of MAO (Methylaluminoxane)" submitted by Eva Zurek in partial fulfillment of the requirements for the degree of Master of Science.

_____
Dr. T. Ziegler, Supervisor, Department of Chemistry

_____
Dr. W. Piers, Department of Chemistry

_____
Dr. T. Chivers, Department of Chemistry

_____
Dr. E. Donovan, Department of Physics

Sept 13 2002.
Date

ii

Abstract

Single-site homogenous catalysts need to be activated by a co-catalyst, or counter-ion. The high activity imparted by MAO (methylaluminoxane) has caused it to be one of the most important activators. However, despite intensive studies MAO has remained a 'black box.' The presence of multiple equilibria between different $(AlOMe)_n$ oligomers coupled with the interaction between MAO and TMA (trimethylaluminum) has hindered experimental structural assignment of MAO. This has made it nearly impossible to characterize the dormant and active species present in olefin polymerization and therefore to theoretically investigate the mechanism of this process.

Using theoretical methods (DFT for energies, MM for enthalpies and entropies) we have put forward a structural model for 'pure' and TMA containing MAO. Via comparison of calculated and experimental ^1H and ^{13}C NMR chemical shifts, we have also proposed the most likely structures for the dormant and active species. Finally, we have studied the mechanism of olefin polymerization.

Within this study we also provide an answer to the question: *"Why is an excess amount of MAO necessary in order for polymerization to occur?"*

Preface

The material presented in this thesis has been published in the following articles:

1) Zurek, E.; Woo, T.K.; Firman, T.K.; Ziegler, T.; "Modeling the Dynamic Equilibrium Between Oligomers of $(AlOCH_3)_n$ in Methylaluminoxane (MAO). A Theoretical Study Based on a Combined Quantum Mechanical and Statistical Mechanical Approach." *Inorganic Chemistry*, **2001**, *40*, 361-370.

2) Zurek, E.; Woo, T.K.; Firman, T.K.; Ziegler, T.; "Modeling MAO (Methylaluminoxane)." *Organometallic Catalysts and Olefin Polymerization: Catalysts for a New Millenium*; Blom, R.; Follestad, A.; Rytter, E.; Tilset, M.; Ystenes, M., Eds,; Springer: New York, 2001.

3) Zurek, E.; Ziegler, T.; "A Combined Quantum Mechanical and Statistical Mechanical Study of the Equilibrium of Trimethylaluminum (TMA) and Oligomers of $(AlOCH_3)_n$ Found in Methylaluminoxane (MAO)." *Inorganic Chemistry*, **2001**, *40*, 3279-3292.

4) Zurek, E.; Ziegler, T.; "Toward the Identification of Dormant and Active Species In MAO (Methylaluminoxane)-Activated, Dimethylzirconocene-Catalyzed Olefin Polymerization." *Organometallics*, **2002**, *21*, 83-92.

A large part of the material in the second chapter was part of Eva Zurek's undergraduate thesis. It is presented here since the Master's thesis heavily relies on these results.

Acknowledgements

I would like to thank my supervisor, Professor Tom Ziegler for his guidance, insight, support and understanding. I am grateful for the freedom he has given me in working on this project, and for the weekly meetings which kept me in line. It has been a great pleasure working for Tom: he has taught me not only how to do computational chemistry but how to work independently and to not be scared of a difficult project. I am also thankful for his friendship and humor.

Many members of the Ziegler team have helped me out directly on this and other projects. They include Cory Pye, Kumar Vanka, Tom Woo, Tim Firman, & Zhitao Xu. Of course, this work could not have been completed without the great system administrators, Serguei Patchkovski and Jochen Autschbach. Other members who have also given advice and support include Artur Michalak, Michael Seth and Hans Martin Senn. For those of you who participated, I really enjoyed the hiking, skiing, dinners and beer. A special thanks goes out to the editors of my thesis: you know who you are!

I would like to thank the members of my supervisory committee: Professors Warren Piers, Tristram Chivers and Eric Donovan. I hope you have fun reading this and stick it out till the end. A special thanks to Dr. Piers for the letters of reference he has written.

Financial support has come from the University of Calgary as well as the Alberta Ingenuity Fund. The MACI-alpha cluster has supplied a great deal of the computational power necessary to obtain these results; without it the NMR calculations would have never been done and the mechanistic study would have taken ages to complete.

I would like to thank Jochen for all the good things.

And finally, I would like to thank my parents for all of the sacrifices they have made, for teaching me how to work hard and be independent. They have also cooked me delicious dinners and have given me great friendship and support throughout the years.

Dla Rodziców

Table of Contents

          Zurek, E.; Woo, T.K.; Firman, T.K.; Ziegler, T. *Inorg. Chem.* **2001**, *40*,
          361.
          Zurek, E.; Woo, T.K.; Firman, T.K.; Ziegler, T. *Organometallic Catalysts*
          and Olefin Polymerization: Catalysts for a New Millenium; Blom, R.;
          Follestad, A.; Rytter, E.; Tilset, M.; Ystenes, M., Eds,; Springer: New
          York, 2001.

List of Tables

List of Figures

xiii

xiv

I am Feynman.

I am Dirac. (Silence)

It must be wonderful to be the discoverer of that equation.

That was a long time ago. (Pause) *What are you working on?*

Mesons.

Are you trying to discover an equation for them?

It is very hard.

One must try.

A conversation between Richard Feynman and Paul Dirac.

James Gleick, *Genius: The Life and Science of Richard Feynman.*

Chapter 1

Introduction

1.1 General Introduction

In recent years, single-site homogeneous catalysts for olefin polymerization have received increasing attention due to their high stereoselectivity, high activity and the narrow molecular weight distribution of the polymer they produce.[1] The catalysts are structurally well defined, with the general formula $L^1L^2MR^1Me$ (M=Ti, Zr; Me=methyl; R=methyl, propyl, etc; L=Cp, NPR_3, NCR_2, etc). Modification of the metallocene ligands results in the production of polymers with specific properties, thereby allowing for the possibility of rational catalyst design. These catalysts however do not work alone: they must be activated by a co-catalyst or anion. There are two main modes of activation, shown in Equations 1.1 and 1.2. Both result in the formation of an ion-pair. Traditionally, it was assumed that the ion-pairs undergo total dissociation leading to the production of a naked cationic species.

$$L_1L_2MRMe + A \quad [L_1L_2MR]^+[MeA]^- \qquad [1.1]$$

Typically A = $B(C_6F_5)_3$ or MAO (methylaluminoxane)

$$L_1L_2MRMe + [C(C_6H_5)_3{}^+][B(C_6F_5)_4{}^-] \quad {}_{-MeC(C_6H_5)_3} \quad [L_1L_2MR]^+[B(C_6F_5)_4{}^-] \qquad [1.2]$$

The reaction mechanism for olefin insertion is generally accepted to be the Cossée-Arlman mechanism[2], shown in Figure 1.1 for $L^1=L^2$=Cp. The olefin approaches the free cation forming a -complex. Next, the C -$C_{ethylene}$ distance decreases resulting in the formation of a four-membered cyclic transition state. After insertion has taken place a new vacant coordination site is formed to which the next olefin may complex. Many computational studies disregarding the influence of the anion have been performed, using this mechanism as a starting point. We will refer to only a few here where polymerization with the naked cationic species, Cp_2ZrR^+, (R=methyl, ethyl), as the catalyst was examined.[3]

In recent years increasing computational resources have made it possible to investigate the role of the activator.[4,5] These studies suggest that total dissociation between cation and anion does not occur. Thus, in order to understand the mechanism of polymerization the influence of the anion must be taken into consideration.

M = Zr, Ti
R = Me, Prop
====== = ethylene
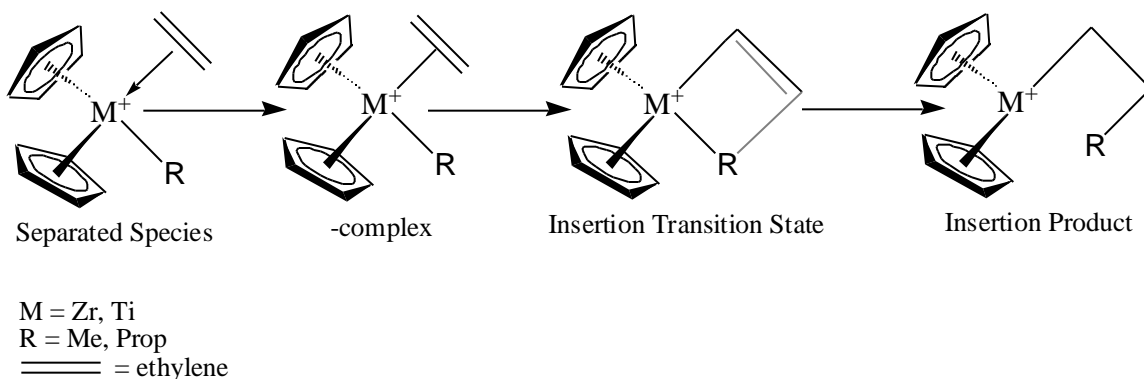
Figure 1.1: The Cossée-Arlman Mechanism

One of the most important activators in single-site olefin polymerization is MAO. It was discovered in 1980 when Sinn and Kaminsky found that addition of water to systems such as $Cp_2ZrMe_2/(AlMe_3)_2$ caused this rather unreactive system to become highly active in ethylene polymerization.[6] It was suspected that partial hydrolysis of $(AlMe_3)_2$ (TMA or trimethylaluminum) resulted in the formation of MAO.

Despite intensive experimental[7-20], theoretical[21-23], and combined[24,25] studies, MAO has remained a "black box". The presence of multiple equilibria between different $(AlOMe)_n$ oligomers coupled with the interaction between MAO and TMA, which to some extent is always present in a MAO solution, has hindered its experimental structural characterization. Moreover, these difficulties have made it nearly impossible to characterize the dormant[a] and active[b] species and therefore to theoretically study the mechanism of olefin polymerization with MAO as the anion. In order to do this a structural model for MAO must first be proposed.

---

[a] Species which react with the catalyst, yet do not react with olefin to produce polymer
[b] Species which react with the catalyst and produce polymer

The main goal of this thesis is to propose a model for MAO and study how MAO influences the mechanism of ethylene polymerization. This thesis will be organized as follows. The remaining section of this chapter will outline the computational details. In Chapter 2 we propose a model for 'pure' MAO; in Chapter 3 this model is extended to 'real' or TMA-containing MAO. Chapter 4 identifies possible structures for the dormant and active species present in polymerization. Chapter 5 examines the mechanism of olefin uptake and insertion with the model active and dormant species. In Chapter 6 we provide a general conclusion and comment briefly on possible future projects. Within this thesis we also try to answer one of the most perplexing questions about MAO: *"Why is an excess of MAO necessary in order for polymerization to occur?"* (Typical conditions have an Al/catalyst ratio of $10^3 – 10^4$.)

1.2 Computational Details

The density functional theory calculations were carried out using the Amsterdam Density Functional (ADF[26]) program versions 2.3.3 and 2000 developed by Baerends *et al.*[27] and vectorized by Ravenek.[28] The numerical integration scheme applied was developed by te Velde *et al.*[29] and the geometry optimization procedure was based on the method of Verslius and Ziegler.[30] For total energies and geometry optimizations the gradient corrected exchange functional of Becke[31] and the correlation functional of Perdew[32] was utilized in conjunction with the LDA parametrization of Vosko et al.[33] The electronic configurations of the molecular systems were described by a double- STO basis set with one polarization function for H, C, Al and O together with a triple- STO basis set for Zr. A 1s frozen core was used for C and O, while an [Ar] frozen core was used for Al and a [Kr] frozen core for Zr. A set of auxiliary s, p, d, f and g STO functions centered on the nuclei was used to fit the molecular density in order to allow for an effective calculation of the Coulomb potential and density derivatives in each SCF cycle.[34]

In ADF, frequencies were calculated via single-point numerical differentiation of energy gradients. The UFF2[35] code was then parametrized to reproduce the thermodynamic corrections calculated with ADF. Next, it was used to calculate entropic

and finite temperature enthalpy corrections to the Gibbs free energy for large MAO cages, for which DFT calculations were not feasible.

Solvation calculations were performed using the COSMO (COnductor-like Screening MOdel) method[36a] as implemented in ADF.[36b] The solvent excluding surface was used along with a dielectric constant of 2.379 for the solvent toluene. Atomic radii used were 2.4, 2.3, 1.5, 2.0 and 1.16 Å for Zr, Al, O, C and H, respectively. Single-point calculations on gas phase geometries were performed (the geometry was not optimized in solution).

Calculations of NMR chemical shifts were carried out using the GIAO (Guage Including Atomic Orbitals) implementation in ADF 2000.[37] Single-point calculations were performed on geometries obtained with the previously mentioned basis sets. However, here we employed a triple- basis set with two polarization functions for H and C, a double- basis set with one polarization function for Al and O along with a triple- basis set for Zr, in order to obtain meaningful chemical shifts.

A Mulliken analysis[38] was used to analyze the charge distribution.

Transition state geometries and energies were obtained by performing a series of geometry optimizations along a fixed reaction coordinate. The transition state geometry was determined as the point along the reaction coordinate where the gradient was less than the threshold set for the optimization procedure, usually 0.001 au/Å. Frequency calculations were not carried out for verification of the transition state. This would be exceptionally computationally expensive because of the size of the systems being studied. The reaction coordinate used to find insertion barriers has been chosen as the distance between the -carbon and one of the carbon atoms of the approaching ethylene.

Chapter 2

The Dynamic Equilibrium Between Oligomers of (AlOMe)$_n$: A Model for 'Pure' Methylaluminoxane.

2.1 Introduction

The determination of the structure of MAO can be linked to the determination of the structures of alumoxanes in general. Alumoxanes are intermediates in the hydrolysis of organoaluminum compounds to aluminum hydroxides. They were originally proposed as consisting of linear **1** or cyclic **2a**, **2b**, **2c** chain structures which were composed of alternating three-coordinate aluminum and two-coordinate oxygen atoms.[7] The first crystallographic evidence for the presence of four-coordinate aluminum atoms was given by Atwood and co-workers in their structural determination of the (Al$_7$O$_6$Me$_{16}$)$^-$ anion **3**.[8] This result encouraged many groups to propose structures consisting of fused four or six membered rings, or both, **4** for MAO.[7] While these structures were more reasonable than those of **1** and those similar to **2a**, **2b** and **2c**, they still contained a peripheral aluminum atom which remained three-coordinate.
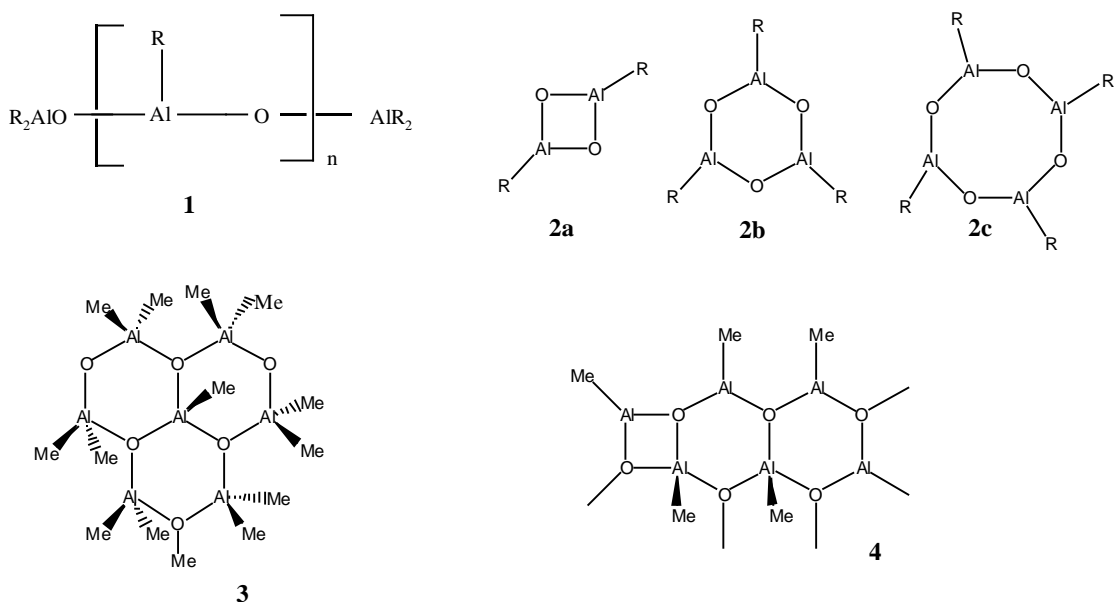
Figure 2.1: Proposed Structures of Alkylaluminoxanes

Methyl bridges and/or the presence of trimethylaluminum groups were suggested[7], but these resulted in structures whose chemical formula substantially deviated from the generally accepted formula of 'pure' MAO, $(AlOMe)_n$ where n is an integer.

Replacement of the methyl substituents in MAO with bulkier *t*-butyl groups made the first structural determination of alkylalumoxanes possible. Barron and co-workers synthesized a series of compounds, $[(^tBu)Al(\mu_3\text{-}O)]_n$, where n = 6, 7, 8, 9 and 12[9,10]. These correspond to structures **5**, **6**, **7**, **8** and **9**, respectively. It was noted that in all of them, the number of square faces was equal to 6, while the number of hexagonal faces was equal to n - 4 (Smith's rule). The synthesis of these compounds led to the suggestion that MAO has a three-dimensional cage structure with four-coordinate aluminum centers bridged by three-coordinate oxygen atoms.[9]

5   **6**   **7**

8   **9**

t-Butyl groups omitted for clarity
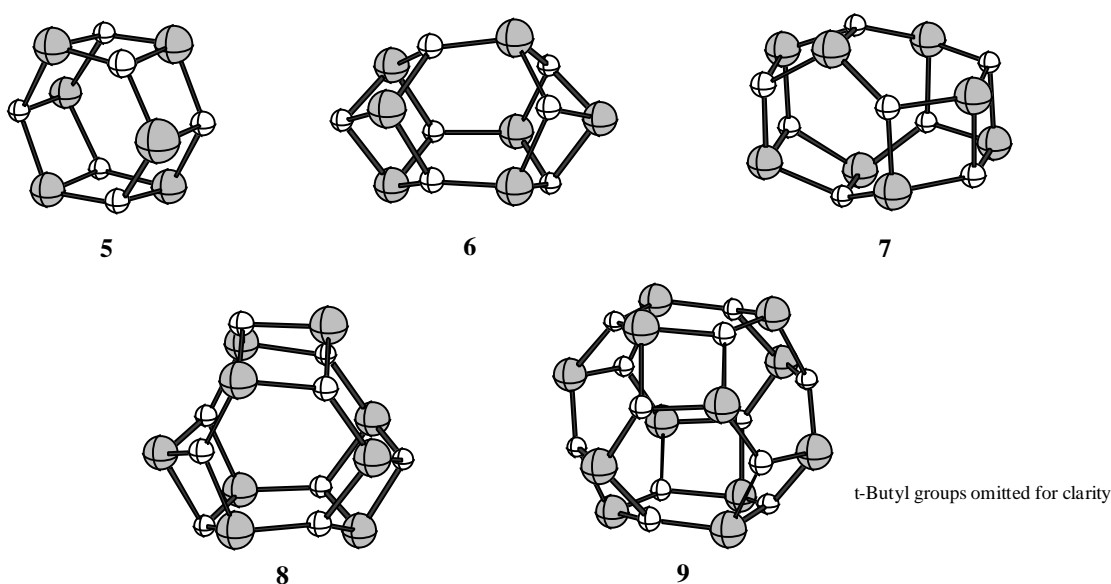
Figure 2.2: Synthesized $[(^tBu)Al(\mu_3\text{-}O)]_n$, ($n$ = 6, 7, 8, 9 and 12) Cage Structures

Barron's $[(^tBu)Ga(\mu_3\text{-}S)]_n$ (n = 6, 7, 8) cubane underwent structural rearrangements under extreme conditions.[9] However, in the case of MAO, it has been proposed that this occurs under normal conditions. In other words, it is believed that there exists a dynamic equilibrium between the different MAO cage structures, as seen in the following equation. Here x, y, z, n and m are integers and $x = y+z = n+m$.

$$(\text{MeAlO})_x \quad (\text{MeAlO})_y + (\text{MeAlO})_z \quad (\text{MeAlO})_n + (\text{MeAlO})_m \qquad [2.1]$$
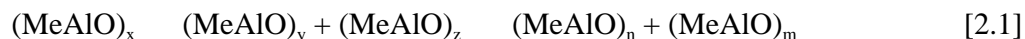
Species of exceptional Lewis acidity are found in MAO solutions, but four-coordinate aluminum centers are not thought of as being exceptionally Lewis acidic. In order to explain this phenomenon, Barron and co-workers developed the concept of Latent Lewis Acidity (LLA). LLA is a consequence of the ring strain present in the cluster. If it is assumed that four-coordinate aluminum and three-coordinate oxygen atoms prefer tetrahedral and trigonal planar geometries, then a qualitative determination of the LLA of a cage compound may be found by calculating the sum of the angular distortions from the ideal.[11] Work has also been done on quantitatively establishing the most acidic of Barron's *t*-butyl compounds.[12]

Estimates of the size range for a typical MAO oligomer have been made using spectroscopic methods. For example, the linewidths of ^{27}Al NMR have predicted that *n* ranges between 9 and 14 at high temperatures and between 20 and 30 at ambient conditions.[13a] EPR studies have been performed via the addition of a spin probe to a MAO solution. This method found that *n* ranges between 14 to 20.[13b]

 It is well known that residual TMA (trimethylaluminum) is present in all MAO solutions. It is also accepted that TMA participates in an equilibrium with MAO oligomers, and that the Al/Me/O ratio in 'real' MAO is not exactly 1:1:1. Within this chapter we will focus upon establishing a model for a pure (TMA free) MAO solution. In the next chapter we will build upon this model in order to propose one for 'real' or TMA-containing MAO.

The objective of this study is to establish the percent abundance of different MAO structures. In an equilibrium mixture, the Gibbs free energy determines the stability of a given structure. The Gibbs free energy can be written as:

$$G(T,n) = H(T,n) - TS(T,n), \qquad [2.2]$$

where *H(T,n)* and *S(T,n)* are the enthalpy and entropy of $(AlOMe)_n$ at a given temperature.

Section 2.2.1 discusses different structural alternatives (sheets, cages, fused cages) showing that cage structures are energetically the most stable. Section 2.2.2 derives formulae used to determine the topologies of cage structures. Section 2.2.3 proposes a method by which the energies of MAO cages can be predicted. In Section 2.2.4 we discuss and provide methods to estimate enthalpic corrections and in Section 2.2.5 the same is done for entropies. Finally, Section 2.2.6 examines the Gibbs free energy and percent abundance of different MAO structures. It is not feasible to look at all of the possible structures for a given $(AlOMe)_n$ without imposing any restrictions; even for a relatively small *n*, the amount of possibilities is large. Thus, throughout the discussion we will try to make generalizations about the properties of the most stable structures for a given *n*. In such a way we will limit our study to the most likely possibilities and the study of the structure of MAO will become a tractable one.

2.2 Results and Discussion

2.2.1 Energetics of Sheet/Cage/Fused Cage Structures

Experimental evidence suggests that MAO consists of three-dimensional cage structures. However, a preliminary investigation on the relative stability of sheet, cage and fused cage structures still ought to be performed. Figure **2.3** presents a selection of the fused-ring and fused cage structures upon which calculations were performed.

The electronic binding energy per monomer unit is defined as:

$$BE(n) \; = \; \frac{1}{n}\left(E(AlOMe)_n - n \times E(AlOMe)\right). \qquad [2.3]$$

It corresponds to the energy which is gained per monomer (AlOMe unit) when a certain geometry is formed from *n* monomers. The more negative the binding energy per monomer, the more stable the given structure is. Table 2.1 gives the binding energies per monomer unit for ring and fused-ring structures.

2 fused hexagons   1 hexagon, 1 octagon

1 octagon, 1 square   2 fused hexagonal cages
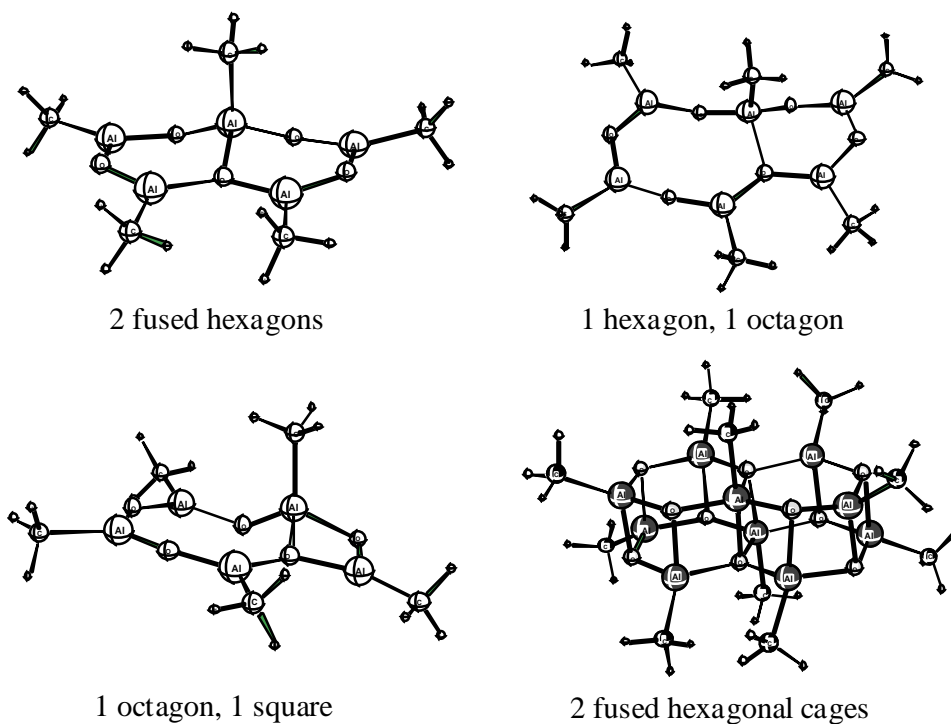
Figure 2.3: A Selection of Fused-Ring and a Fused-Cage Structure

When single ring structures are considered, the binding energy per monomer decreases until it reaches a minimum for an octagonal ring (-78.83 kcal/mol), before slightly increasing again. For the fused ring structures the binding energy per monomer appears to level off at approximately –80 kcal/mol. The optimization of the fused cage

Table 2.1: Binding Energies Per Monomer (kcal/mol) for Sheet Structures[a]

Structure	BE/monomer	Structure	BE/monomer
Square	-61.62	2 Hexagons	-80.18
Hexagon	-77.33	1 Square, 1 Hexagon	-77.29
Octagon	-78.83	1 Hexagon, 1 Octagon	-79.27
Decagon	-78.59	1 Square, 1 Octagon	-78.49
Dodecagon	-78.30	2 Octagons	-79.35

[a]All Energies given in kcal/mol

structure yielded a cage structure (the former is not a minimum on the calculated potential energy surface). That is, the five-coordinate Al and four-coordinate O bonds broke giving four-coordinate Al and three-coordinate O atoms. This shows that fused cage structures are unstable alternatives for MAO.

The binding energies of cage structures can be found in Table 2.2. With the exception of $(AlOMe)_4$, the other cages correspond to **5-9** shown in Figure 2.2 (the MAO analogues of Barron's synthesized structures). Even for a very strained structure such as $(AlOMe)_4$, the binding energy per monomer is approximately 9 kcal/mol lower than for any of the sheet structures. This indicates that MAO cage structures consisting of three-coordinate oxygen and four-coordinate aluminum atoms are much more energetically stable than sheet or fused cage structures.

Table 2.2: Binding Energies Per Monomer (kcal/mol) for Cage Structures[a]

Structure	BE/monomer	Structure	BE/monomer
$(AlOMe)_4$	-88.73	$(AlOMe)_8$	-99.05
$(AlOMe)_6$	-95.93	$(AlOMe)_9$	-100.17
$(AlOMe)_7$	-96.35	$(AlOMe)_{12}$	-102.30

[a]All Energies given in kcal/mol

Accordingly, in our investigation of possible MAO geometries we decided to focus on three dimensional cage structures. The faces of these cages consist of polygons which must consist of an even number of atoms, since there are no O–O or Al–Al bonds in MAO. It is not possible within such a study to look at all possible types of faces. Thus, we decided that cage compounds composed only of square, hexagonal and octagonal faces would be considered.

2.2.2   Mathematical Relationships

In order to perform a study on the relative energies of different MAO cages, we first of all need a method which may be used to construct possible structures. In this section we view the MAO cages as polyhedrons (neglecting the methyl groups) and

propose a procedure how to obtain possible topologies. This method is derived from mathematics, however we impose upon it chemically sensible constraints. For example, all of the polyhedrons may be composed of only square, hexagonal and octagonal faces and exactly three edges must form a vertex. The former constraint is based upon the aforementioned assumption about the topologies of the MAO cages whereas the latter guarantees that all of the atoms in the cage are three-coordinate (addition of methyl groups to the cage will make the Al atoms four-coordinate). All of the MAO structures on which explicit calculations have been performed have been created using this method. We shall also derive a formula relating the number of square faces to the number of octagonal faces found within a polyhedron. This result will prove useful in explaining the large ratio of Al/Zr needed in order for polymerization to occur. Finally, we will derive mathematical relationships used to construct large MAO cages.

A convenient way by which one can construct polyhedrons is via the drawing of Schlegel diagrams.[39] A Schlegel diagram is a projection of a three dimensional object onto a plane surface, an example of which is shown in Figure 2.4. On the left is a Schlegel Diagram of the three dimensional object, which is shown on the right. The first

Schlegel Diagram   3-D Representation
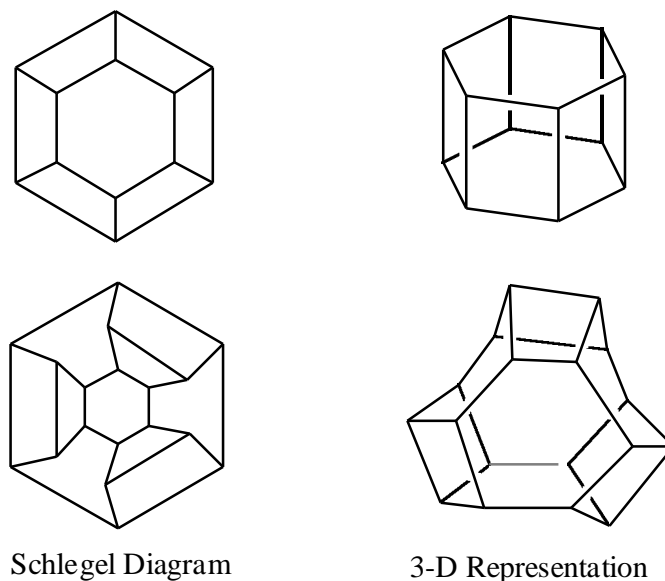
Figure 2.4: Schlegel Diagrams and 3-D Representations of $(AlOMe)_6$ and $(AlOMe)_9$ MAO Cage Structures

diagram is of the $(AlOMe)_6$ cage and the second is of $(AlOMe)_9$. The only rules followed while drawing the diagrams for this particular chemical system were:

- The faces were square, hexagonal or octagonal
- Each point was connected by three lines

Despite the fact that it is not possible to derive all of the possible connectivities present in a polyhedron corresponding to a given number of atoms, some assertions can be made. The first deals with the relationship between the number of square, hexagonal and octagonal faces comprising a given polyhedron.

From the mathematical study of Polytopes , it is known that[39]:

$$F + P = C + 2, \qquad\qquad\qquad [2.4]$$

where F is the number of faces of a given polyhedron, P is the number of points or vertices within the polyhedron and C is the number of connectivities. In this case, P corresponds to the number of atoms in the cage structure, N. For a given $(AlOMe)_n$, $N = 2n$. Within the cage structure itself each atom bonds to three others. Since each connectivity belongs to two atoms, C is equal to $1.5N$. Thus, Equation 2.4 simplifies to:

$$F = 0.5N + 2. \qquad\qquad\qquad [2.5]$$

Each atom belongs to three faces. Thus, if O, H and S correspond to the number of octagonal, hexagonal and square faces within a given cage structure, we have that

$$\frac{8}{3} O + \frac{6}{3} H + \frac{4}{3} S = N, \qquad\qquad\qquad [2.6]$$

and that

$$O + H + S = F. \qquad\qquad\qquad [2.7]$$

Equating 2.5 and 2.7, then substituting 2.6 for *N*, we find

$$S = O + 6. \qquad [2.8]$$

Equation 2.8 gives the relationship between the number of octagonal and square faces within a MAO cage. It also shows that the minimum amount of square faces which can exist in such a polyhedron is six and that this occurs when the number of octagonal faces is zero, that is when the polyhedron is made up solely of square and hexagonal faces.

We have derived other relationships which are valid only when square and hexagonal faces are present. The atoms (points) in such a polyhedron may be found in one of four bonding environments. Let us define:

- = the number of atoms which are part of 3 square faces (in a 3S environment)
- = the number of atoms part of 2 square and 1 hexagonal face (in a 2S+H environment)
- = the number of atoms part of 1 square and 2 hexagonal faces (in a 2H+S environment)
- = the number of atoms part of 3 hexagonal faces (in a 3H environment).

Descartes showed[39] that in a polyhedron if the face-angles at a vertex amount to 360^0 - $_i$, where $_i$ is known as the deficit, then

$$\sum_i \delta_i = 720^0. \qquad [2.9]$$

Within our structures the deficits for an atom in the aforementioned bonding environments are, 90^0, 60^0, 30^0 and 0^0, respectively. Hence, by 2.9:

$$90^0 \ + 60^0 \ + 30^0 \ = 720^0, \qquad [2.10]$$

which can be simplified to yield

$$3 \quad + 2 \quad + \quad = 24. \qquad [2.11]$$

Substituting $\quad + \quad + \quad + = N$ into 2.11 and using the fact that $4S + 6H = 3N$ gives

$$\quad + 2 \quad +3 \quad = 3N - 24 = 6H. \qquad [2.12]$$

Take into consideration a large MAO cage consisting of square and hexagonal faces only. As the cage grows, the number of hexagonal faces increases while the number of square faces stays fixed at 6. For a large cage one can imagine that the probability that an atom is part of 3 square faces is very small. Similarly, so is the probability that an atom is part of 2 square and 1 hexagonal face. If we make this assumption, and can be put to zero in 2.11 and 2.12. Of course, this does not guarantee that such a topology exists. For confirmation a Schlegel diagram must be drawn.

2.2.3 Energetic Considerations

The energies of thirty-six different $(AlOMe)_n$ structures, where n ranged between 4 and 16 were determined via DFT calculations. Some representative structures composed of square and hexagonal faces are shown in Figure 2.5. For $(AlOMe)_{14}$ only the most stable structural alternative is shown. Figure 2.6 displays three isomers of $(AlOMe)_8$ along with their relative energies. The geometries of all structures were found via drawing a Schlegel diagram and next constructing the corresponding three-dimensional structure.

It was found that the stability of a given MAO cage is heavily dependent upon the bonding environment of the atoms and not only upon the type of faces present. For example, two of the cages shown in 2.6 have 2 octagonal and 8 square faces, however, their energies differ by 9.27 kcal/mol. In view of this, we performed a least squares fit using the bonding environments as an index. The fit resulted in the following energy expression (in kcal/mol) for any given MAO structure:

$$E(n) = -373.57 \quad - 377.49 \quad - 381.13 \quad - 381.80 \quad - 377.14 \quad - 380.59 \quad - 381.03 \quad -$$
$$378.86\mu - 365.51 \quad . \qquad [2.13]$$

15

*methyl groups omitted for clarity
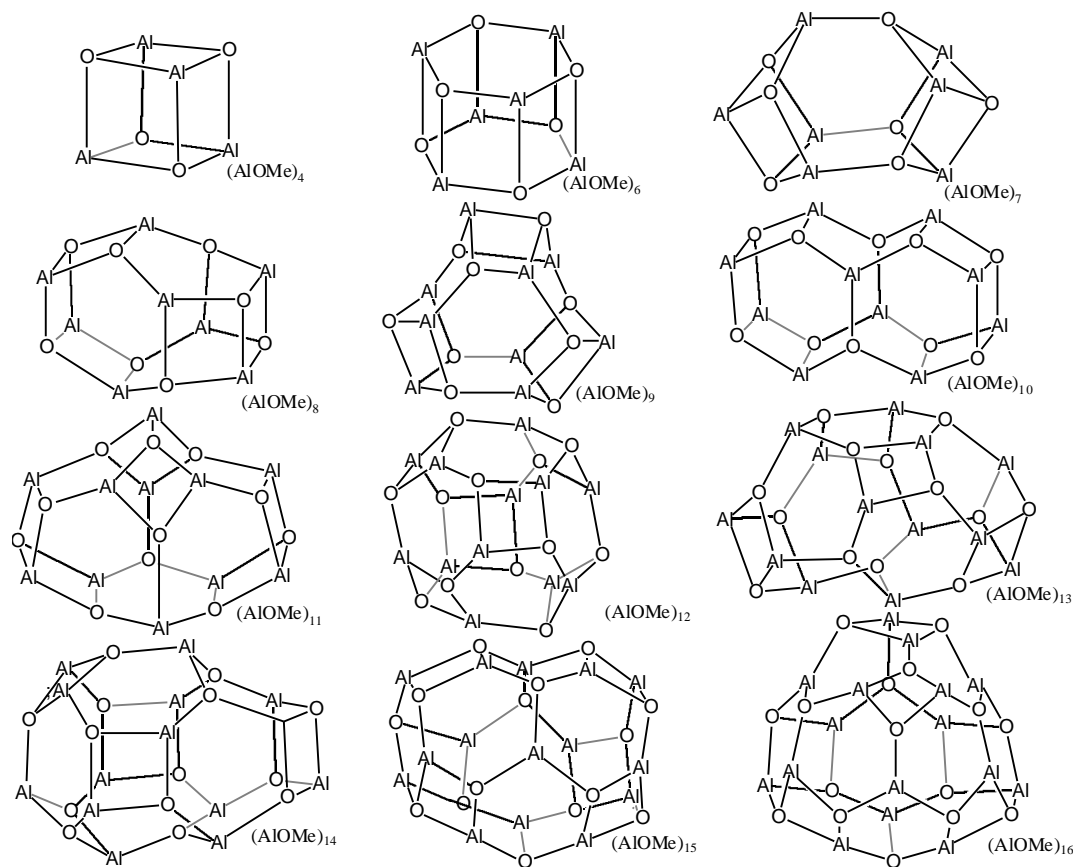
Figure 2.5: MAO Cage Structures Composed of Square and Hexagonal Faces for

(AlOMe)$_4$-(AlOMe)$_{16}$

32.61 kcal/mol   0 kcal/mol

41.88 kcal/mol

*methyl groups omitted for clarity
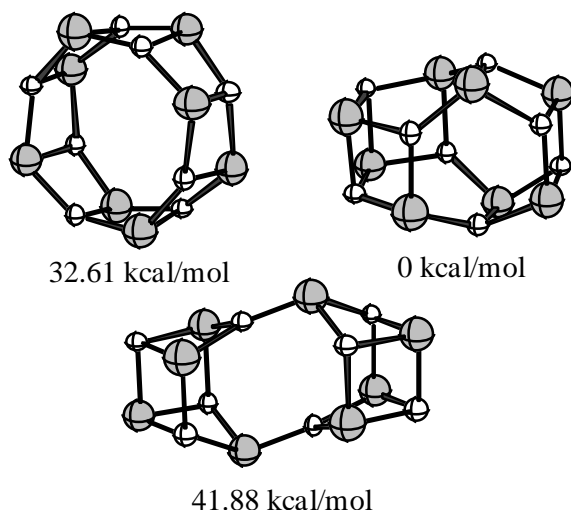
Figure 2.6: Isomers of (AlOMe)$_8$ and their Relative Energies

, , , and   have been previously defined and   is the number of atoms part of two square and one octagonal face (in a 2S+O environment),   is the number of atoms in a 2O+S environment,   the number of atoms in a H+O+S environment, μ is the number of atoms in a 2H+O environment and   in a 2O+H environment. None of the structures which we have considered contained an atom in a 3O environment. In order for such an environment to be present, the cage would have to be quite large. The root-mean square deviation for the total energy was 4.70 kcal/mol. The fit was checked on $(AlOMe)_{14}$ from Figure 2.5 for which the predicted and calculated energies differed by 5.51 kcal/mol. Figure 2.7 shows the predicted and calculated energy values for ten $(AlOMe)_{12}$ isomers, along with the $x = y$ line. The fit is not perfect, but it performs reasonably well in reproducing the trend.

The coefficients pertaining to each specific bonding environment provide a means by which one can gauge the stability of a particular environment. The more negative the coefficient, the more stable the environment. The order of stability is 3H > 2H+S > H+O+S > 2O+S > 2H+O > 2S+H > 2S+O > 3S > 2O+H. Thus, an atom bonded to three hexagonal faces is the most stable, while an atom bonded to two octagonal and one hexagonal face is the least stable.
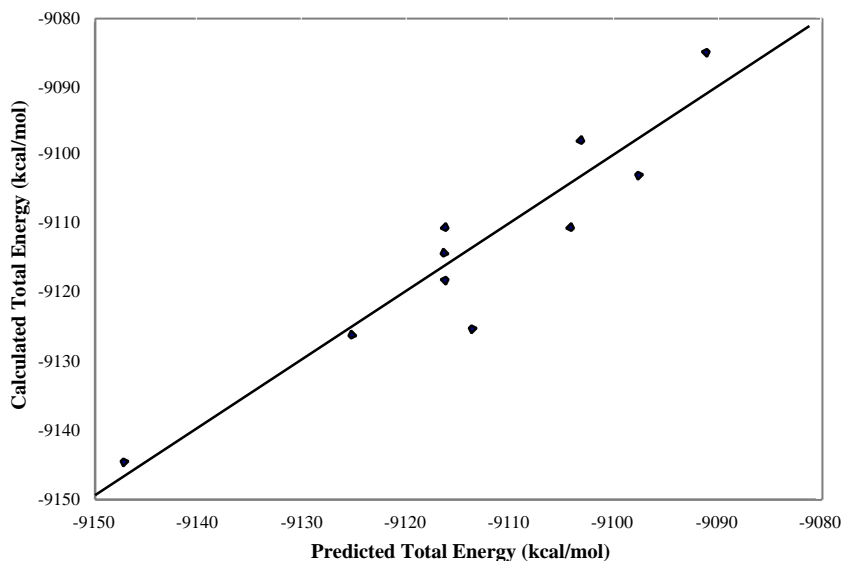
Figure 2.7: Calculated Energies and those Predicted by Equation 2.13 for Isomers of $(AlOMe)_{12}$

Structures composed simply of square and hexagonal faces were found to have the lowest energies for a given n with the exception of $(AlOMe)_{10}$ where another structure was 0.38 kcal/mol more stable. This can be attributed to the fact that the number of square faces within a structure is equal to the number of octagonal faces plus six. Thus, the minimum possible number of square faces occurs when no octagonal faces are present. The square faces exhibit a large amount of ring strain therefore destabilizing the structure. Hence, the cages with the least amount of square faces present for a given n, have the lowest energies.

Figure 2.8 shows the Energy per Monomer Unit versus n for structures composed of square and hexagonal faces only. For $n =$17, 18, 20, 21, 25 and 30, the bonding environments were found using Equations 2.11 and 2.12. We verified that such a topology was possible by drawing the corresponding Schlegel diagram. Equation 2.13 was used to predict the energies, hence error bars are present.
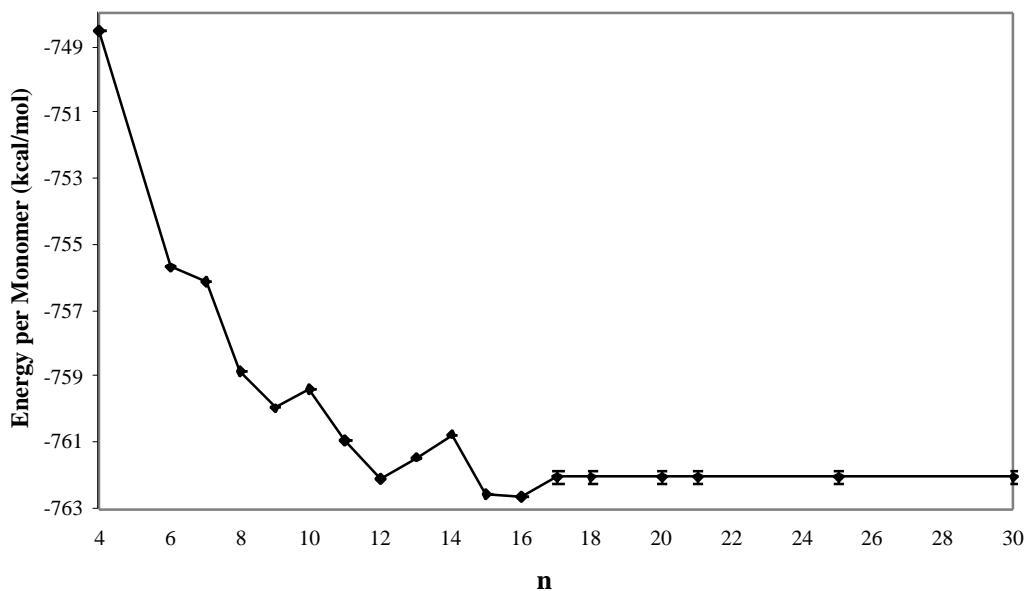
Figure 2.8: Energy per Monomer Unit vs. n

The first notable aspect of Figure 2.8 is that the energy per monomer approaches a plateau as n increases. Equations 2.11 and 2.12 show that as a MAO cage increases in

size the number of atoms found in a 2H+S environment is 24, while the number of atoms in a 3H environment increases as a function of n. Equation 2.13 assigns certain energies to atoms in each environment. Thus, for large n, the energy of a structure becomes a linear function of n and hence the energy per monomer unit reaches a plateau with increasing n. The graph displays an almost smooth curve, with the exception of three local maxima points which are present at $n = 7$, 10 and 14.

More energetically stable structural alternatives for these oligomers could not be found. Their relative instability is due to the presence of a greater amount of strained bonds (atoms in 3S or 2S+H environments) as compared to their neighbours. For example, $(AlOMe)_6$ contains twelve 2S+H atoms, $(AlOMe)_7$ contains two 3S, six 2S+H and six 2H+S atoms, $(AlOMe)_8$ contains eight 2S+H and eight 2H+S atoms. Thus, the presence of atoms in a 3S environment destabilizes $(AlOMe)_7$ in comparison with its neighbours. Note that Equation 2.13 shows that for structures with square and hexagonal faces only the order of stability is 3H > 2H+S > 2S+H > 3S.

Consider the growth of a MAO cage by two monomer units as shown in Figure 2.9. All of these structures are composed of square and hexagonal faces only and are possible structural alternatives for $(AlOMe)_n$ where $n = 6$, 8, 10… . Such structures contain six atoms in a 2S+H environment which is energetically destabilizing. Other more stable structural alternatives were found for $n > 10$. The entries given in Figure 2.8 correspond to the most stable isomer.
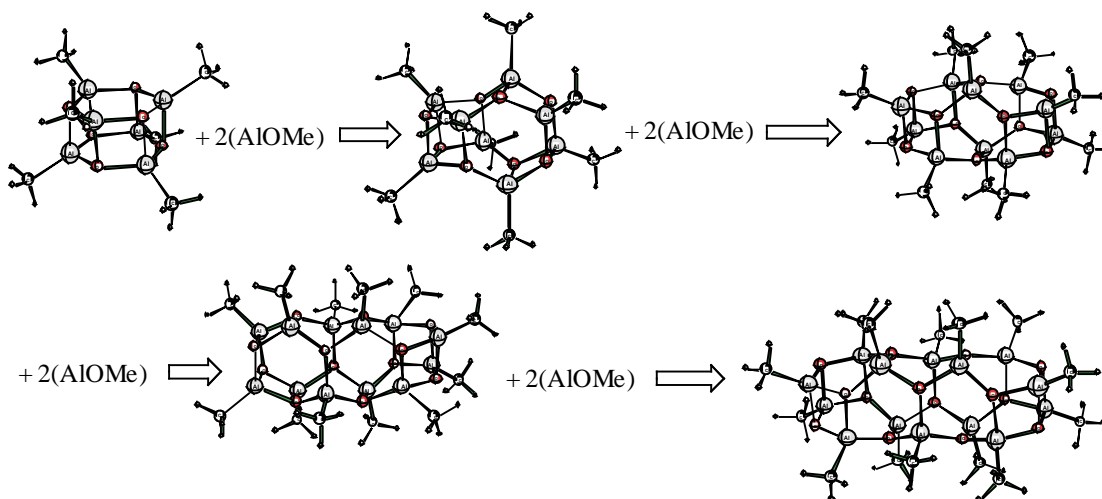
Figure 2.9: Growth of a MAO Cage by Two AlOMe Units

2.2.4   Enthalpic Considerations

Finite temperature enthalpies and entropies can be calculated from standard expressions[40] provided that all the vibrational frequencies are known. Unfortunately, full quantum mechanical frequency calculations are computationally too expensive to be calculated for all structures. Thus, another approach was taken, based on molecular mechanics calculations using the Universal Force Field 2.[35]

It was necessary to parametrize UFF2 so that the frequencies reproduced those calculated with ADF. The results of the ADF and UFF2 calculations are given below in Table 2.3. The parametrization was performed on $(AlOMe)_4$ and $(AlOMe)_6$ then checked on $(AlOMe)_8$-II and $(AlOMe)_8$-III. As Table 2.3 shows, zero-point energies and entropies of all of the structures are reproduced extremely well. Moreover, so are the differences for the two $(AlOMe)_8$ isomers. The parametrization was performed on MAO structures composed solely of square and hexagonal faces, yet good values are also obtained for $(AlOMe)_8$-II, which contains two octagonal faces. The thermodynamic values obtained using UFF2 are quite reliable: they reflect the differences between isomers, and can be used for structures consisting of square, hexagonal and octagonal faces.

Table 2.3: Comparison of Thermodynamic Quantities Obtained Using UFF2 and ADF[a]

Structure	ADF ZPE	UFF2 ZPE	ADF Entropy	UFF2 Entropy
$(AlOMe)_4$	100.14	98.87	126.22	130.88
$(AlOMe)_6$	148.21	149.12	162.21	159.01
$(AlOMe)_8$-II	197.89	198.81	211.61	207.58
$(AlOMe)_8$-III	198.72	199.46	219.59	221.28

[a]ZPEs given in kcal/mol; entropies in cal/molK at 298.15K.

The total enthalpy is given as:

$$H(T, n) = E(n) + H_{EC}(T, n), \hspace{4cm} [2.14]$$

where $E(n)$ is the energy and $H_{EC}(T, n)$ is the finite temperature enthalpy correction. For a liquid the latter can be decomposed into the rotational, translational and vibrational finite temperature enthalpy corrections as:

$$H_{EC}(T, n) = H_{rot}(T, n) + H_{trans}(T, n) + H_{vib}(T, n) . \qquad [2.15]$$

We have performed a parametrization so that $H_0(n)$, the zero-point energy, and $H_{vib}(T, n)$ could be calculated for large MAO structures ($n > 16$) whose geometries were not optimized with ADF (see appendix for discussion of fit). The different enthalpy contributions can be found via the following (in kcal/mol):

$$H_0(n) = 25n \text{ kcal/mol} \qquad [2.16a]$$
$$H_{rot}(T, n) = H_{trans}(T, n) = 1.5RT \qquad [2.16b]$$
$$H_{vib}(T,n) = H_0(n) + \ln(T) \times (0.0028T - 0.3548) \qquad [2.16c]$$

Equation 2.16a has a root mean square deviation of 1.16 kcal/mol, Equation 2.16b is exact and for 2.16c, the root mean square deviations are 3.28, 0.78, 1.32 and 3.36 kcal/mol at 198.15K, 298.15K, 398.15K and 598.15K, respectively.

Figure 2.10 shows the finite temperature enthalpy correction per monomer unit $\frac{H_{EC}(T,n)}{n}$ as a function of n at different temperatures. The values are plotted for the most stable oligomer composed of square and hexagonal faces only. Error bars are given for $n =17, 18, 20, 21, 25$ and 30, where Equations 2.16a - 2.16c were used for predicting values. Otherwise, the results of the parametrized UFF2 code were used. It shows that the enthalpy correction per monomer unit is almost the same for all MAO oligomers at the plotted temperatures. Hence, for a given disproportionation reaction $H_{EC}(T, n)$ will be nearly zero and does not contribute to the relative stability of the MAO oligomers.
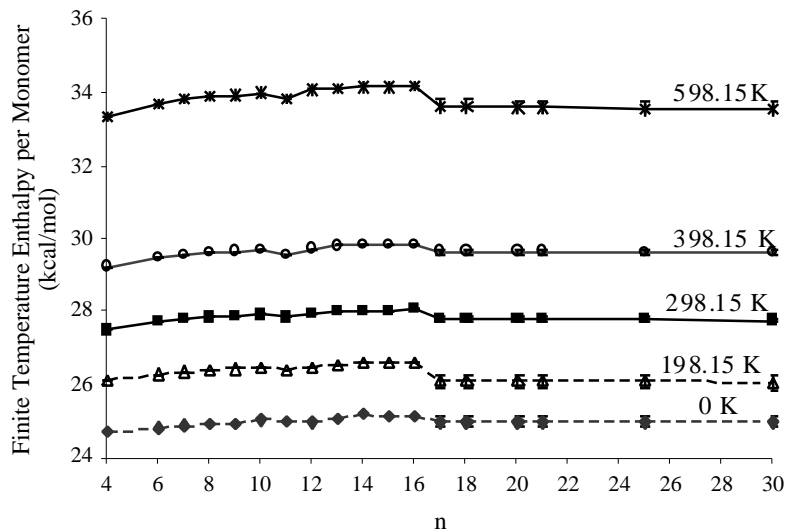
Figure 2.10: Enthalpy per Monomer Unit vs. *n*

2.2.5 Entropic Considerations

For *n* < 17, entropies were calculated via the parametrized UFF2 code. The total entropy of an (AlOMe)$_n$ oligomer at temperature *T* is given by

$$S(T, n) = S_{trans}(T, n) + S_{rot}(T, n) + S_{vib}(T, n),$$ [2.17]

where $S_{trans}(T, n)$, $S_{rot}(T, n)$, $S_{vib}(T, n)$ are the translational, rotational and vibrational contributions to the entropy. The following equations predict the different entropic contributions at 298.15K in cal mol^{-1} K^{-1} (see appendix for discussion of fit),

$$S_{trans}(298.15, n) = 0.351n + 41.16\!$$ [2.18a]

$$S_{rot}(298.15, n) = 0.573n + 30.57\!$$ [2.18b]

$$S_{vib}(298.15, n) = 7.91 + 8.30 + 10.20 + 8.49 + 10.41 + 9.50 +$$
$$10.45 + 7.32\mu + 0 ,$$ [2.18c]

where   corresponds to the number of atoms bonded to three square faces and so on. The root mean square deviation for $T \times S(298.15, n)$ is 1.78 kcal/mol. Entropic corrections are temperature dependent and hence we parametrized equations which could be used to predict entropies at different temperatures given those at 298.15K. They are the following in cal mol^{-1} K^{-1}:

$$S_{trans}(T_2, n) = S_{trans}(T_1, n) + \frac{T_2}{T_1} + (0.014)T_2 - 5.47 \qquad [2.19a]$$

$$S_{rot}(T_2, n) = S_{rot}(T_1, n) + \frac{T_2}{T_1} + (0.0077)T_2 - 3.28 \qquad [2.19b]$$

$$S_{vib}(T_2, n) = \frac{T_2}{T_1} - \frac{1}{\left(0.0006T_2^2 - 0.5355T_2 + 108.85\right)} S_{vib}(T_1, n), \qquad [2.19c]$$

where $S_{trans}(T_2, n)$ is the translational entropy at temperature T_2 and so on. Equations 2.19a and 2.19b are nearly exact while Equation 2.19c gives a root mean square deviation of 0.27 kcal/mol, 1.70 kcal/mol, and 4.09 kcal/mol at 198.15K, 398.15K and 598.15K, respectively for $T \times S(T, n)$.

Figure 2.11 shows $\frac{-TS(T, n)}{n}$ versus n for different temperatures. For $n = 17$, 18, 20, 21, 25 and 30, Equations 2.18a - 2.19c were used to predict the entropies, hence error bars are present. At low temperatures $\frac{-TS(T, n)}{n}$ is not very significant: it is approximately the same for all n. As the temperature increases $\frac{-TS(T, n)}{n}$ becomes important in stabilizing smaller structures. At all temperatures the same trends are followed, yet the differences between adjacent points become greater with increasing temperature. The graph in Figure 2.11 displays an almost smooth curve, with a local minimum present at $n = 12$.
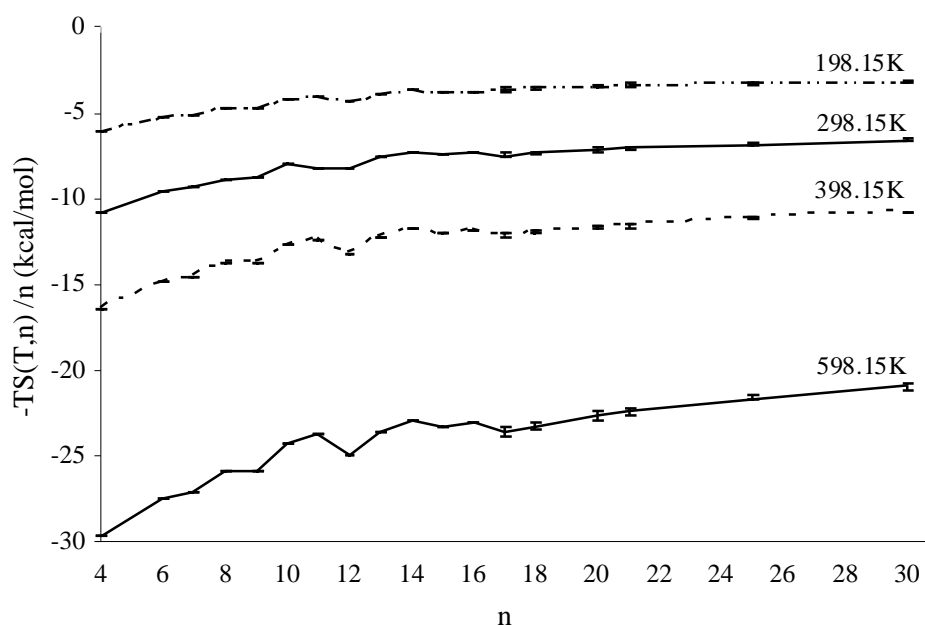
Figure 2.11: Entropy per Monomer Unit vs. *n*

2.2.6 The Gibbs Free Energy

The Gibbs free energy per Monomer is given as:

$$\frac{G(T,n)}{n} = \frac{H(T,n)}{n} - \frac{TS(T,n)}{n}.$$

[2.20]

It is plotted in Figure 2.12 for the most stable oligomers (those which *do not* follow the growth scheme shown in Figure 2.9 for *n* > 10) composed of square and hexagonal faces. It was found that these structures give the lowest Gibbs free energy for a given *n*, with one exception, that is of $(AlOMe)_{10}$ where a structure containing octagonal faces is 2.59 kcal/mol more stable. Error bars are present for *n* = 17, 18, 20, 21, 25 and 30 where Equations 2.11 and 2.12 were used to find the connectivities and the methods described earlier were used to estimate the Gibbs free energy.
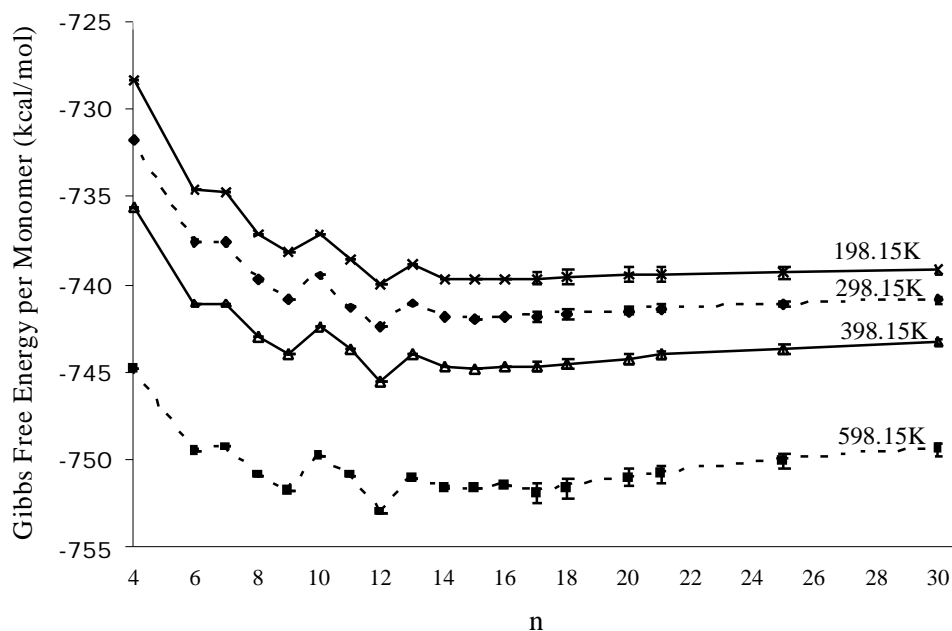
Figure 2.12: Gibbs Free Energy per Monomer Unit vs. *n*

The same general trend is followed at all temperatures, with $(AlOMe)_{12}$ being the most stable oligomer. At lower temperatures, $(AlOMe)_{16}$ is almost as stable as $(AlOMe)_{12}$, while at high temperatures the difference increases. This can be attributed to entropic effects, which are expected to be more important at higher temperatures. Local maxima at $n = 7$, 10 and 13 are found at all temperatures. They are due to the bonding environments present in the given structures (a greater amount of atoms in 3S and 2S+H environments as compared to their neighbours). The most important temperatures are 298.15K and 398.15K, since typical polymerization conditions are within this range.

Equation 2.8 shows that there are six square faces present in a MAO structure composed of square and hexagonal faces. We have shown that these structures have the lowest free energy for a given *n*. Moreover, the structures which are most stable do not have atoms in 3S or 2S+H environments, that is they do not contain square-square edges. Bonds which are made up of square-square edges (for example in the structures shown in Figure 2.9) are more strained and less stable and are therefore the sites with greatest

LLA. This suggests that there are not many acidic or active sites present in MAO. This topological consequence could explain the high Al/Catalyst ratio necessary for polymerization to occur.

The Gibbs free energy which one monomer gains by binding with other monomers to form $(AlOMe)_n$ is given by:

$$G(T,n) = \frac{G(T,n)}{n} - G(T,1).$$

[2.21]

If $\Delta G(T,n)$ is defined in such a way, then Equation 2.22 may be used to calculate equilibrium constants between a free monomer and one found in $(AlOMe)_n$. For $n = 17$, 18, 20, 21, 25 and 30 the equilibrium constants were obtained using the estimated Gibbs free energies for $(AlOMe)_n$. For $n = 19$, 22 - 24, and 26 - 29 the Gibbs free energies were found via interpolation and next the equilibrium constants were calculated. As a check, structures were found via drawing a Schlegel diagram for $n = 19$, 22 and 24 then the Gibbs free energy were predicted using the aforementioned formulae. All of the interpolated Gibbs free energies fell within the given error bars.

$$K_{eq}(T,n) = \exp\frac{-G(T,n)}{RT}$$

[2.22]

Next, it is possible to find the percent abundance of a given structure according to Equation 2.23. This procedure (using Equations 2.21-2.23) is equivalent to assuming that the monomers obey a Boltzmann probability distribution at constant temperature and pressure.

$$\%(AlOMe)_n(T) = \frac{K_{eq}(T,n)}{\sum_i K_{eq}(T,i)} \times 100\%$$

[2.23]

Table 2.4: Percent Abundance of MAO Oligomers at Different Temperatures

n	198.15K	298.15K	398.15K	598.15K	n	198.15K	298.15K	398.15K	598.15K
4	0.00	0.00	0.00	0.02	18	6.62	5.93	6.37	6.17
6	0.00	0.01	0.08	1.05	19	5.76	5.02	5.26	4.88
7	0.00	0.01	0.09	0.92	20	5.01	4.26	4.35	3.87
8	0.01	0.23	0.96	3.33	21	4.45	3.69	3.69	3.20
9	0.18	1.29	3.36	7.40	22	4.05	3.30	3.24	2.73
10	0.01	0.14	0.45	1.27	23	3.68	2.94	2.84	2.33
11	0.50	3.00	2.49	3.43	24	3.34	2.63	2.50	1.99
12	16.24	20.11	21.86	20.22	25	3.04	2.35	2.19	1.70
13	0.98	2.16	3.12	3.83	26	2.84	2.17	2.00	1.53
14	4.85	8.38	4.43	4.87	27	2.66	2.00	1.82	1.37
15	10.37	9.22	8.49	6.65	28	2.49	1.85	1.66	1.23
16	10.60	8.85	7.89	5.99	29	2.33	1.71	1.52	1.10
17	7.79	7.20	7.96	7.93	30	2.18	1.58	1.39	0.99

Table 2.4 gives the percent abundance of the MAO's at different temperatures. This is also plotted in Figure 2.13. The most abundant species at all temperatures is $n = 12$ which ranges between 16-22% in abundance. These values agree well with experimental data.[13] However, it is not clear if the experiments report n for $(AlOMe)_n$, or $n + m$ for $(AlOMe)_n \cdot (TMA)_m$. Since small MAO cages contain more acidic sites (strained bonds), our results predict that as the temperature increases the number of acidic sites will also increase. Higher temperatures stabilize smaller species (which can be seen in the large increase of $n = 9$ at 598.15K), while lower temperatures stabilize larger species (which can be seen in the increase of n ≥ 15 at 198.15K). This is also evident in the average value of n which is 18.41, 17.23, 16.89 and 15.72 at 198.15K, 298.15K, 398.15K and 598.15K, respectively.
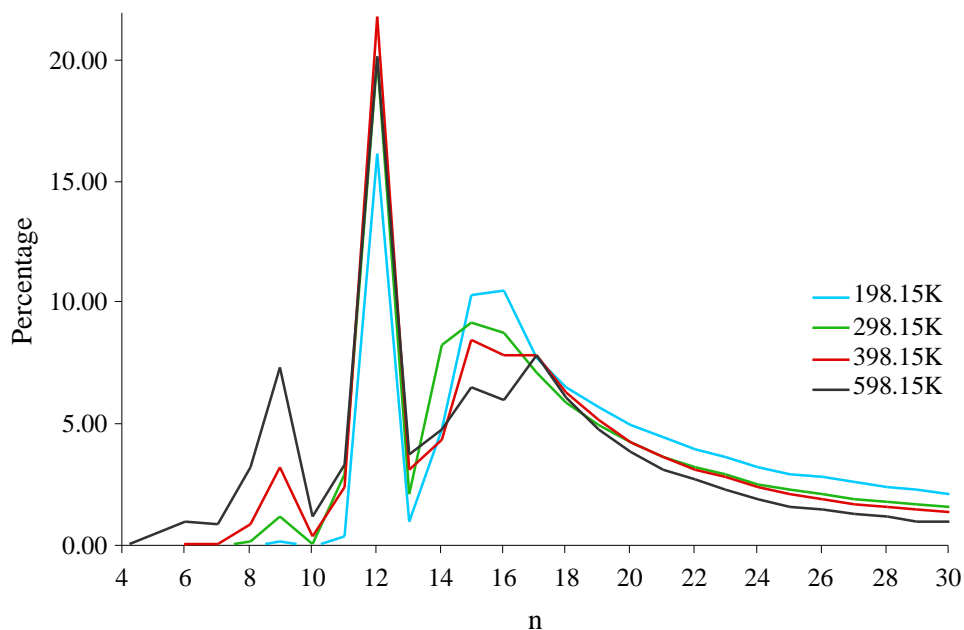
Figure 2.13: Percentage of $(AlOMe)_n$ at Different Temperatures

2.3 Conclusions

In this study we have found possible structures for MAO cages with a 1:1:1 ratio of Al/O/Me via drawing Schlegel diagrams. Using topological arguments, we have shown that the most stable MAO structures have only six square faces and few square-square edges. These faces exhibit high ring strain and therefore such square-square edges should have the highest LLA (be the more active sites). We propose the low abundance of these faces and edges to explain the high Al/catalyst ratio required for polymerization to occur. In short, we have found that the most stable and abundant 'pure' MAO species are the least active. We have also calculated the percent distribution of $(AlOMe)_n$ at different temperatures. This predicts that the average MAO oligomer has the formula $(AlOMe)_{18.41}$, $(AlOMe)_{17.23}$, $(AlOMe)_{16.89}$ and $(AlOMe)_{15.72}$ at 198.15K, 298.15K, 398.15K and 598.15K, respectively, in good agreement with experimental data. We have also outlined a method which may be used to investigate the composition of any solution composed of an equilibrium mixture of oligomers.

2.4 Appendix

Energies

The energy of a given MAO cage structure was found to be heavily dependent upon the structure of the cage itself. Assigning certain coefficients to atoms in different bonding environments proved to be an effective means to predict energies. Al and O atoms are not equivalent and should therefore give different contributions to the energy, even if their bonding environments are the same. Only two cases were found where the structure was not symmetric with respect to interchange of the Al and O atoms. For isomers of $(AlOMe)_9$ and $(AlOMe)_{12}$, interchanging the Al and O atoms resulted in an energy difference of 3.2 kcal/mol and 7.6 kcal/mol, respectively. Such differences correspond to 0.05% and 0.08% of the total energy and are not very significant. Thus, it is reasonable to assume that Al and O atoms contribute equally to the energy of a given structure when found in a similar bonding environment. The energies were fitted via a least squares analysis, with the bonding environments as parameters.

Enthalpies

Standard expressions[40] give the translational and rotational contributions to the enthalpy as being $\frac{3}{2} RT$. Hence, it is only necessary to fit the vibrational contribution to the enthalpy. The fit was performed only on structures composed of square and hexagonal faces, since they gave energies per monomer which were much lower than those also containing octagonal faces.

Entropies

The translational entropy is dependent only upon the mass of the molecule while the rotational entropy is dependent upon the moment of inertia, which is in turn dependent upon mass (and geometry). Hence, it is natural to model the translational and rotational entropy as a function of *n*. Linear regression was used to obtain Equations 2.18a and 2.18b, which are valid only at 298.15K.

The vibrational entropy varied considerably between different isomers and hence could not be modeled in a similar fashion. Thus, it was natural to model it in the same way as the energies. A least squares analysis with the bonding environments as parameters was used to fit the entropies at 298.15K.

The extension to different temperatures was performed on structures consisting of square and hexagonal faces only. Formulae were fit so that entropies at different temperatures could be acquired if those at 298.15K were known. If we assume that the vibrational entropy at temperature T_2 is proportional the vibrational entropy at T_1, we find that

$$nR \sum_i \left[\frac{1}{u_i(T_1)\exp[u_i(T_1)] - 1} - \ln\left(1 - \exp[-u_i(T_1)]\right) \right] =$$

$$CnR \sum_i \left[\frac{1}{u_i(T_2)\exp[u_i(T_2)] - 1} - \ln\left(1 - \exp[-u_i(T_2)]\right) \right] \qquad [2.24]$$

where C is some constant to be determined and $u_i = \dfrac{h v_i}{kT}$. For a given i,

$$\frac{h v_i}{kT_1}\left[\exp\left(\frac{h v_i}{kT_1}\right) - 1\right]^{-1} - \ln\left[1 - \exp\left(-\frac{h v_i}{kT_1}\right)\right] =$$

$$C\left\{ \frac{h v_i}{kT_2}\left[\exp\left(\frac{h v_i}{kT_2}\right) - 1\right]^{-1} - \ln\left[1 - \exp\left(-\frac{h v_i}{kT_2}\right)\right] \right\} \qquad [2.25]$$

Since $\dfrac{h v_i}{kT}$ is of the order of magnitude of about 10, we can assume that $\exp\left(\dfrac{-h v_i}{kT_i}\right) \approx 0.$

This implies that $\ln\left[1 - \exp\left(\dfrac{h v_i}{kT_i}\right)\right] \approx \ln(1) = 0$. Simplifying [2.25] and solving for C, we obtain:

$$C = \frac{T_1}{T_2} \exp\left(\frac{hv_i}{kT_2} - \frac{hv_i}{kT_1}\right) .$$ [2.26]

Using a Taylor Series expansion we obtain,

$$C = \frac{T_1}{T_2} \, (1 + \text{higher order terms}).$$ [2.27]

The higher order terms will be neglected and instead, a correction factor will be added. The correction factor was found to be $(0.0006T^2 - 0.5353T + 108.85)^{-1}$.

The root mean square deviation for the vibrational entropy was calculated to be 0.27 kcal/mol, 1.70 kcal/mol and 4.09 kcal/mol for 198.15K, 398.15K and 598.15K, respectively. This is a good fit, especially taking into account the fact that the entropies were estimated over a 400 K temperature range. As the temperature rises, the approximation that $\exp\left(\frac{-hv_i}{kT_i}\right) \to 0$ becomes less appropriate. Hence, the root mean square deviation increases with increasing temperature and becomes comparably large at 598.15K.

Chapter 3

The Dynamic Equilibrium Between Trimethylaluminum (TMA) and Oligomers of (AlOMe)$_n$: A Model for 'Real' Methylaluminoxane.

3.1 Introduction

In the previous chapter, we have examined possible structural alternatives for oligomers of (AlOMe)$_n$, where $4 \leq n \leq 30$. We have found that the most stable structures are cages consisting of square and hexagonal faces only. For larger cages, when there is more than one possible isomer, those with the least amount of atoms in 3S (three square) and 2S+H environments are more stable. Moreover, we have calculated a percent distribution for this system, finding an average unit formula of (AlOMe)$_{18.41}$, (AlOMe)$_{17.23}$, (AlOMe)$_{16.89}$, and (AlOMe)$_{15.72}$ at 198.15K, 298.15K, 398.15K and 598.15K respectively.

Unfortunately, this system is only hypothetical and as of yet has not been determined experimentally. This is due to the fact that there is always residual TMA found within a MAO solution. It is generally accepted that the TMA exists as the free and bound species according to the following equilibrium:

$$(AlOMe)_n \; + \; \frac{m}{2}(AlMe_3)_2 \quad \rightleftharpoons \quad (AlOMe)_n \cdot (AlMe_3)_m . \qquad\qquad [3.1]$$
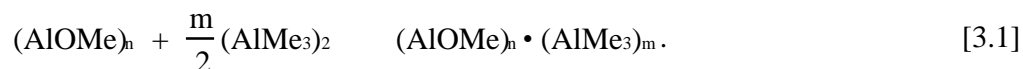
Several experimental attempts have been undertaken to establish the degree to which TMA is coordinated to MAO.[7,14] Moreover, the effect of addition of TMA to a MAO mixture has been examined.[15] However, the conclusions drawn from these studies are to some degree uncertain due to experimental difficulties. Proton NMR gives a spectrum in which the peaks from MAO and TMA overlap and removal of volatiles produces more free TMA upon standing. Moreover, using Lewis bases in such an analysis (in titration or as a probe molecule in heteronuclear NMR) is unreliable due to the fact that most bases not only interact with TMA, but also with MAO. Some experimental methods claim to have overcome these difficulties yielding a Me/Al ratio of 1.4[14c] or 1.5[14d] when free TMA has been removed or corrected for. Barron has

characterized two isomers as the products of the reaction of $[(^tBu)_6Al(\mu_3\text{-}O)]_6$ and TMA.[16] They are shown in Figure 3.1.

In this chapter we examine the degree to which TMA is coordinated to MAO as well as the bonding mode of this coordination. We will build upon the model which we have proposed for 'pure' MAO and establish a percent abundance of 'real' MAO species with the general formula $(AlOMe)_n \bullet (TMA)_m$ where $4 \quad n \quad 30$ and $0 \quad m \quad 4$, depending upon the structural properties of the parent cage.
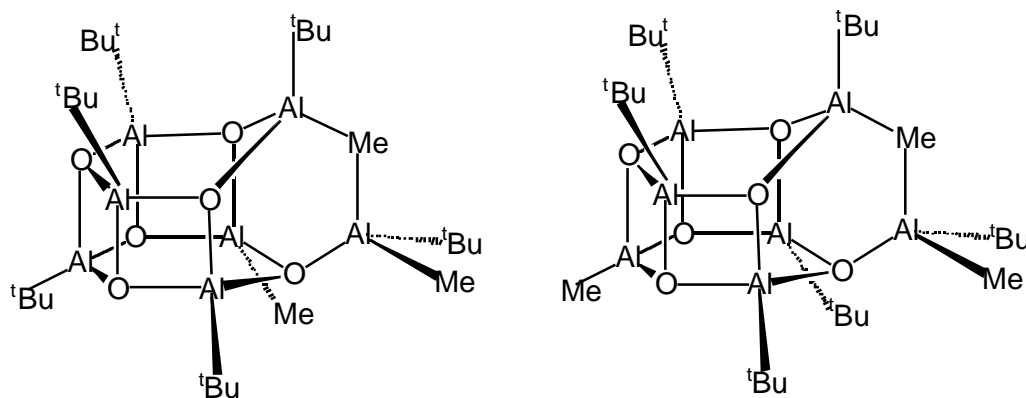
Figure 3.1: Isomers of $[Al_7(\mu_3\text{-}O)_6(^tBu)_6Me_3]$

Section 3.2.1 discusses the different ways in which TMA may interact with MAO. Section 3.2.2 examines the sites of greatest Latent Lewis Acidity on MAO cages. Sections 3.2.3, 3.2.4 and 3.2.5 discuss the energetic, enthalpic and entropic contributions to the Gibbs free energy when one to four TMA groups are added to different MAO cages. In Section 3.2.6 the Gibbs free energy is used to find the percent abundance of each species within the temperature range of 198.15K-598.15K and the ratio of Me/Al groups is calculated. Finally, in Section 3.2.7 the accuracy of the theoretical and experimental results is examined.

3.2 Results and Discussion

3.2.1   How TMA Bonds to MAO

In this section we study how TMA bonds to MAO. Calculations have been performed on six different structural alternatives for $(AlOMe)_6 \bullet (TMA)$, shown in Figure

3.2. The E values for the reaction shown in 3.1 with $n = 6$ and $m = 1$ are given in Table 3.1. All energies are with respect to the TMA dimer, since this is the most likely species to exist in solution.

unimportant methyl groups omitted for clarity
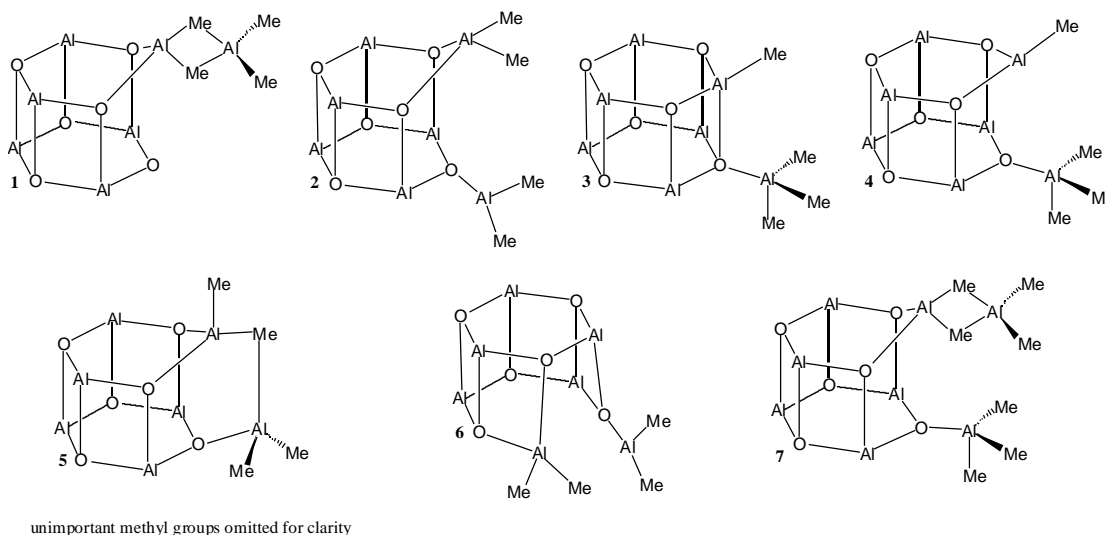
Figure 3.2: Possible Structures for $(AlOMe)_6 \cdot (TMA)$ and $(AlOMe)_6 \cdot (TMA)_2$

Table 3.1: E for Reaction of $\frac{1}{2}(TMA)_2 + (AlOMe)_6$

Structure	E^a (kcal/mol)	Structure	E^a (kcal/mol)
1	14.89	4	6.26
2	-13.06	5	-7.79
3	-1.01	6	5.15

$^a E$ is the electronic contribution to the enthalpy

In **1** the strained square-square (s-s) bond has broken and a TMA group has bonded to the corresponding Al atom via two bridging methyl groups. It is surprising to find that for this reaction E is equal to 14.89 kcal/mol and hence this bonding mode is highly unfavorable. One reason for this might be that the oxygen prefers to be three-coordinate. The strained s-s bond in **2** has also broken. Yet, here the TMA has bonded to the O atom and a methyl transfer to the Al has occurred. This reaction has the lowest E,

and hence this is the preferred bonding mode. Structures **3** and **4** are quite similar. However, in **4** the strained s-s bond is broken, whereas in **3** it is not. Neither structure is a favorable alternative. In **5** an s-s bond has broken, the Al of the TMA has bonded to an O on the parent cage, and to an Al via a methyl bridge, yielding a structure similar to that shown in Figure 3.1 for $[Al_7(\mu_3\text{-}O)_6(^tBu)_6Me_3]$. This reaction also has a negative E, however it is not as low as in the case of **2**. In fact, **5** can be considered as an intermediate between $(AlOMe)_6 + \frac{1}{2}(TMA)_2$ and **2**, as shown in Figure 3.3. Other groups[24] have proposed that TMA bonds to MAO in a manner similar to that shown in **5**, however they did not consider a structure similar to **2**. The exact same bonding has taken place in **6** as in **2**, yet the bond broken was a square-hexagonal (s-h) one. The E here is positive showing that it is not only *how* TMA bonds to MAO which is important, but also *where*.

$1/2(TMA)_2$
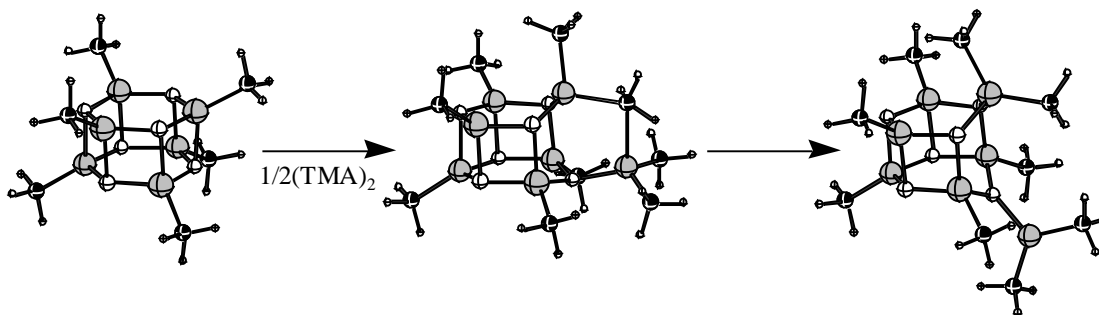
Figure 3.3: Interaction of TMA with $(AlOMe)_6$

The s-s bond is much more strained than the s-h bond, and is therefore more acidic. Other groups[21] have proposed that the preferred bonding mode of TMA is that shown in **7**. Here we have two TMA groups bonding to the MAO cage simultaneously. However, our calculations show that E for the formation of **7** from $(AlOMe)_6$ and $(TMA)_2$ is 4.02 kcal/mol and this is therefore an unfavorable reaction. Thus, it can be concluded that TMA bonds to MAO as shown in **2**. Structures with methyl bridges (**5**) and weak ion-pairs (**3**) may be present in MAO to some extent, but the completely ring-opened cage (**2**) is the predominant binding mode of TMA to MAO.

3.2.2 Sites of Greatest Latent Lewis Acidity Within Cage MAO Structures

We performed geometry optimizations on a number of $(AlOMe)_n \bullet (TMA)$ structures where $6 \leq n \leq 13$. The MAO cages chosen were the most stable ones consisting of square and hexagonal faces only and the bonding mode of TMA was the same as for structure **2**, shown in Figure 3.2. Also, for a given MAO cage, we optimized structures where TMA was bonded to a number of different sites. Figure 3.4 displays only the sites on the pure MAO cages for which the reaction given in Equation 3.1, with $m = 1$ was exothermic. A structure for $(AlOMe)_{12} \bullet (TMA)$ is not shown, since the reaction was endothermic.
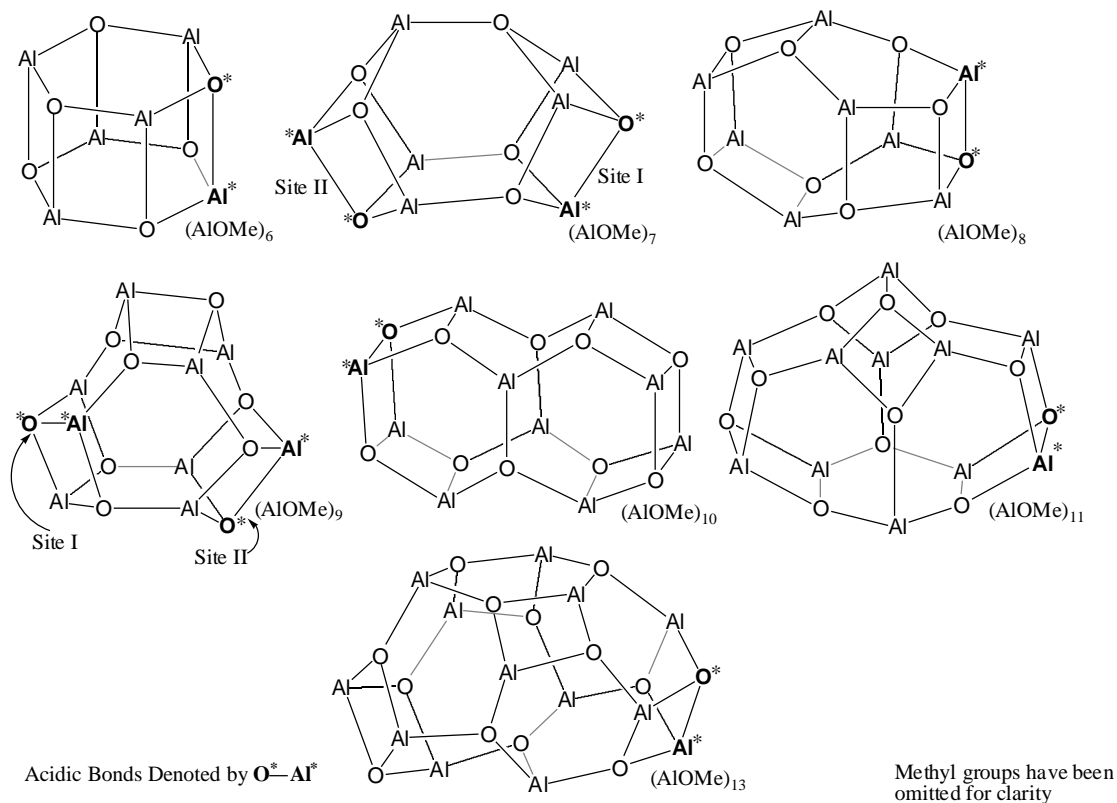
Figure 3.4: $(AlOMe)_n$ Cage Structures Containing Acidic Bonds

Three variables are necessary in characterizing the most Lewis Acidic Site. The first is what type of bond was broken (s-s, s-h or h-h), the second and third correspond to the bonding environments of the O and Al atoms before the bond was broken (3S, 2S+H,

2H+S or 3H). For example, in **2** above, the most acidic site has O and Al atoms in 2S+H environments and an s-s bond was broken. Intuitively speaking, s-s bonds and atoms in 3S environments ought to experience higher ring strain and therefore be the most acidic. We shall now examine this in more detail.

Table 3.2: E (kcal/mol) for the Reaction of $(AlOMe)_n + \frac{1}{2}(TMA)_2$

n	site	E	n	site	E
6	I	-13.06	9	II	-4.30
7	I	-7.82	10	I	-10.56
7	II	-4.73	11	I	-5.20
8	I	-6.98	12	I	1.70
9	I	-9.82	13	I	-7.70

Table 3.3: Variables Characterizing the Most Lewis Acidic Site for $(AlOMe)_n$

n	Al environment	O environment	Bond Broken
6	2S + H	2S + H	s-s
7	2S + H	3S	s-s
8	2S + H	2S + H	s-s
9	2H + S	2S + H	s-h
10	2S + H	2S + H	s-s
11	2S + H	2S + H	s-s
13	2S + H	2S + H	s-s

Table 3.2 lists E for each particular site and Table 3.3 shows the three variables characterizing the most acidic site for each $(AlOMe)_n$. In all cases but one the most Lewis acidic site is an s-s bond with an Al in a 2S+H environment. The O is either in a 2S+H or 3S environment. For $(AlOMe)_9$ the site which is most acidic is an s-h bond with an Al in a 2H+S environment and O in a 2S+H environment. It is probably more acidic than the site consisting of an s-s bond with O and Al atoms in 2S+H environments due to less

steric congestion in the ring opened product. Equation 2.13 shows that the order of stability of a given bonding environment for a cage composed of square and hexagonal faces only is 3S < 2S+H < 2H+S < 3H. The data in Table 3.2 and Table 3.3 shows that the least stable bonding environments are also the most acidic.

Table 3.3 suggests that $(AlOMe)_{12}$, the most stable $(AlOMe)_n$ structures, will not have any acidic sites, since all of the atoms in $(AlOMe)_{12}$ belong to 2H+S environments and all of the bonds are s-h or h-h. When TMA was added to an s-h bond of $(AlOMe)_{12}$ (which ought to be more acidic than an h-h bond), E was 1.70 kcal/mol indicating that this reaction will not occur. Since the most stable oligomers for n 14 consist of atoms in 2H+S and 3H environments, we can conclude that TMA will not react with $(AlOMe)_n$ where n =12 and n 14 , due to the lack of strained bonds present in the most stable structural alternative.

3.2.3 Energetic Considerations

We have performed geometry optimizations on thirty-two different structures with the general formula $(AlOMe)_n \bullet (TMA)_m$ where 6 n 13 and n 12. The maximum m is dependent upon the number of acidic bonds present in the parent cage and ranges between 2 and 4. We also took into account the different possible ways TMA could bind to the MAO cage. For example, in $(AlOMe)_7$ there are two types of acidic sites and therefore two possible ways how a TMA monomer may bind to the parent cage. Moreover, due to the geometry of the parent cage two TMA monomers can bind to it in two different ways. Not enough acidic sites are present to which a third TMA can bind. In Figure 3.5 we show $E(n, m)$ for the reaction given in Equation 3.1. Only the most exothermic value is given for a specified n and m. For example, the addition of three TMA groups to $(AlOMe)_9$ can be done in four different ways with $E(n, m)$ ranging from between -3.87 kcal/mol to -9.23 kcal/mol. Only the value for the structure lowest in energy is given in Figure 3.5.
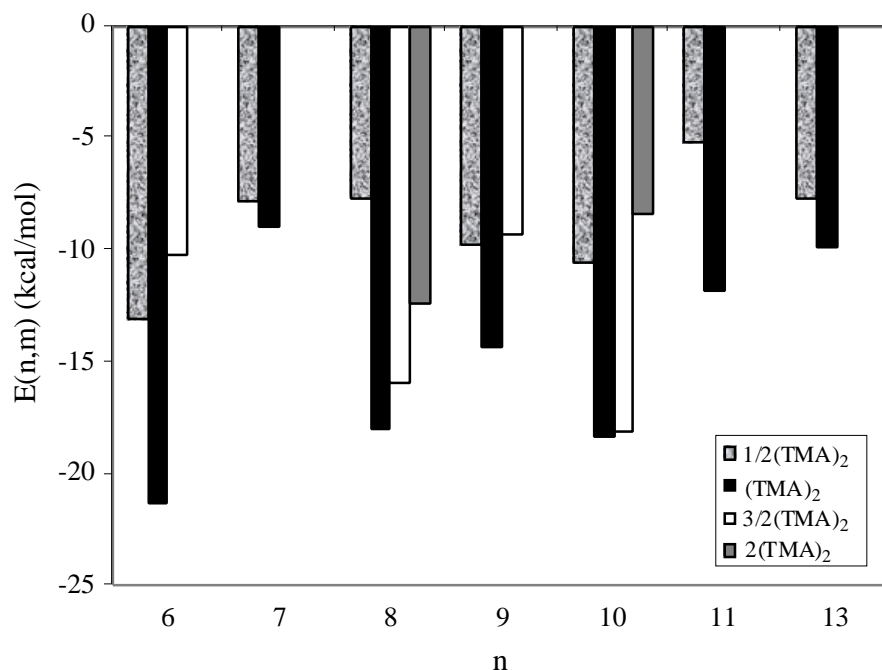
Figure 3.5: $E(n, m)$ for $(AlOMe)_n + \dfrac{m}{2}(TMA)_2 \rightarrow (AlOMe)_n \cdot (TMA)_m$

Figure 3.5 underlines that for a given n, the most negative $\Delta E(n, m)$ occurs when $m = 2$. If the topology of the parent cage is such so that it can react with more than two TMA groups then $\Delta E(n, 2) < \Delta E(n, 3) < \Delta E(n, 4)$. This occurs due to increased steric repulsion. Closer examination of the structures containing acidic bonds shows that each structure has two such bonds on opposite ends of the MAO cage. Hence it is possible to add two TMA groups to a MAO cage with little steric crowding. However, the third TMA must always be in close proximity to one of the other TMA groups. Thus, energetically speaking it is unfavorable to add more than two TMA groups to any MAO cage where $6 \le n \le 13$ and $n \ne 12$. If $n = 12$ or $n \ge 14$ then it is energetically unfavorable to add even one TMA group to the MAO cage.

Previously we have demonstrated that structures containing octagonal faces were less stable than those containing square and hexagonal faces only. Yet, we must take into account the possibility that this is not the case when the interaction with TMA is considered. These structures are less stable due to the fact that they contain more strained

acidic bonds. However, when they react with TMA a sufficient amount of strain could be released so that they become lower in energy than the structures we have considered so far. This may be due to the fact that $E(n, m)$ for a given n and m is lower or because of the fact that more TMA groups can be added to some of these cages.

We have explored the first option on two compounds. The energy of an $(AlOMe)_9 \bullet (TMA)_2$ structure containing one octagonal face (the TMA's were arranged in such a way as to minimize steric interactions) was still 20.22 kcal/mol *higher* than that of the *least* stable $(AlOMe)_9 \bullet (TMA)_2$ structure whose parent cage consisted of square and hexagonal faces only. There is much steric interaction present in $(AlOMe)_8 \bullet (TMA)_4$, whose parent cage is composed of square and hexagonal faces only. An alternative structure containing two octagonal faces has much less steric hindrance. Yet, this structure has an energy which is still 6.45 kcal/mol higher.

The number of acidic bonds present in the parent cage with which TMA may react is greatly dependent upon the topology of the cage. For example, in $(AlOMe)_8$ up to four TMA groups can react with the cage, independent of whether it contains octagonal faces or not. For the case of $(AlOMe)_{11}$ only two TMA groups can be added to the cage without octagonal faces whereas up to five TMA groups can be added when octagonal faces are present. However, such a structure should have quite a lot of steric hindrance and entropically be unfavorable. Hence, within this study we decided to focus upon structures whose parent cages do not contain octagonal faces.

3.2.4   Enthalpic Considerations

The total enthalpy and finite temperature enthalpy corrections have been previously defined in Equations 2.14 and 2.15. The only difference is that now they are also dependent upon m (in the last chapter m was set to zero, that is there were no TMA groups bound to the MAO cages). In this chapter we will write $H(T, n, m)$, $H_{EC}(T, n, m)$ and so on.

For the systems being studied, fully quantum mechanical frequency calculations are currently computationally too expensive. In the previous chapter, these contributions were computed using a parametrized version of the Universal Force Field 2 (UFF2). We

will follow the same method here, but first parameters for a two-coordinate oxygen atom need to be obtained. (In the previous chapter, parameters for four-coordinate aluminum and three-coordinate oxygen were found.) The parametrization was performed on $(AlOMe)_6 \cdot (TMA)_1$ and checked on $(AlOMe)_6 \cdot (TMA)_2$ and $(AlOMe)_8 \cdot (TMA)_1$. Results of the ADF and UFF2 calculations for the finite temperature enthalpy corrections and entropies at 298.15K are given below in Table 3.4.

Table 3.4: Comparison of Thermodynamic Quantities Obtained Using UFF2 and ADF[a]

Structure	ADF $H_{EC}(T, n, m)$	UFF2 $H_{EC}(T, n, m)$	ADF Entropy	UFF2 Entropy
$(AlOMe)_6 \cdot (TMA)_1$	235.12	236.39	216.27	210.20
$(AlOMe)_6 \cdot (TMA)_2$	306.31	305.73	262.77	253.88
$(AlOMe)_8 \cdot (TMA)_1$	291.57	293.93	255.88	248.70

[a]$H_{EC}(T, n, m)$ given in kcal/mol; entropies in cal/molK at 298.15K.

For the finite temperature enthalpy correction at 298.15K, the UFF2 estimates differ from values calculated by ADF by 1.27 kcal/mol, -0.58 kcal/mol and 2.36 kcal/mol for $(AlOMe)_6 \cdot (TMA)_1$, $(AlOMe)_6 \cdot (TMA)_2$ and $(AlOMe)_8 \cdot (TMA)_1$. At 298.15K UFF2 underestimates the entropy by 1.81 kcal/mol, 2.65 kcal/mol and 2.14 kcal/mol for these same structures. These deviations are reasonable and represent an error of only a few percent (relative error is less than 1% in all of the above calculations). Moreover, the error does not increase when more than one TMA group is added to the parent cage. In fact, in this particular case the error is smaller for $(AlOMe)_6 \cdot (TMA)_2$ than for $(AlOMe)_8 \cdot (TMA)_1$. We can also consider the error in $G(298.15K, n, m)$ for the Equation given in 3.1. For the formation of $(AlOMe)_6 \cdot (TMA)_1$, $(AlOMe)_6 \cdot (TMA)_2$ and $(AlOMe)_8 \cdot (TMA)_1$ it is 2.11 kcal/mol, 1.12 kcal/mol and 4.96 kcal/mol. Thus, we can expect that this error is within 5 kcal/mol.
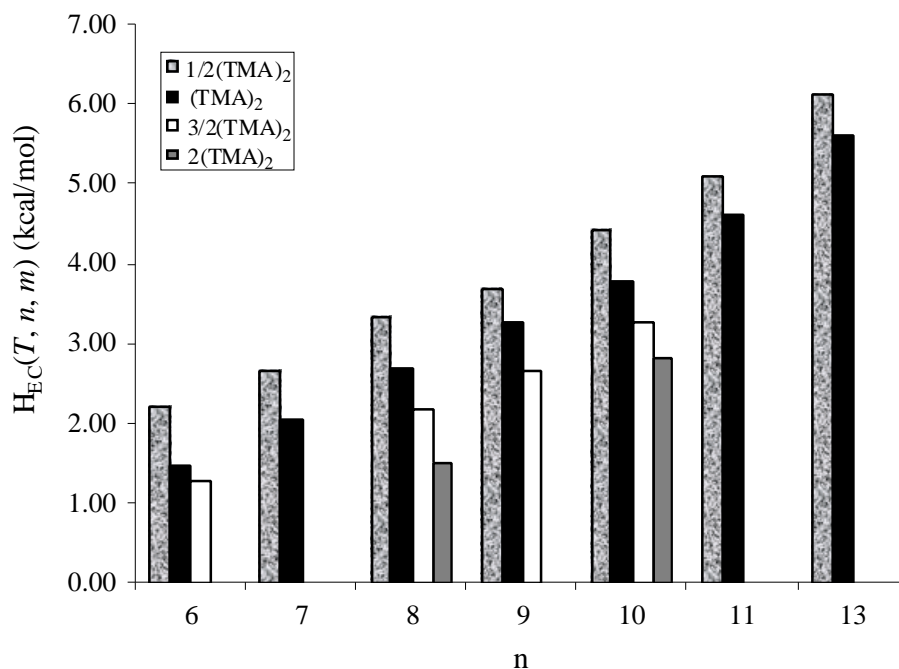
Figure 3.6: ΔH_{EC}(298.15K, *n*, *m*) for $(AlOMe)_n + \dfrac{m}{2}(TMA)_2 \quad (AlOMe)_n \quad (TMA)_m$

Figure 3.6 shows the difference in the finite temperature enthalpy correction for the reaction in Equation 3.1, for the most stable structural alternatives. It is given as a function of *n*; *m* ranges between 1 and 4 (depending upon the topology of the parent cage) at 298.15K. H_{EC}(298.15K, *n*, *m*) increases linearly with increasing *n* for a given *m*. Thus, H_{EC}(298.15K, *n*, 1) = (0.569*n* - 1.254) kcal/mol with a root-mean square deviation of 0.08 kcal/mol; H_{EC}(298.15K, *n*, 2) = (0.597*n* - 2.095) kcal/mol with a root-mean square deviation of 0.07 kcal/mol. For *m* = 3, 4 no linear regression was performed due to the lack of data points present. As *m* increases H_{EC}(298.15K, *n, m*) decreases for a given *n*. From the few data points available, this also appears to follow a linear relationship. At different temperatures, the aforementioned relationships for the addition of TMA to MAO hold. Moreover, H_{EC}(*T, n, m*) increases with increasing temperature. For *n* = 6, *m* = 1 it is 1.64 kcal/mol, 2.24 kcal/mol, 2.74 kcal/mol and 3.57 kcal/mol at 198.15K, 298.15K, 398.15K and 598.15K.

3.2.5 Entropic Considerations

Entropic values were calculated using the newly parametrized UFF2 code. The total entropy was previously defined in Equation 2.17 for the case when $m = 0$. Now it is also dependent upon m, and thus we write $S(T, n, m)$.
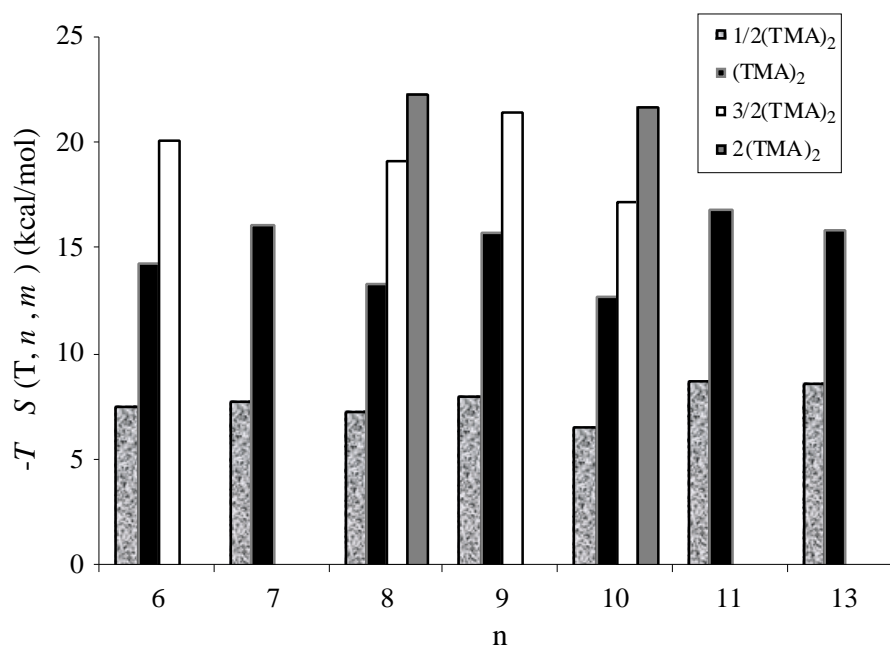
Figure 3.7: $-T\ S$(298.15K, n, m) for $(AlOMe)_n + \dfrac{m}{2}(TMA)_2 \quad (AlOMe)_n (TMA)_m$

Figure 3.7 displays $-T\ S$(298.15K, n, m) for the reaction given in Equation 3.1 for the most stable structural alternative of a given n and m. $-T\ S$(298.15K, n, 1) varies between 6.54 - 8.69 kcal/mol with an average value of 7.77 kcal/mol. Thus, on average the enthalpy for the addition of one TMA to a MAO cage must be at least -7.77 kcal/mol in order for this to be a favorable reaction. $-T\ S$(298.15K, n, 2) varies between 12.73 - 16.85 kcal/mol, with an average value of 7.50 kcal mol^{-1} m^{-1}; $-T\ S$(298.15K, n, 3) varies between 17.23 - 21.48 kcal/mol with an average value of 6.50 kcal mol^{-1} m^{-1}; for $-T\ S$(298.15K, n, 4) the average is 5.43 kcal mol^{-1} m^{-1}. Thus $-T\ S$(298.15K, n, m) per TMA unit decreases for every TMA being added.

In general, $-T\ S(T, n, m)$ increases at higher temperatures. For example $-T\ S(T,$ 9, 2) is 11.24 kcal/mol, 15.71 kcal/mol, 20.01 kcal/mol and 28.43 kcal/mol at 198.15K, 298.15K, 398.15K and 598.15K, respectively. This underlines the fact that at higher temperatures the relative stability of smaller structures is increased due to entropic effects.

3.2.6   The Gibbs Free Energy and Percent Abundance

The Gibbs free energy has already been defined in Equation 2.2, however now it is also dependent upon m and will therefore be written as $G(T, n, m)$. The free energy change, $G(T, n, m)$, for the reaction given in Equation 3.1 is plotted for the most stable structural alternatives in Figures 3.8a – 3.8d at 198.15K, 298.15K, 398.15K and 598.15K, respectively. At 298.15K there are only four reactions with negative $G(298.15K, n, m)$ values. They are for the addition of one and two TMA groups to $(AlOMe)_6$ and the addition of two TMA groups to $(AlOMe)_8$ and $(AlOMe)_{10}$. The fact that these values are quite small, coupled with the low abundance of the parent cages in 'pure' MAO (0.01%, 0.23% and 0.14% for $n = 6, 8, 10$) indicates that very little TMA is bound to MAO.

As the temperature increases and entropic effects become more important in destabilizing larger compounds, even fewer $G(T, n, m)$ values are negative. At 398.15K they occur when one and two TMA groups are added to $(AlOMe)_6$, while at 598.15K no negative values are found. However, at higher temperatures the equilibrium shifts towards smaller MAO cages. Thus, despite the fact there are few, if any, negative $G(T, n, m)$ values are present, since the parent cages have a higher percent abundance, more TMA will be bound to MAO. At lower temperatures the opposite occurs. That is, there are ten reactions with negative $G(198.15K, n, m)$ values, however, when only 'pure MAO' is taken into consideration the percent abundance of the parent cages is 0%, 0%, 0.01%, 0.18% and 0.01% for $n = 6, 7, 8, 9$ and 10 respectively. Thus, even in this case not much TMA will be bound to MAO.
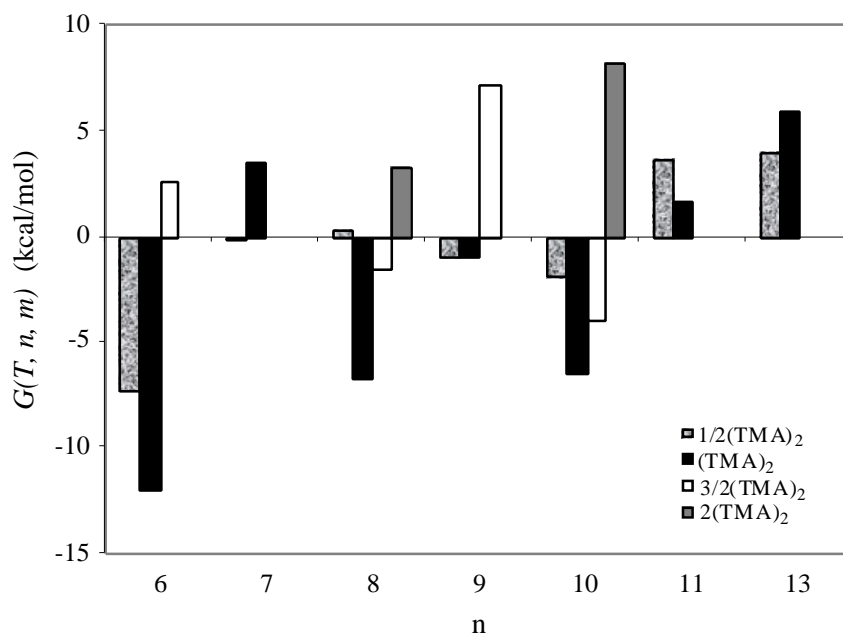
Figure 3.8a: $G(198.15K, n, m)$ for $(AlOMe)_n + \dfrac{m}{2}(TMA)_2 \rightarrow (AlOMe)_n \cdot (TMA)_m$
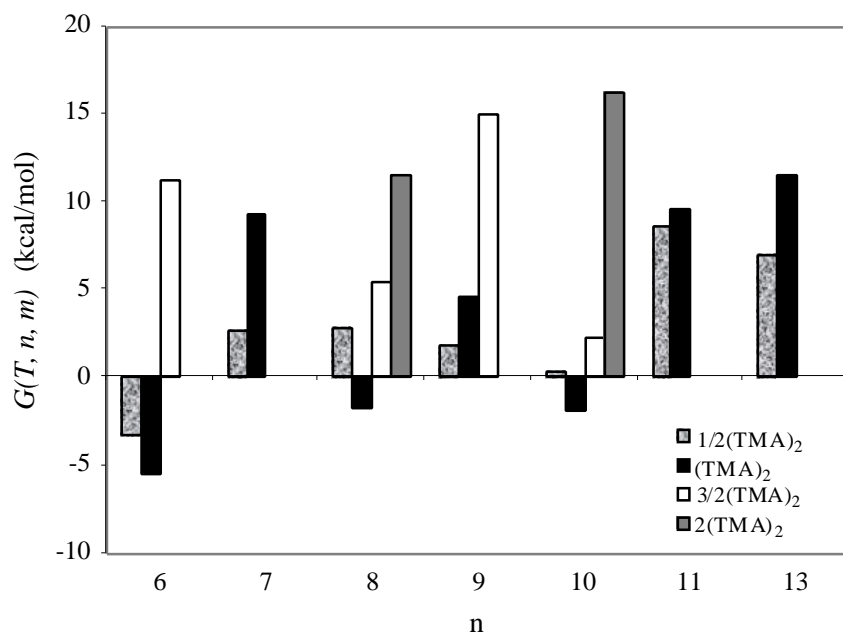
Figure 3.8b: $G(298.15K, n, m)$ for $(AlOMe)_n + \dfrac{m}{2}(TMA)_2 \rightarrow (AlOMe)_n \cdot (TMA)_m$
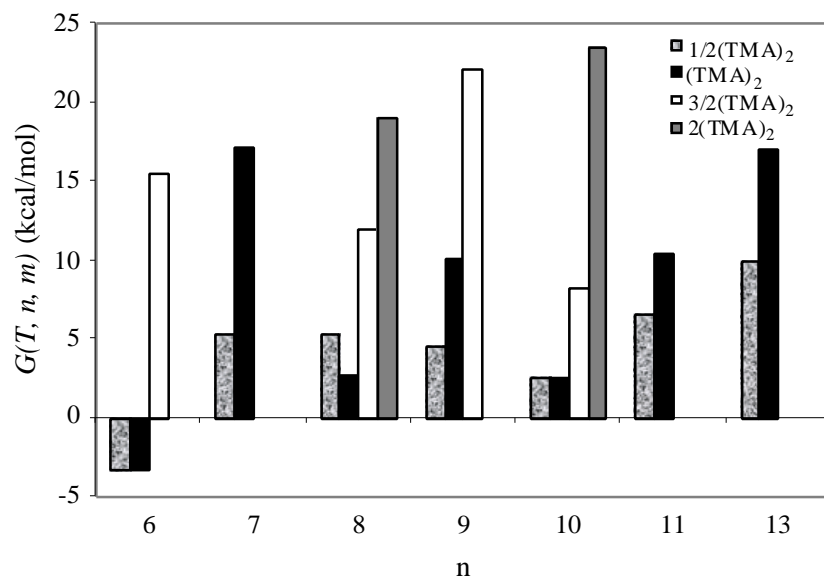
Figure 3.8c: $G(398.15K, n, m)$ for $(AlOMe)_n + \dfrac{m}{2}(TMA)_2 \rightleftharpoons (AlOMe)_n \cdot (TMA)_m$
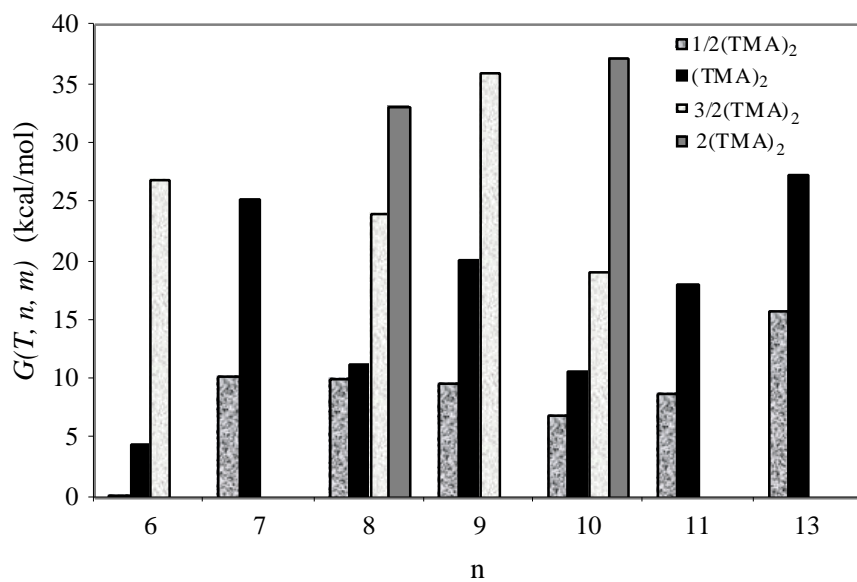
Figure 3.8d: $G(598.15K, n, m)$ for $(AlOMe)_n + \dfrac{m}{2}(TMA)_2 \rightleftharpoons (AlOMe)_n \cdot (TMA)_m$

The Gibbs free energy which one AlOMe monomer gains by binding with others and with TMA to form $(AlOMe)_n \cdot (TMA)_m$ is given by:

$$\frac{G(T,n,m)}{n} = \frac{G(T,n,m)}{n} - G(T,1,0) - \frac{m}{2n} G(T,0,2). \qquad [3.1]$$

The equilibrium constant for this process is given in Equation 3.2. The percent abundance of this species can be found by using 3.3.

$$K_{eq}(T,n,m) = \exp\frac{-G(T,n,m)}{RT} \qquad [3.2]$$

$$\%(AlOMe)_n \cdot (TMA)_m (T) = \frac{K_{eq}(T,n,m) \times [(TMA)_2]^{\frac{m}{2n}}}{\sum_{m} \sum_{n} K_{eq}(T,n,m) \times [(TMA)_2]^{\frac{m}{2n}}} \times 100\% \qquad [3.3]$$

The percent abundance of the possible $(AlOMe)_n \cdot (TMA)_m$ structures at 198.15K, 298.15K, 398.15K and 598.15K are given in Table 3.5, for 1 mol/L TMA. The numbers are a sum of the percentage of all possible isomers considered for a given n and m. Changing the TMA concentration has little effect on the overall Me/Al ratio. For small concentrations $[(TMA)_2]^{m/2n}$ approaches zero and the ratio goes to 1, while for concentrations within the range of 1 – 20 mol/L, $[(TMA)_2]^{m/2n}$ is approximately equal to 1. Even at concentrations of 100 mol/L, at 398.15K the Me/Al ratio is only 1.03. Increasing the concentration of TMA changes the percentages of individual components slightly but the overall Me/Al ratio remains virtually unchanged. Table 3.6 gives the Me/Al ratio as well as the percent of Al found as bound TMA of the total aluminum content in MAO (free TMA is neglected) at 1 mol/L TMA. The latter ratio is more sensitive to the change of TMA concentration than the former, for example, it increases to 1.33 at a TMA concentration of 20 mol/L at 398.15K.

Table 3.5: Percent Abundance of $(AlOMe)_n \cdot (TMA)_m$ at Different Temperatures (in Kelvin)

n	m	198.15	298.15	398.15	598.15	n	m	198.15	298.15	398.15	598.15
6	0	0.00	0.01	0.07	0.86	11	2	0.32	0.54	0.65	0.71
6	1	0.00	0.02	0.15	0.84	12	0	15.27	19.05	18.92	16.56
6	2	0.00	0.04	0.15	0.46	13	0	0.91	2.02	2.70	3.13
6	3	0.00	0.00	0.00	0.02	13	1	0.42	0.81	1.02	1.13
7	0	0.00	0.01	0.08	0.76	13	2	0.29	0.45	0.52	0.53
7	1	0.00	0.00	0.04	0.31	14	0	8.30	7.90	6.88	5.23
7	2	0.00	0.00	0.00	0.07	15	0	9.67	8.77	7.33	5.45
8	0	0.01	0.22	0.83	2.74	16	0	9.92	8.33	6.88	4.89
8	1	0.01	0.12	0.36	0.95	17	0	7.31	6.80	6.88	6.51
8	2	0.17	0.60	1.05	1.73	18	0	6.28	5.56	5.55	5.06
8	3	0.02	0.07	0.13	0.22	19	0	5.46	4.73	4.56	3.99
8	4	0.00	0.02	0.04	0.08	20	0	4.75	4.03	3.75	3.16
9	0	0.17	1.22	2.91	6.03	21	0	4.18	3.46	3.22	2.62
9	1	0.26	1.12	2.18	3.75	22	0	3.80	3.09	2.82	2.24
9	2	0.35	0.92	1.44	2.08	23	0	3.46	2.76	2.47	1.91
9	3	0.05	0.18	0.36	0.61	24	0	3.14	2.46	2.17	1.63
10	0	0.01	0.13	0.39	1.04	25	0	2.86	2.20	1.90	1.40
10	1	0.02	0.12	0.28	0.58	26	0	2.67	2.03	1.73	1.25
10	2	0.12	0.39	0.70	1.14	27	0	2.50	1.88	1.58	1.12
10	3	0.03	0.09	0.14	0.21	28	0	2.34	1.74	1.44	1.01
10	4	0.00	0.01	0.02	0.05	29	0	2.19	1.61	1.32	0.90
11	0	0.47	2.36	2.15	2.81	30	0	2.05	1.49	1.20	0.81
11	1	0.20	0.63	1.01	1.42						

Our results lead to the conclusion that very little TMA is bound to MAO within the temperature range of 198.15K - 598.15K. Most TMA exists as the free dimer in solution. Higher temperatures somewhat facilitate the binding of TMA to MAO, but only

very slightly. This is due to the fact that small MAO structures containing the greatest amount of acidic sites are more stable at higher temperatures due to entropic effects. The Me/Al ratio is ~1 at all temperatures and does not agree with experimental data which suggests a number near 1.5. We shall comment on this discrepancy in the next section.

Table 3.6: The Me/Al Ratio and Percent of Aluminum Found as Bound TMA for a Solution Containing 1 mol/L TMA

Temperature (K)	Me/Al	$Al_{TMA}/Al_{Total} \times 100\%$
198.15	1.00	0.21
298.15	1.01	0.62
398.15	1.02	1.05
598.15	1.03	1.76

3.2.7 Analysis of Theoretical and Experimental Results

We shall now discuss the possible sources of error in the experimental and theoretical procedures used to determine the bound TMA content in MAO.

Errors in the Calculations

We have calculated the free energy of dimerization for TMA as being G_d^0 = O.3kcal/mol at 298.15K. This value is larger than the experimental estimate[41] of -7.46 kcal/mol. We note that the deviation is larger than the standard error of ± 5 kcal/mol associated with DFT calculations. To determine if the discrepancy between theory and experiment is due to systematic errors in the calculated numbers we must find out how much the numbers must change for the Me/Al ratio to increase to 1.5.

Table 3.7 shows how changing G(298.15K, n, 2) for the reaction in Equation 1 would influence the Me/Al ratio. A negative number denotes a decrease in the calculated G(298.15K, n, 2); a positive number an increase. In light of the error present in the Gibbs free energy of dimerization, it is reasonable to assume that the G(298.15K, n, 2) values for the reaction shown in Equation 1 are good to within at least ± 10 kcal/mol . Table 3.7 shows that decreasing G(298.15K, n, m) by 10 kcal/mol for every dimer of

TMA present in the reaction raises the Me/Al ratio to 1.06 and increasing it by 10 kcal/mol lowers it to 1.00. In order to achieve the experimental ratio, $G(298.15K, n, m)$ would have to be decreased by 32 kcal/mol for each TMA dimer present in the reaction. It is highly unlikely that errors of this magnitude would be present in a DFT calculation. Note that in these calculations we assumed that MAO cages where $n = 12$ and n 14 would not react with TMA, that is that the $G(298.15K, n, 2)$ is not affected.

Table 3.7: The Effect of Changing $G(298.15K, n, 2)$ on the Me/Al Ratio

$G(298.15K, n, 2)$	Me/Al	$G(298.15K, n, 2)$	Me/Al
10	1.00	-20	1.27
-10	1.06	-25	1.39
-15	1.14	-30	1.47

Solvent Effects

MAO solutions are often made by the controlled hydrolysis of TMA in toluene or other hydrocarbon solvent and it can be quite difficult to remove all of the solvent from the MAO solution.[14d] Thus, we decided to examine if the inclusion of solvent effects had an impact on the calculated results. Solvent parameters for toluene were used. The inclusion of solvent effects for the reaction in Equation 3.1 for $n = 6$, $m = 1$, increased $E(6,1)$ by 0.76 kcal/mol in comparison to the gas phase value, showing that solvent effects are negligible.

Other Possible Bonding Modes

We have studied six possible bonding modes of a single molecule of TMA to a MAO cage. To our knowledge, there are no other reasonable ways in which this may be done. We have also studied one bonding mode of two TMA groups to a single MAO cage (structure **7**), showing that this is not a favorable alternative. Despite the fact that there may exist other ways in which one or more TMA groups can bind to a single MAO cage, it seems unlikely that these will be more stable alternatives to that shown in structure **2** (for example TMA trapped inside a MAO cage).

Analysis of Experimental Data and Techniques

Simeral and co-workers have developed a technique to determine the amount of bound and free TMA in a MAO solution using proton NMR.[14c] They found that the addition of tetrahydrofuran (THF) to MAO resulted in the signals attributed to TMA moving downfield due to the formation of a THF-TMA adduct. The signals attributed to MAO moved downfield only slightly and in such a manner the two peaks became nearly resolved. It was then possible to determine the amount of H atoms, and hence CH_3 groups, which belong to TMA and those to MAO. Total Al content was determined via wet chemical methods and ICP-AE (inductively coupled plasma atomic emission). Knowing the total Al, total TMA and the amount of Me present in MAO it was then possible to determine the Me/Al ratio when free TMA had been accounted for. They found this ratio to be 1.4-1.5.

The validity of this method relies on the assumption that THF does not facilitate the bonding of TMA to MAO. Figure **9** shows a number of possible reactions which could occur when THF is added to MAO along with the energy change for the reaction. Reaction **1** corresponds to the formation of an adduct between THF and free TMA. The energy change is -14.17 kcal/mol underlining that this does indeed occur. Reaction **2** has a E value of only -6.56 kcal/mol demonstrating that THF hardly binds to MAO. In reaction **3**, the O of the THF bonds to an Al on the MAO. Moreover, an Al from a free TMA group bonds to an O on the MAO. A strained square-square bond is broken in the process. This reaction has a E of -23.15 kcal/mol. This suggests that the THF facilitates the bonding of a TMA group to a MAO cage thereby inflating the Me/Al ratio. This result also shows us that the presence of basic impurities in the MAO mixture can increase the amount of TMA which is bound to the $(AlOMe)_n$ cages. Moreover, it may lead to the formation of a MAO solution with a smaller average *n* value.

1)

$1/2 \ (TMA)_2 \ +$ $\longrightarrow$

E = -14.17 kcal/mol

2)

 $+$ $\longrightarrow$

E = -6.56 kcal/mol

3)

 $+$ $+ \ 1/2 \ (TMA)_2 \longrightarrow$

E = -23.15 kcal/mol
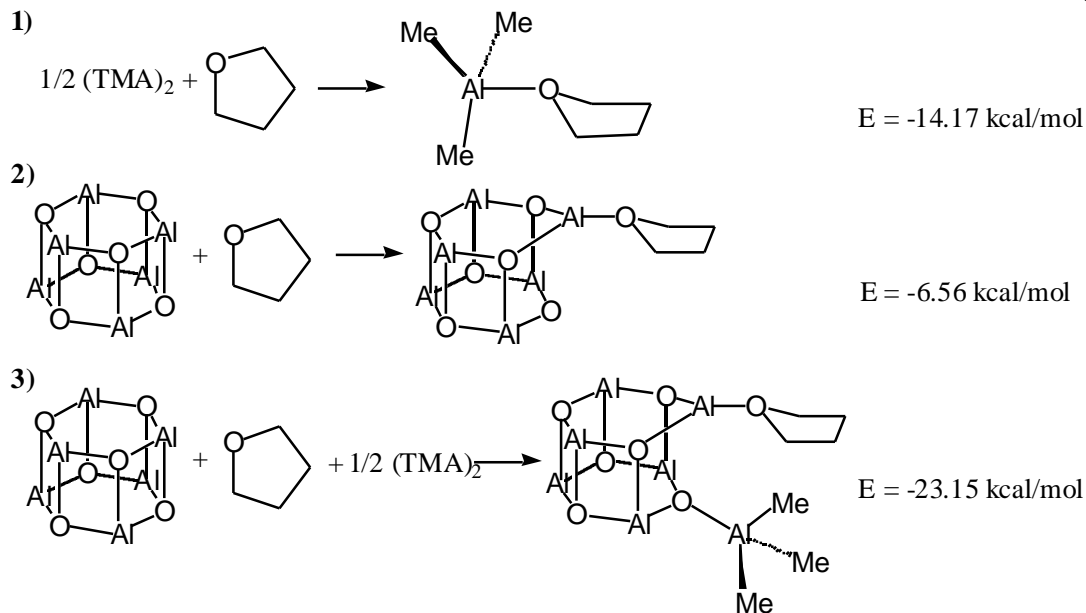
Figure 3.9: Possible Reactions in a Solution Containing (AlOMe)$_6$, TMA and THF

Decomposition of (AlOMe)$_n$

It has been shown experimentally that a MAO solution from which TMA has been removed develops more free TMA upon standing.[14b] This has been attributed to the equilibrium shown in Equation 3.1 shifting to the left. Our calculations show that there is very little TMA bound to MAO, thus we propose that (AlOMe)$_n$ undergoes a slow decomposition which results in the formation of aluminoxane and TMA dimer. This can be seen most clearly in Equation 3.4. Upon removal of TMA the equilibrium shifts to the right and more free TMA is observed.

$$(AlOMe)_n \qquad Al_{(n-2)}O_nMe_{(n-6)} + (TMA)_2 \qquad\qquad [3.4]$$

3.3 Conclusions

Within this chapter we have proposed a model for TMA containing, or 'real' MAO. Our results indicate that TMA binds to strained, acidic sites in MAO. An AlMe$_2$ group attaches to an O atom on the cage and a Me is transferred to an Al atom. The acidic sites for MAO cages where n ranges from 6 to 13 have been determined. With one

exception ($n = 9$), the most acidic sites consist of a bond made up of two square faces with O and Al atoms in (2S+H) environments.

According to our calculations, it has been found that very little TMA is actually bound to MAO within the temperature range of 198.15K - 598.15K. The addition of more than two TMA groups to a single MAO cage is energetically unfavorable due to increased steric hindrance of the ring-opened compound. Moreover, for $(AlOMe)_n$ where $n = 12$ or n 14, the addition of even one TMA group to the parent cage is endothermic since these cages do not contain strained, acidic sites. For 1 mol/L TMA, the Me/Al ratio has been calculated as being 1.00, 1.01, 1.02 and 1.03 and average unit formulae of $(AlOMe)_{18.08} \cdot (TMA)_{0.04}$, $(AlOMe)_{17.04} \cdot (TMA)_{0.11}$, $(AlOMe)_{15.72} \cdot (TMA)_{0.17}$ and $(AlOMe)_{14.62} \cdot (TMA)_{0.26}$ have been obtained for 198.15K, 298.15K, 398.15K and 598.15K. Somewhat more TMA is bound to MAO cages at higher temperatures due to the fact that smaller structures which contain acidic bonds are entropically more stable and are present in greater abundance.

Our results do not agree with experimental estimates of a Me/Al ratio of approximately 1.5. However, we have shown that one of the experimental procedures is likely to inflate the calculated Me/Al ratio. This result also indicates that the presence of basic impurities within the mixture ("dirty MAO") may have the effect of binding TMA to the MAO cages and furthermore lowering the average n value.

In conclusion, our findings suggest that the most stable and therefore most abundant 'pure' MAO species do not contain acidic sites. TMA binds to exactly these same sites, however the reaction is not exothermic enough to make the $(AlOMe)_n \cdot (TMA)_m$ cages more stable than the pure MAO cages without strained bonds. Thus, very little TMA is bound to MAO and most exists as the free species in solution.

Chapter 4

Towards the Identification of Active and Dormant Species in MAO-Activated, Cp$_2$ZrMe$_2$-Catalyzed Olefin Polymerization.

4.1 Introduction

In Chapter 3, we built upon our model for 'pure' MAO in order to put one forward for 'real' (TMA-containing) MAO. We found that 'real' MAO consists of three-dimensional cage structures with the general formula $(AlOMe)_n \cdot (TMA)_m$, where n ranges between 6~30 and m between 0~4, depending upon the topology of the parent cage. Most MAO structures contain very few strained, Lewis acidic bonds. For example, $(AlOMe)_{12}$, the species of greatest abundance at all temperatures, has no such sites. The average unit formula is about $(AlOMe)_{18.08} \cdot (TMA)_{0.04}$, $(AlOMe)_{17.04} \cdot (TMA)_{0.11}$, $(AlOMe)_{15.72} \cdot (TMA)_{0.17}$ and $(AlOMe)_{14.62} \cdot (TMA)_{0.26}$ at 198.15K, 298.15K, 398.15K and 598.15K, respectively. Since the reaction between TMA and MAO is minimal, increasing the concentration of TMA has very little effect on m. Most TMA is present as the free dimer and very little is actually bound to MAO. Having established a model for 'real' MAO, we will now try to determine the structures of the active and dormant species in olefin polymerization.

Within the last few years there have been several spectroscopic investigations on mixtures of MAO and Cp$_2$ZrMe$_2$.[11, 17, 18] Barron and co-workers examined the reaction of Cp$_2$ZrMe$_2$ with $[(^tBu)Al(\mu_3\text{-}O)]_n$ where n = 6, 7 and 9.[11] ^{1}H NMR spectroscopy was successfully used to characterize the species [Cp$_2$ZrMe][($^tBu)_6Al_6O_6Me$], shown in Figure
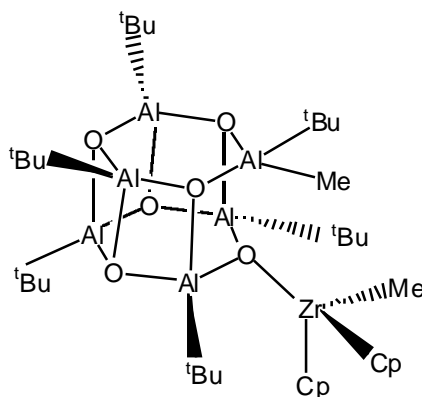
Figure 4.1: Structure[11] of [Cp$_2$ZrMe][($^tBu)_6Al_6O_6Me$]

4.1. Separate resonances for the two Cp ligands indicated that rotation about the Zr-O bond is slow on the NMR time scale. This was attributed to be the result of steric interactions between the Cp ligands and *t*-butyl groups or to an Al-Me ---Zr interaction.

Experimental evidence suggests that the catalytic species in polymerization is formed only when both MAO and TMA are present.[14d,16] For example, Barron's study on the polymerization of 1,5-hexadiene by $[Me_2C(Cp)(Flu)]ZrBz_2$ revealed that the activity of the alumoxanes adhered to the following trend: $[(^tBu)_6Al(\mu_3-O)]_6/(AlMe_3)_6 > MAO > [Al_7(\mu_3-O)_6(^tBu)_6Me_3] >> [(^tBu)_6Al(\mu_3-O)]_6$.[16] The first compound is thought to be a mixture of the two isomers of $[Al_7(\mu_3-O)_6(^tBu)_6Me_3]$ (see Figure 3.1) where all of the *t*-butyl substituents have been replaced with methyl groups. It has higher activity than $[Al_7(\mu_3-O)_6(^tBu)_6Me_3]$ due to decreased steric hindrance.

Tritto and co-workers have performed ^1H and ^{13}C NMR measurements on mixtures of MAO and Cp_2ZrMe_2 with different Al/Zr ratios[17a] and in the presence of ethylene.[17b] They have observed the formation of three complexes which have been identified as $[(Cp_2ZrMe)_2(\mu-Me)]^+[MeMAO]^-$ (**2**), $[Cp_2ZrMeAlMe_3]^+[MeMAO]^-$ (**3**), and $[Cp_2ZrMe]^+[MeMAO]^-$ (**4**), see Figure 4.2.[17a] Species **3** is observed only at Al/Zr ratios greater than or equal to 20. It is present in very small amounts, likely due to the fact that the removal of non-deuterated toluene also removes residual TMA. An increase in the Al/Zr ratio results in the broadening of Cp and Me signals for **3**, possibly indicating fluxional equilibria, such as methyl transfer.

Recently, Babushkin and co-workers have performed similar NMR investigations with Al/Zr ranging from 10-4000.[18] Several species which are present in a MAO, Cp_2ZrMe_2 solution at different Al/Zr ratios have been identified. Their structural assignments are given in Figure 4.2. Note that Tritto did not observe signals which correspond to the weak complex **1**. Babushkin found that **1**, **2** and **4** form at low Al/Zr ratios. As the ratio increases, **1** and **2** gradually disappear while the proportions of **3** and **4** increase. At high Al/Zr ratios the concentration ratio of **4**/**3** was found as being 1-4 depending upon the TMA content of the MAO solution.

The change in the ^1H NMR signals of the Cp rings as a function of zirconium concentration was monitored for **3**. It led to the conclusion that **3** exists in solution as the

contact ion-pair (**3a**) and the separated ion-pair (**3b**). The dissociation of **3** would form [Cp$_2$ZrMe]$^+$, which is the species capable of binding the olefinic substrate and hence the active species in polymerization.
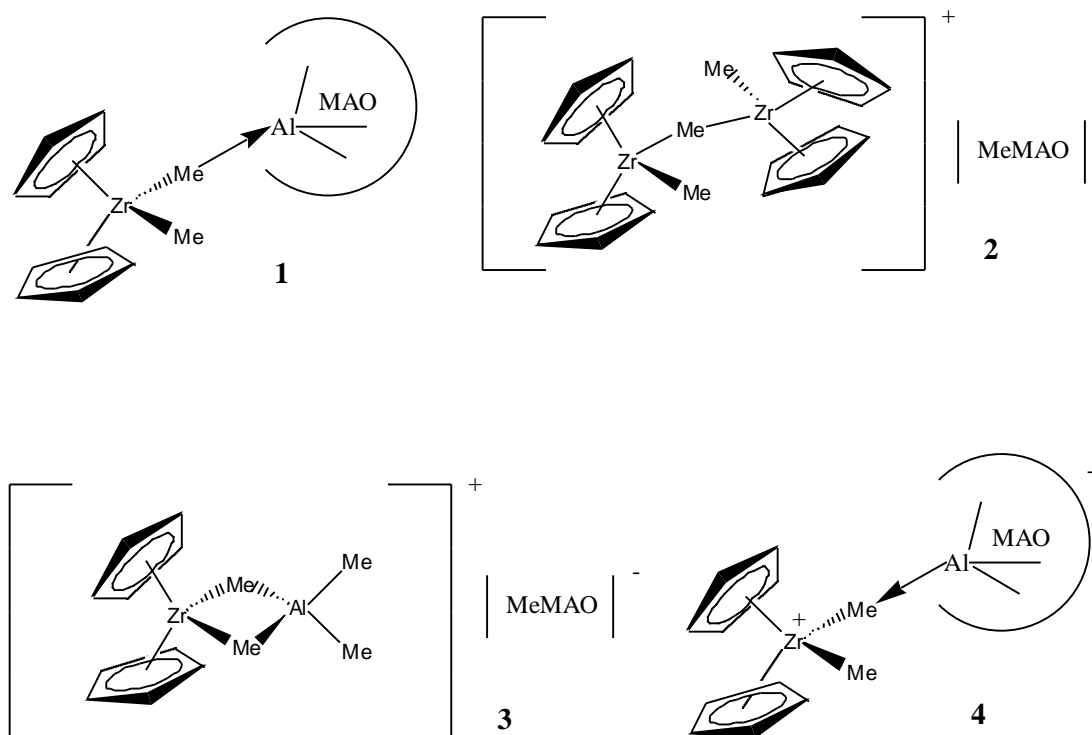
Figure 4.2: Proposed Species[18] Formed in a Mixture of MAO and Cp$_2$ZrMe$_2$

Species **4** is considered as being a "tight" ion-pair (unable to undergo dissociation) and hence the dormant state of the active site in olefin polymerization. Various groups have assumed this to be an oxygen bound complex similar to that shown in Figure 4.1[19, 20]. Babushkin and co-workers, however identify it as being a μ-Me bound species. They reach this conclusion from the observance of a μ-Me group in **4**, which was only detected when a MAO sample enriched with 70% ^{13}C was used. (We note that in a later paper, the same authors propose an oxygen bound structure for the dormant species.[22])

Within this chapter we will use our current knowledge of MAO, along with the clues provided by experimental NMR data to determine the most likely structures of **3** and **4**, the active and dormant species in olefin polymerization. In section 4.2.1 we shall discuss

the relative energies in gas-phase and in solution for possible structures for **3**. In section 4.2.2 we shall compare experimental and calculated NMR chemical shifts for the most stable structure. The relative energies of structural alternatives for **4** will be examined in section 4.2.3 and the NMR data in 4.2.4. Section 4.2.5 will look at the different ways in which **3** may be formed, along with the ion-pair formation and ion-pair dissociation energies for both **3** and **4**. In Section 4.2.6 we will examine how the Al/Zr ratio of a MAO/TMA/Cp$_2$ZrMe$_2$ mixture composed of the proposed structures influences the **4/3** ratio.

4.2 Results and Discussion

4.2.1   Structural Alternatives for 3 and their Relative Energies

Figure 3.4 shows the MAO cages with Lewis acidic bonds. These are the only species in MAO which can react with TMA and therefore with other bases. Hence, we will refer to them as the seven active forms of MAO. Experimentally[17a,18] it has been determined that **3** contains a MAO cage to which at least one TMA group is bound (see Figure 4.2). For reasons of computational expediency, we will model this by (AlOMe)$_6$•(TMA). We note that there is very little of this species present in a real MAO solution (~0.02% at 298.15K) and that more realistic choices would be (AlOMe)$_9$•(TMA) (~1.12%), or (AlOMe)$_9$•(TMA)$_2$ (~0.92%) or (AlOMe)$_{13}$•(TMA) (~0.81%). However, these species are still too large in order for us to be able to calculate their NMR chemical shifts using a reasonable amount of computational effort. Therefore we will model them via (AlOMe)$_6$•(TMA) and assume that they will undergo the same reaction with Cp$_2$ZrMe$_2$ and yield a similar NMR spectrum.

Five structural alternatives for the catalytically active species, **3**, are shown in Figure 4.3. In **A** a Lewis acidic site on the MAO has broken. A methyl group is transferred to an aluminum atom on the MAO cage and [TMACp$_2$ZrMe]$^+$ binds to the oxygen on the MAO cage. **A** has two bridging μ-Me groups between aluminum and zirconium, whereas **C** only has one. **B** is similar to **A** in the respect that it contains two bridging methyl groups. However, the oxygen--aluminum bond between [MAOMe]$^-$ and [TMACp$_2$ZrMe]$^+$ has broken forming the separated ion-pair. In **D**, the zirconocene is

bound via a methyl bridge directly to an aluminum atom on the MAO cage. **E** can be formed from the reaction of any of **A**-**D** with another $\frac{1}{2}$ (TMA)$_2$. Here two bridging μ-Me groups are present as well.
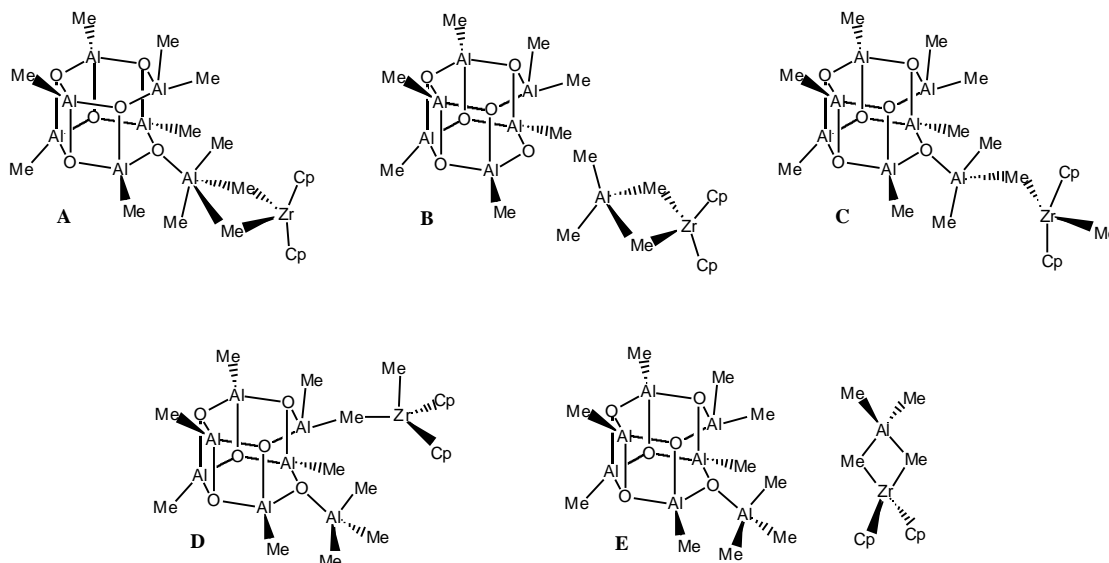
Figure 4.3: Possible Structural Alternatives for **3** (the 'Active' Species)

The NMR data of Babushkin and co-workers shows evidence for two bridging μ-Me groups, which would suggest that **A**, **B** or **E** are the likely candidates for **3**. However, **A** does not correspond to a minimum on the calculated potential energy surface and optimizes to give **C**. This is not surprising, since five-coordinate aluminum is rare. **C** is 46.80 kcal/mol *more stable* than **B** in gas phase. Solvation effects ought to stabilize **B** over **C** due to the fact that in the separated ion-pair the charges are more polarized. However, we still find in toluene that **C** is 30.90 kcal/mol *more stable* than **B**. The energy difference illustrates the fact that an Al–O bond is much stronger than a μ–Me-Al bond. **C** is 6.05 kcal/mol and 6.30 kcal/mol *more stable* than **D** in gas phase and toluene solution. *E* for the formation of **E** (from **C** and $\frac{1}{2}$ (TMA)$_2$) is 15.27 kcal/mol and 8.02 kcal/mol in gas phase and toluene solution, respectively. Our calculations show that **C** is energetically the most favorable structural alternative for **3**. Since free rotation about the

O-[AlMe$_3$Cp$_2$ZrMe$^+$] and μ−Me −[ZrCp$_2$Me$^+$] bonds can occur, different conformers of **C** may be found. We have optimized four possible structures whose energies differed by up to 2.52 kcal/mol (gas phase). This small energy difference indicates that a variety of different conformers will be present in solution.

Comparison of relative energies for the possible candidates for **3** suggests that **C**, with a single bridging methyl group is the predominant species among **A**, **B**, **C**, **D** and **E** in solution. The fact that **C** will be in greatest abundance among the candidates for **3** can be reconciled with the NMR observations of two μ−Me groups in **3** by considering the exchange mechanism shown in Figure 4.4. The Al-μ−Me$_I$ bond is broken; next the Al-μ−Me$_{II}$ bond is formed, following a possible rotation of the AlMe$_2$ group about the Al-O bond. In this scenario, the NMR signals should integrate to give two Me groups for which the chemical shift would be the average of one μ-Me and one Zr-Me.
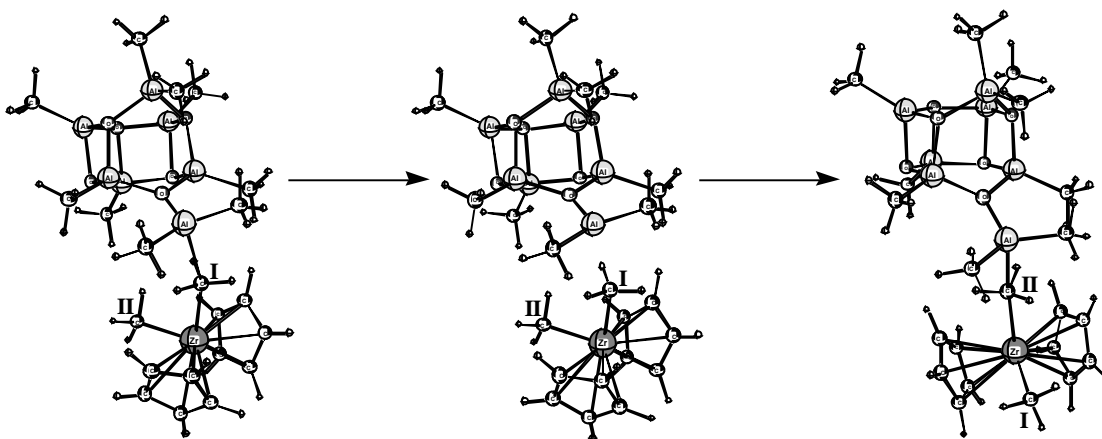
Figure 4.4: Exchange of two Methyl Groups in **C**

Two signals attributed to Al-Me ought to be present as well. Since the μ-Me bond is quite weak, it is likely that this exchange will occur quickly on the NMR time scale. The calculated bond strength is given by the ion-pair formation energy of **C** (from (AlOMe)$_6$•TMA and Cp$_2$ZrMe$_2$) and ranges between –3.18 to –5.70 kcal/mol (gas phase) to –3.68 to –5.00 kcal/mol (toluene), depending upon the conformer of **C** chosen.

4.2.2 NMR of Species 3

For all of the NMR calculations, TMS (trimethylsilane) was used as a reference. Due to the fact that chemical shifts are temperature and solvent dependent, we have tried to gauge the inherent error present in our calculations via comparison of the calculated and experimental ^{1}H and ^{13}C NMR spectrum of Cp$_2$ZrMe$_2$, shown in Table 4.1. In all cases the values are slightly overestimated by the computational methods employed. These values suggest that an error of approximately 3 ppm for ^{13}C shifts and 0.5 ppm for ^{1}H shifts is to be expected between the calculated and experimental spectra.

Table 4.1: Experimental and Calculated ^{1}H and ^{13}C Chemical Shifts for Cp$_2$ZrMe$_2$[b]

	exp[a]	calc	
^{13}C (Cp)	109.11	111.65	2.54
^{1}H (Cp)	5.64	6.12	0.48
^{13}C (Me)	29.26	32.47	3.21
^{1}H (Me)	-0.15	-0.08	0.07

[a]Reference 18. [b]Chemical Shifts in ppm.

Table 4.2: Experimental and Calculated ^{1}H and ^{13}C Chemical Shifts for (TMA)$_2$[b]

	exp[a]	calc	
μ-Me ^{13}C	-5.34	-5.80	-0.46
μ-Me ^{1}H	-0.005	0.53	0.53
terminal ^{13}C	-8.025	-9.46	-1.44
terminal ^{1}H	-0.535	-0.64	-0.10

[a]Reference 42. [b]Chemical Shifts in ppm.

We have also calculated the ^{1}H and ^{13}C NMR spectrum of the TMA dimer and compared it with experimental data that was taken at -78^{0}C in a solution of toluene-d_8.[42] Table 4.2 shows that we underestimate the ^{13}C shifts by up to 1.44 ppm. ^{1}H shifts differ from experiment by up to 0.53 ppm. The agreement is good, indicating that we should be

able to reproduce the chemical shifts of Al containing systems with bridging and terminal methyl groups.

Table 4.3 gives the experimental spectrum for **3** and the calculated one for a conformer of **C**. The last two rows show the average value of the calculated ^{1}H and ^{13}C chemical shifts of the Zr-Me and μ-Me groups. An averaging of these two values corresponds to the exchange of the two Me groups, as shown in Figure 4.4. The average ^{13}C chemical shift of 30.54 ppm differs by 7.53 ppm from the experimental shift of 38.07 ppm assigned to two μ-Me groups. This is somewhat higher than the expected error of about 3 ppm, however errors of this magnitude are not uncommon for calculated ^{13}C chemical shifts. The average of the shifts corresponding to the Zr-Me and μ-Me protons was found as being 0.24 ppm while an experimental shift of -0.27 ppm was observed for the μ-Me protons. This falls close to the expected error. The calculated (-1.21 ppm) and experimental (-6.00 ppm) ^{13}C shifts of the Al-Me groups differ by 4.79 ppm. The ^{1}H

Table 4.3: Experimental Chemical Shifts for **3** and Calculated Chemical Shifts for **C**, the Proposed Active Species[b]

	exp^{a}	Integration $_{\text{exp}}$[a]	calc	Integration $_{\text{calc}}$
^{13}C (Cp)	115.73	10C	113.60	10C
^{1}H (Cp)	5.5	10H	6.35	10H
^{13}C (Zr-Me)	-	-	41.7	1C
^{1}H (Zr-Me)	-	-	0.41	3H
^{13}C (μ-Me)	38.07	2C	19.38	1C
^{1}H (μ-Me)	-0.27	6H	0.07	3H
^{13}C (Al-Me)	-6.00	2C	-1.21	2C
^{1}H (Al-Me)	-0.58	6H	-0.47	6H
^{13}C $_{\text{average}}$*	N/A	N/A	30.54	2C
^{1}H $_{\text{average}}$*	N/A	N/A	0.24	6H

[a]Reference 18. * Corresponds to average chemical shift of Zr-Me and μ-Me for ^{13}C and ^{1}H

[b]Chemical Shifts in ppm.

shifts of Al-Me agree quite closely, with a calculated value of -0.47 ppm and an experimental one of -0.58 ppm. The calculated (113.60 ppm, 6.35 ppm) and experimental (115.73 ppm, 5.5 ppm) shifts corresponding to the Cp rings agree reasonably well.

Chemical shifts are known to be quite sensitive to changes in geometry. Hence, the different conformers of **C**, despite having similar energies, may have different chemical shifts. This may also explain the deviation between calculated and experimental values. Ideally, the shifts of all the conformers would be calculated and averaged, which is computationally not a feasible option. In general, correspondence between the shifts is very good, indicating that Species **3** might have the structure suggested in **C**.

4.2.3 Structural Alternatives for 4 and their Relative Energies

Three structural alternatives for **4** are shown in Figure 4.5. In **F** a methyl from Cp_2ZrMe_2 binds to an Al atom from the MAO thereby becoming a μ-Me group. This corresponds to the structure proposed by Babushkin and co-workers. In **G** a bridging methyl group is present as well, along with an oxygen bound zirconium. This is a structure similar to the intermediate formed when TMA reacts with MAO (see Figure 3.3). **H** is the oxygen bound, ring opened product, containing no μ-Me groups. Such an oxygen bound compound has been proposed as being the dormant state for the catalyst in olefin polymerization.[19,20]

Babushkin and co-workers have evidence for the presence of a bridging μ-Me group in **4**. However, this group was only observed when a sample enriched with 70% ^{13}C was used. Otherwise, the detection was impossible. This suggests that **H** cannot be the species seen. Yet, once again the relative energies of the different species must be taken into consideration.
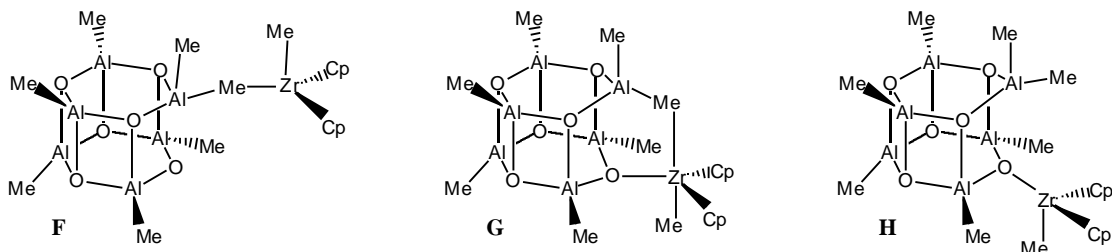
Figure 4.5: Possible Structural Alternatives for **4** (the 'Dormant' Species)

The first thing to note is that **G** is not a minimum on the calculated potential energy surface and when optimized gave **H**. When looking at the interaction of TMA and MAO, we optimized a similar structure, however the fully ring opened product was lower in energy by 5.27 kcal/mol. Perhaps, the steric bulk of the Cp rings prevents **G** from being a stable structural alternative.   he formation of **H** from $(AlOMe)_6$ and Cp_2ZrMe_2 was found to be exothermic by 16.58 kcal/mol (gas) and 16.12 kcal/mol (toluene). For **F**, these values are calculated as being -0.02 kcal/mol (gas) and 1.63 kcal/mol (toluene). This shows that **F** is a weakly bound species, and **H** is a tight ion-pair. From comparison of relative energies we can conclude that **H** is the most likely candidate for **4**.

4.2.4   NMR of Species 4

Table 4.4 shows the experimental ^1H and ^{13}C chemical shifts of **4** along with the calculated ones for **H**. For the Cp rings, the calculated shifts (115.78, 6.40) are slightly higher than the experimental values (113.90, 5.70). We also overestimate the ^{13}C shifts for Zr-Me by 4.77 ppm. The ^1H shifts of the Zr-Me protons were not detected, however we calculate them to be 0.38 ppm. The calculated NMR shifts for **H** are in good agreement with those obtained experimentally for **4**. However, **H** lacks the experimentally observed μ-Me group.

Table 4.4: Experimental Chemical Shifts for **4** and Calculated Chemical Shifts for **H**, the Proposed Dormant Species[b]

	exp^a	Integration $_{exp}{}^a$	calc	Integration $_{calc}$
^{13}C (Cp)	113.90	10C	115.78	10C
^1H (Cp)	5.70	10H	6.40	10H
^{13}C (Zr-Me)	42.00	1C	46.77	1C
^1H (Zr-Me)	-	-	0.38	3H
^{13}C (μ-Me)	9.00	1C	-	-
^1H (μ-Me)	-	-	-	-

[a]Reference 18. [b]Chemical Shifts in ppm.

It is possible that a structure similar to **G** is a minimum on the potential energy surface when one of the other active cages of MAO is considered. It would be less stable than the fully ring-opened product (as was the case for TMA reacting with MAO), and hence found in small abundance. This would explain the fact that the signal attributed to μ-Me was only observed when a sample enriched with 70% ^{13}C was used. We note that when Barron studied the *t*-butyl analogue of **H**, he observed two separate resonances for the protons in the Cp groups.[11] One explanation was the presence of an Al-Me ---Zr interaction which would also indicate the formation of a species similar to **G**.

Table 4.5: Experimental Chemical Shifts for **1** and Calculated Chemical Shifts for **F**, the Proposed Weakly Bound Species[b]

	$_{exp}$[a]	Integration $_{exp}$[a]	$_{calc}$	Integration $_{calc}$
^{13}C (Cp)	112.0	10C	115.83	10C
^{1}H (Cp)	5.7	10H	6.67	10H
^{13}C (Zr-Me)	29.5[c]	1C	42.33	1C
^{1}H (Zr-Me)	-	-	0.66	3H
^{13}C (μ-Me)	29.5[c]	1C	13.41	1C
^{1}H (μ-Me)	-	-	0.50	3H
^{13}C $_{average}$*	N/A	N/A	27.87	2C
^{1}H $_{average}$*	N/A	N/A	0.58	6H

[a]Reference 18. [b]Chemical Shifts in ppm. [c]Only one band with double intensity revealed

* Corresponds to the average chemical shift of Zr-Me and μ-Me for ^{13}C and ^{1}H

The NMR spectrum of **F** was also calculated and is compared with the observed spectrum for **1**, the weakly bound species, in Table 4.5. The last two rows give the average shift of Zr-Me and μ-Me, which corresponds to a rapid exchange of the two methyl groups. This is likely to occur due to the fact that **1** is a very weakly bound species. Experimentally one band with double intensity is seen at 29.5 ppm. This compares well to the average shift of 27.87 ppm. The calculated values (115.83, 6.67) of the Cp shifts somewhat overestimate ones obtained experimentally (112.0, 5.7).

Correspondence between the calculated and experimental shifts is very good, indicating that Species **1** might have the structure suggested in **F**.

4.2.5 The Formation/Dissociation of Species C

The ion-pair dissociation energy for **H** is 111.72 kcal/mol in gas phase and 62.60 kcal/mol in toluene solution. This underlines the Zr-O bond strength and supports the conjecture that this species is dormant during polymerization. Structure **C** can be formed in one of two ways, which are given in Equations 4.1 and 4.2 below**.** The E values for these reactions, in gas phase as well as in toluene solution can be found in Table 4.6. The process is also illustrated in Figure 4.6.

$$(AlOMe)_6 + \frac{1}{2}(TMA)_2 \quad (AlOMe)_6 \cdot (TMA) \qquad [4.1a]$$

$$(\mathbf{C}) \quad (AlOMe)_6 \cdot (TMA) + C p_2 ZrMe_2 \quad [TMA(AlOMe)_6 Me]^- [Cp_2 ZrMe]^+ \qquad [4.1b]$$

$$(\mathbf{H}) \quad (AlOMe)_6 + C p_2 ZrMe_2 \quad [(AlOMe)_6 Me]^- [Cp_2 ZrMe]^+ \qquad [4.2a]$$

$$(\mathbf{C}) \quad \begin{array}{l} [(AlOMe)_6 Me]^- [Cp_2 ZrMe]^+ + \frac{1}{2}(TMA)_2 \\[6pt] \qquad [TMA(AlOMe)_6 Me]^- [Cp_2 ZrMe]^+ \end{array} \qquad [4.2b]$$
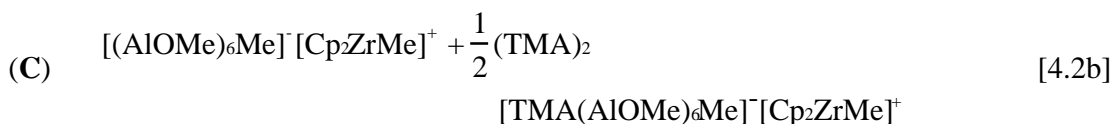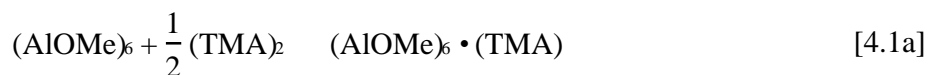
Table 4.6: E for Equations 4.1a, 4.1b, 4.2a and 4.2b[a]

Reaction	$E_{(gas\ phase)}$	$E_{(solv)}$
4.1a	-13.06	-12.32
4.1b	-3.82	-4.32
4.2a	-16.58	-16.12
4.2b	-0.30	-0.52

[a]All Energies given in kcal/mol

The ion-pair dissociation energy for **C** is 92.70 kcal/mol in gas phase and 48.39 kcal/mol in toluene solution. This is substantially lower than that of **H**, showing that this is a viable

candidate for the active species in polymerization. In the next chapter we will examine the olefin uptake and insertion mechanism in order to verify these conjectures.
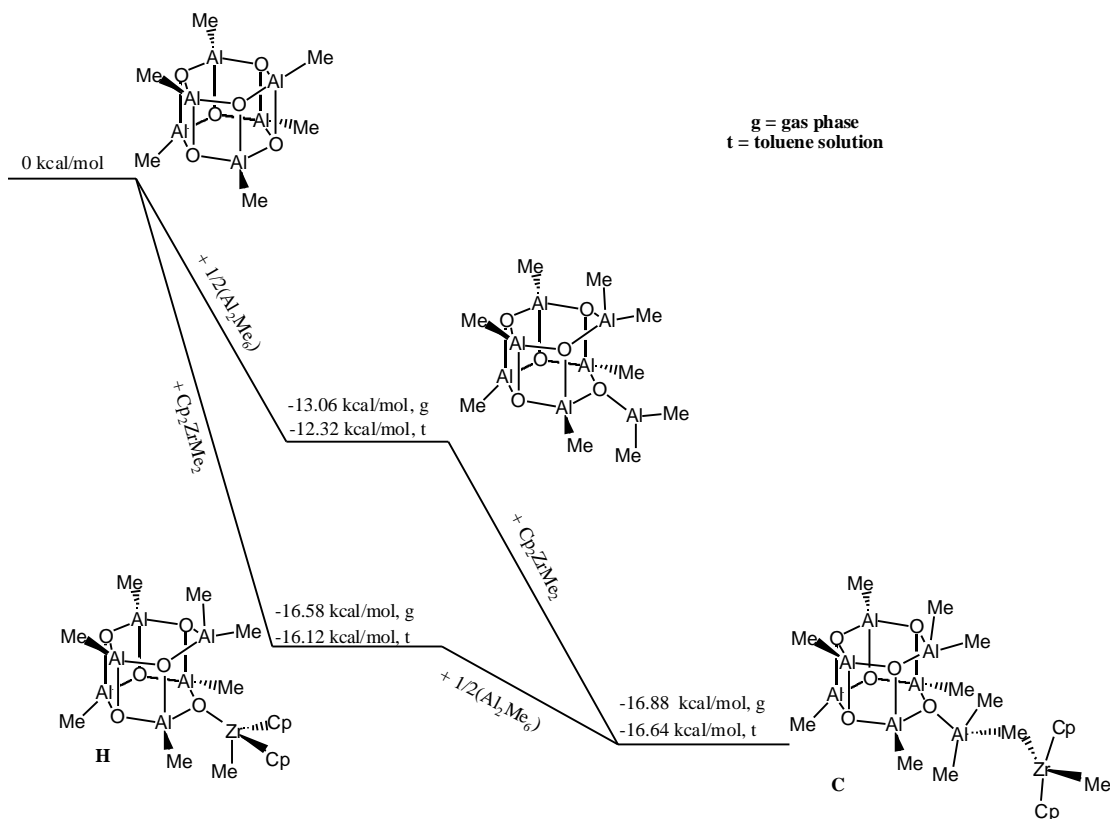
Figure 4.6: Energetic Relationships Between (AlOMe)$_6$, (AlOMe)$_6\bullet$(TMA), [Cp$_2$ZrMe]$^+$[(AlOMe)$_6$Me]$^-$ (**H**) and [Cp$_2$ZrMeAlMe$_3$]$^+$[(AlOMe)$_6$Me]$^-$ (**C**)

4.2.6 The MAO/TMA/Cp$_2$ZrMe$_2$ Mixture

The Gibbs free energy which one AlOMe monomer gains by binding with others, TMA and Cp$_2$ZrMe$_2$ to form (AlOMe)$_n\bullet$(TMA)$_m\bullet$(Cp$_2$ZrMe$_2$)$_p$ is given by

$$\frac{G(T,n,m,p)}{n} = \frac{G(T,n,m,p)}{n} - G(T,1,0,0) - \frac{m}{2n}G(T,0,2,0) + \frac{p}{n}G(T,0,0,1)$$

[4.3]

The equilibrium constant for this process is given in Equation 4.4 and the percent abundance of a given species by 4.5.

$$K_{eq}(T, n, m, p) = \exp\left[\frac{-\Delta G(T, n, m, p)}{RT}\right] \qquad [4.4]$$

$$\% (\text{AlOMe})_n \bullet (\text{TMA})_m \bullet (\text{Cp}_2\text{ZrMe}_2)_p \, (T) =$$

$$\frac{K_{eq}(T, n, m, p) \times [(\text{TMA})_2]^{\frac{m}{2n}} \times [\text{Cp}_2\text{ZrMe}_2]^{\frac{p}{n}}}{\sum\limits_{m \; n \; p} K_{eq}(T, n, m, p) \times [(\text{TMA})_2]^{\frac{m}{2n}} \times [\text{Cp}_2\text{ZrMe}_2]^{\frac{p}{n}}} \times 100\% \qquad [4.5]$$

In the second chapter on 'pure' MAO, we considered the case when $m = p = 0$ and were able to calculate the percent distribution of structures with the general formula $(\text{AlOMe})_n$; in the third chapter on 'real' MAO, we considered the case when $p = 0$ and were thus able to calculate the percent distribution of structures with the general formula $(\text{AlOMe})_n \bullet (\text{TMA})_m$. Here, we will use the thermodynamic gas phase data from our previous studies along with certain assumptions to examine how the equilibrium of a 'real MAO' mixture is affected in the presence of dimethylzirconocene.

We would like to consider a solution containing Cp_2ZrMe_2 bound to MAO cages in the same way as in **C** and **H**. The MAO cage may be any of the seven active forms of MAO, however the Zr from Cp_2ZrMe_2 must be bound to it either via a single μ-Me or an O atom at a Lewis acidic site. In order to examine this equilibrium, we need to know the values of $\Delta G(T, n, 0, p)$ and $\Delta G(T, n, m, p)$, for structures similar[a] to **H** and **C**. It is computationally not feasible to calculate all of these values, however we can use previously obtained data in order to estimate them. For $\Delta G(T, n, 0, p)$ we note that ΔE for the reaction given in Equation 4.1a is -13.06 kcal/mol while for the reaction given in 4.2a it is -16.68 kcal/mol. Since the change in energy for the two reactions differs only slightly, we will assume this will also be the case for the change in Gibbs Free Energies.

---

[a] By 'similar' we mean that $(\text{AlOMe})_6$ may be replaced by any of the seven active forms of MAO.

We will further assume that ΔG(298.15K, *n*, 1, 0) $\geq$ ΔG(298.15K, *n*, 0, 1) and will only consider the case when $p = 1$, thus only up to one Cp_2ZrMe_2 may be bound to an active MAO cage in a manner similar to **H**.

To estimate ΔG(*T*, *n*, *m*, *p*) we note that ΔE for the reaction shown in Equation 4.1b is -3.82 kcal/mol and predict that ΔG at 298.15K for this reaction will be 2 kcal/mol. We will further assume that ΔG(298.15K, *n*, *m*, 1) = ΔG(298.15K, *n*, *m*, 0) + 2 kcal/mol. Again we will only consider the case when $p = 1$, that is up to one Cp_2ZrMe_2 may be bound to an active MAO cage in a manner similar to **C**, irrespective of how many TMA groups are present. It is highly unlikely that species with $p \geq 2$ would be present in any significant amount due to steric and entropic effects. No other species will be considered in the equilibrium.

A mixture composed of only these species with 1 mol/L TMA and 1 mol/L Cp_2ZrMe_2 at 298.15K would give a ratio of structures similar to **H** to those similar to **C** of 1.76. Experimentally, it was found that at high Al/Zr ratios the molar ratio of **4**/**3** varied between 1 - 4, depending upon the TMA content of the solution and that signals due to species other than **3** and **4** were absent.[18] Thus, the calculated value of 1.76 for the ratio of species similar to **H** to species similar to **C** falls within the experimental range. For this situation we calculate the Al/Zr ratio as being 177:1.

Let us we consider a solution of 0.009M Cp_2ZrMe_2 and 0.5M TMA, with about 30% of the total Al content being due to free TMA. This yields an Al/Zr ratio of 275:1, implying that ratios of approximately this magnitude are necessary in order to guarantee that all of the Cp_2ZrMe_2 is bound to MAO in a manner similar to **H** and **C**. The ratio of structures similar to **H** to those similar to **C** would then increase slightly to 1.83. In Babushkin's study this corresponds to the disappearance of NMR signals due **1**, **2** and free Cp_2ZrMe_2. Weak signals corresponding to **1** and **2** are still seen at Al/Zr = 100, however the ratio at which they disappear is not given.[18]

4.3 Conclusions

Within this chapter we have examined several structural candidates for the active and dormant species found in a $MAO/TMA/Cp_2ZrMe_2$ mixture via comparison of relative

energies in gas phase and toluene solution as well as calculated and experimental ^{1}H and ^{13}C NMR chemical shifts.

The NMR data for species **3** showed evidence for two bridging methyl groups. We found that such a species was either not stable (**A**) or of higher energy (**B**, **E**) than a structure containing one Zr-Me and a single μ-Me (**C**). However the μ-Me bond is very weak (~4 kcal/mol) making it possible for the Zr-Me and μ-Me groups to undergo exchange. If this process (Figure 4.4) is fast on the NMR time scale, the resulting spectrum would integrate to give two Me groups whose chemical shift would be the average of the one μ-Me and one Zr-Me. The calculated NMR spectrum of **C** agreed well with the experimental spectrum for **3** if the average of the two shifts was taken. The presence of conformers with very similar energies could explain the deviation between calculated and experimental chemical shift values. The ion-pair dissociation energy for **C** of 48.39 kcal/mol in toluene, indicates that this is a viable candidate for the active species in polymerization. **D** was found to be 6.30 kcal/mol higher in energy than **C** and very little of it should be found in the reaction mixture.

The NMR data for species **4** showed evidence for one μ-Me group. However, when such a structure was considered it was either unstable (**G**) or much higher in energy (**F**) than the oxygen-bound species with no μ-Me groups (**H**) present. The calculated NMR data for **H** agreed well with experiment, with the exception of the lacking μ-Me group. Yet, it is possible that a structure similar to **G** is a minimum on the potential energy surface when other MAO cages are considered. This structure would be higher in energy than **H** and therefore very few such μ-Me groups would be present at any given time, resulting in a weak signal. In order to see this signal experimentally, it was necessary to use a sample enriched with 70% ^{13}C. The ion-pair dissociation energy for **H** was calculated to be 62.60 kcal/mol in toluene. This high value shows that this is a likely candidate for the dormant species in polymerization. NMR calculations on the μ-Me bridged species **F** gave close agreement with what is seen experimentally for Species **1**, a weak complex between MAO and the pre-catalyst.

The model which we have proposed for MAO implies that high Al/Zr ratios, ~275:1, are necessary in order to bind all of the Cp_2ZrMe_2 to MAO as species **3** and **4** at 298.15K.

Experimentally, the disappearance of signals due to **1** and **2** is observed at Al/Zr ratios of over 100. The reason for this phenomenon is that there are very few acidic sites in MAO. Thus, the concentration of MAO must be much higher than that of catalyst in order to push the equilibrium to the right in the reactions shown in Equations 4.1a and 4.2a and therefore in 4.1b and 4.2b, where $(AlOMe)_6$ is replaced by any of the seven active forms of MAO.

The calculated ratios of 1.76 and 1.83 for structures similar to **H** to those similar to **C** correlate with the experimental observation that at high Al/Zr ratios the ratio of **4/3** varied between 1–4, depending on the TMA content. Structures similar to **H** should be more prevalent than structures similar to **C** since very little TMA is actually bound to MAO and since the Al-μ-Me bond in structures similar to **C** is quite weak.

In conclusion, the model which we propose explains why such a high ratio of Al/Zr is necessary in order for polymerization to occur. Most MAO oligomers do not contain Lewis acidic sites to which TMA may bind, implying that a low percentage of $(AlOMe)_n \bullet (TMA)_m$ species is present. Furthermore, the binding between the pre-catalyst and $(AlOMe)_n \bullet (TMA)_m$ is quite weak, implying a very low abundance of the active species. Thus, the Al/Zr ratio must be very large in order for the active species to be present in any significant amount. *In short, the feature which makes a MAO cage less stable is the same that makes it catalytically active.*

Chapter 5

A Theoretical Study of the Olefin Insertion Mechanism in MAO-Activated, Cp$_2$ZrMe$_2$-Catalyzed Ethylene Polymerization

5.1 Introduction

In Chapter 4 we built upon our model for 'real' MAO in order to identify the structures of the dormant and active species present in Cp$_2$ZrMe$_2$-catalyzed olefin polymerization. The energies of possible structural alternatives for the [Cp$_2$ZrMe]$^+$[AlMe$_3$MeMAO]$^-$ and [Cp$_2$ZrMe]$^+$[MeMAO]$^-$ ion-pairs, where MAO was modeled by (AlOMe)$_6$, were calculated and compared. The structures with the lowest energies are shown in Figure 5.1. Next, we calculated the ^{1}H and ^{13}C NMR chemical shifts of **1** and **2**, showing they matched those observed experimentally[18] for the active and dormant species in olefin polymerization. Based upon these results we proposed that the active and dormant species have the structures given in **1** and **2**, respectively, where (AlOMe)$_6$ is a model for any of the seven active forms of MAO (shown in Figure 3.4). In this chapter we aim to give further evidence for the assignment of **1** and **2**. We also (finally) complete our initial objective: to study the mechanism of olefin polymerization with MAO as the activator.
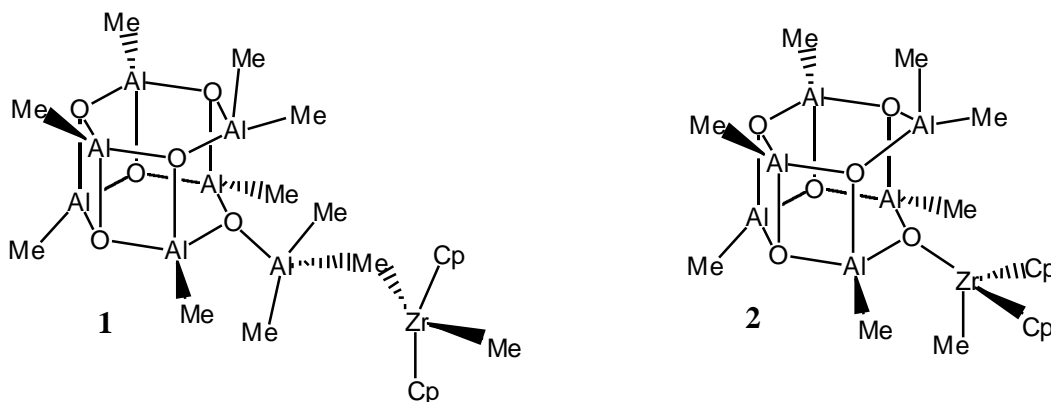

Figure 5.1: The Model Active (**1**) and Dormant (**2**) Species in MAO-Activated, Cp$_2$ZrMe$_2$-Catalyzed Olefin Polymerization

The reaction mechanism for olefin insertion is generally accepted to be the Cossée-Arlman mechanism[2], shown in Figure 1.1. It assumes that the ion-pairs undergo total dissociation, and only considers the naked cationic species. Many computational studies have been performed using this mechanism as a starting point, neglecting the influence of the anion. We will only mention a few involving the catalyst Cp_2ZrMe^+.[3]

In recent years increasing computational resources have made it possible to investigate the role of the activator. For example, ion-pair formation and separation energies have been calculated[4a,b,c,d] and dormant product formation has been examined.[4e] However, studies of the insertion mechanism are still quite limited due to the large computational cost. Lanza et al.[5a] have examined ethylene insertion into the contact ion-pair $[H_2Si(C_5H_4)(^tBuN)Ti(CH_3)]^+[CH_3B(C_6F_5)_3]^-$. Fusco et al.[5b] have studied olefin separated ion-pairs (OSIP) for the system $[Cp_2(Ti/Zr)CH_3]^+[Cl_2Al[O(AlMe_3)AlHMe]_2]^-$, where $[MeAl[O(AlMe_3)AlHMe]_2]$ was used to model MAO. Bernardi et al.[5c] have investigated the reaction of $H_2Al(\mu-Cl)_2TiCl_2CH_3$ with ethylene. Chan et al.[5d] have examined OSIP for different catalysts and the counter-ion $B(C_6F_5)_3^-$, along with ethylene insertion[5e] into the Zr-C bond of $Cp_2ZrEt-\mu-CH_3- B(C_6F_5)_3$. Nifant'ev et al[5f] have performed studies of ethylene insertion into the Zr-C bonds of the $[Cp_2ZrEt]^+[B(C_6F_5)_3CH_3]^-$ and $[Cp_2ZrEt]^+[B(C_6F_5)_4]^-$ ion-pairs. Also, computational and experimental mechanistic studies[5g] on the displacement of $[B(C_6F_5)_3CH_3]^-$ from zirconocene cations by neutral systems, including olefins, have been performed. These studies suggest that total dissociation between cation and anion does not occur, and thus the insertion mechanism must be modified. Further evidence is given by the discrepancy between experimental activation energies and those calculated for the naked cationic species.[3g]

In this investigation we consider a dissociative and an associative mechanism shown in Figures 5.2 and 5.3, respectively. Our investigation shall be limited to the two ion-pairs $[AlMe_3MeMAO]^-[Cp_2ZrR]^+$ and $[MeMAO]^-[Cp_2ZrMe]^+$ with R = methyl, propyl. In both mechanisms, the cation and anion dissociate during the approach of the olefin to the cation, resulting in the formation of a dissociated -complex. The degree of dissociation is dependent upon the nature of the cation, anion and solvent. Next, the ethylene

72

approaches the metal-alkyl bond leading to the formation of a four-membered cyclic insertion transition state. In the dissociative mechanism (Figure 5.2), the transition state occurs when the cation and anion are still separated and the Zr is four-coordinate. In the associative mechanism (Figure 5.3), the μ-methyl bond is only slightly elongated at the transition state and the Zr is five-coordinate. The two modes of approach of the ethylene are *trans* or *cis* to the μ-methyl bridge. The former is shown in Figure 5.2 and the latter in Figure 5.3. The tetrahedral arrangement of the contact ion-pair becomes trigonal bipyramidal during olefin uptake. In the *trans* case the ethylene is in an axial position while in the *cis* case it is found in the equatorial plane.

Separated Species   Uptake Transition State   -complex   Insertion Transition State

R = Me, Prop
A⁻ = anion
olefin
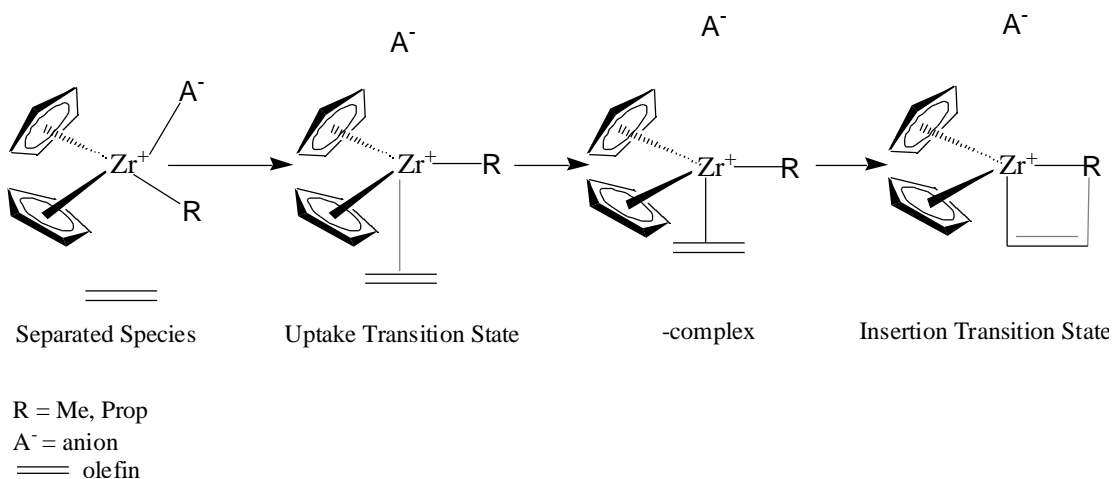
Figure 5.2: The Dissociative Mechanism; *Trans* Approach

Separated Species   Uptake Transition State   -complex   Insertion Transition State

R = Me, Prop
A⁻ = anion
olefin
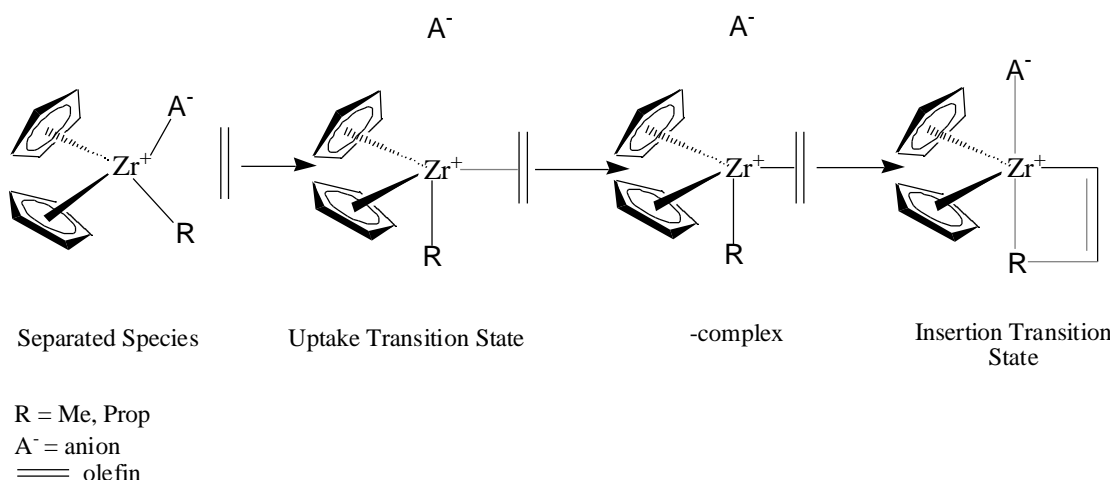
Figure 5.3: The Associative Mechanism; *Cis* Approach

In Section 5.2.1 we look at the -complexes and transition states for the first insertion into the Zr-Me bond of **2**. In Section 5.2.2 we examine the first insertion into the Zr-Me bond of **1**, comparing it to that of the naked cation. In 5.2.3 we look at the second insertion into the Zr-propyl bond of the proposed active species.

5.2 Results and Discussion

5.2.1   Further Evidence for the Assignment of 'Dormant' Species

Within this section we will examine the -complexes and insertion transition states for the first insertion into the Zr-Me bond of **2**. The reaction of $[Cp_2ZrMe]^+[Me(AlOMe)_6]^-$ with C_2H_4 to form $[Cp_2ZrProp]^+[Me(AlOMe)_6]^-$ is exothermic by 19.87 and 18.55 kcal/mol in gas phase and toluene solution.

In Figure 5.4 we show the optimized structures for the first insertion, dissociative mechanism; in Table 5.1 we give the energies of the different species relative to free ethylene and $[Cp_2ZrMe]^+[Me(AlOMe)_6]^-$ in gas phase as well as toluene solution. The Zr-O distance provides a measure for the degree of dissociation of the anion (in **2**, the Zr-O bond is 2.212 Å). We were unable to locate any associated transition states for either mode of approach.

Table 5.1: Energies of -complexes and Insertion Barriers for the Proposed Dormant Species[a]

	Cis, (-complex)	Cis (TS)	Trans, (-complex)	Trans (TS)
Structure Label	3a	3a†	3b	3b†
E_{gas}	31.88	38.80	34.65	35.37
$E_{toluene}$	28.43	35.55	26.96	29.26

[a]All Energies given in kcal/mol

Figure 5.4: π-complexes and Insertion Transition States with the Proposed Dormant Species

In the *cis* (**3a**, **3a†**) and *trans* (**3b**, **3b†**) π-complexes and transition states a large degree of dissociation has occurred between the cation and anion. In both cases, the Zr-O
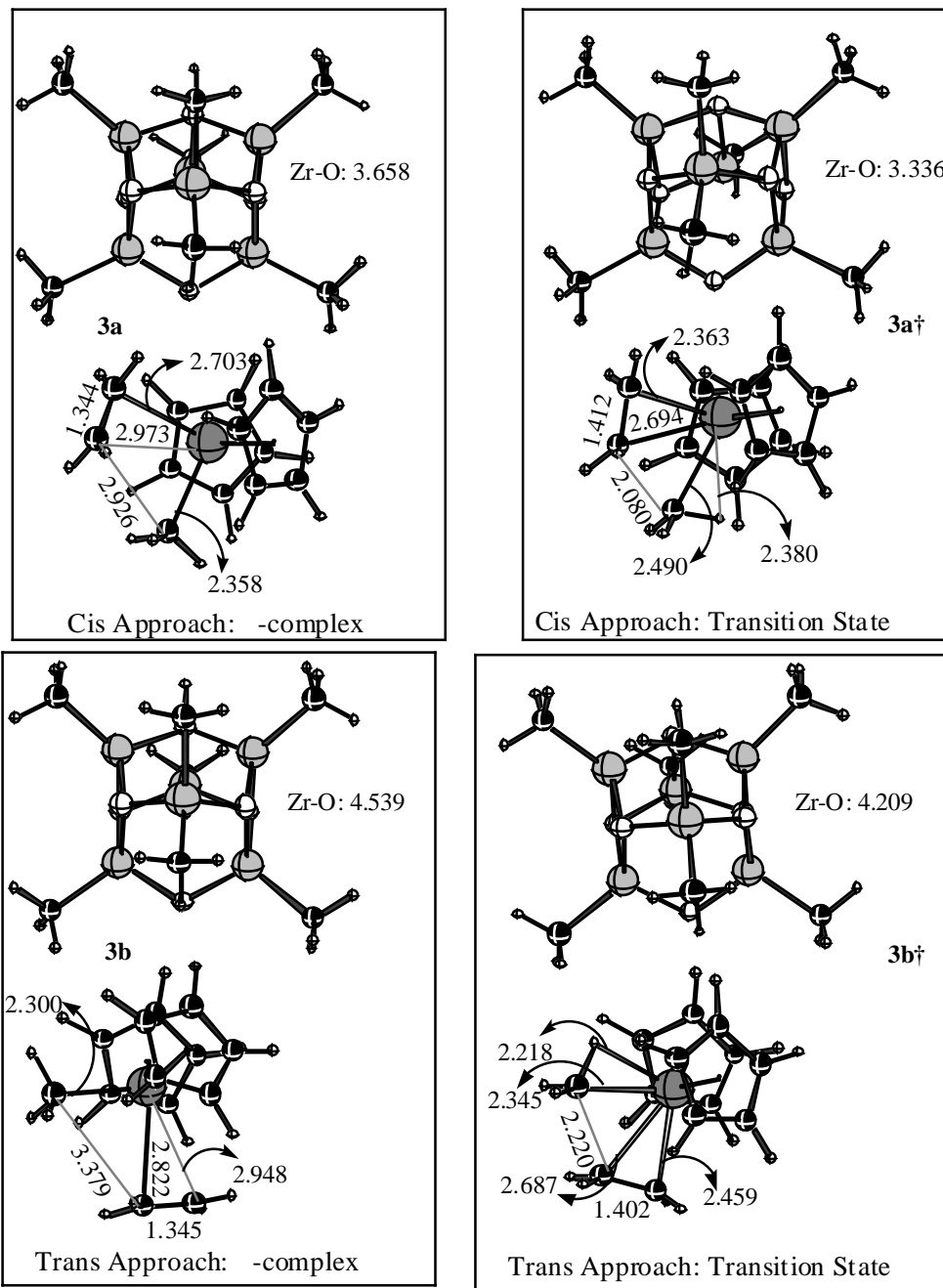
distance of the -complex is greater than that of the insertion transition state. The large charge separation causes the inclusion of solvation effects to lower the energies of the structures by an average amount of ~5 kcal/mol. **3b** and **3b**† are 1.47 kcal/mol and 6.29 kcal/mol lower in energy than **3a** and **3a**†, showing that the *trans* approach is more favorable. In the *trans* approach, the ethylene is competing for the same metal orbital as the anion, hence the displacement between cation and anion must be greater in order for the ethylene to bind. This is evident in the longer Zr-O distance for both **3b** and **3b**†. The insertion barriers of 29.26 and 35.55 kcal/mol are too high in order for the ion-pair to be active in olefin polymerization. In view of this, we did not attempt to calculate the uptake barriers nor do we present the data for the second insertion, dissociative mechanism. (Which gives further confirmation that an oxygen-bound species is dormant, yielding insertion barriers of ~25 kcal/mol.)

5.2.2 First Insertion of Ethylene with the Model Active Species

Within this section we will examine the mechanism for the first insertion, using **1** as the model active species. As was mentioned in Chapter 4, free rotation about the O-[$AlMe_3Cp_2ZrMe^+$] and μ−Me −[$ZrCp_2Me^+$] bonds lead to many possible conformers of **1**. We have optimized four possible structures and show the conformer of lowest energy in Figure 5.5. It is worthwhile to note that the orientation of the Cp rings (we will refer to it as out of the plane of the page) minimizes steric interactions with the MAO cage and that the μ-Me—Zr bond is 2.417 Å long. We have started all of our calculations based upon geometries where the Cp rings have been out of plane, as shown in **5**. In the *trans* case there is only one possible mode of approach of the olefin to the metal center, whereas for the *cis* case there are two, one from above and one from below the cation.

The structures and energies of the optimized -complexes and transition states for the first insertion are given in Figure 5.6 and Table 5.2. The -complexes were found without any geometrical constraints and the transition states using the $C_{ethylene}$-C distance as the reaction coordinate. For comparison, we have also provided the results for the naked cation.
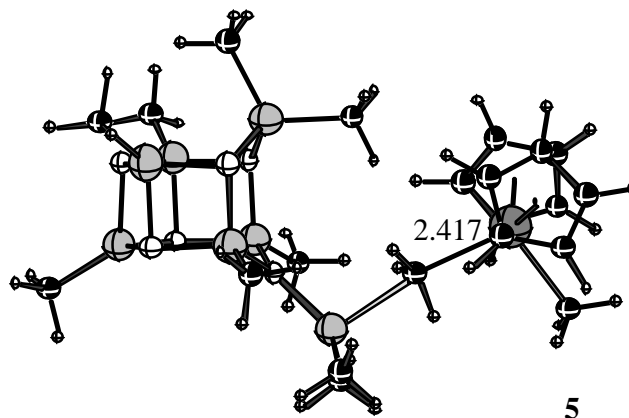
Figure 5.5: Lowest Energy Conformer of [Cp$_2$ZrMe]$^+$[AlMe$_3$Me(AlOMe)$_6$]$^-$
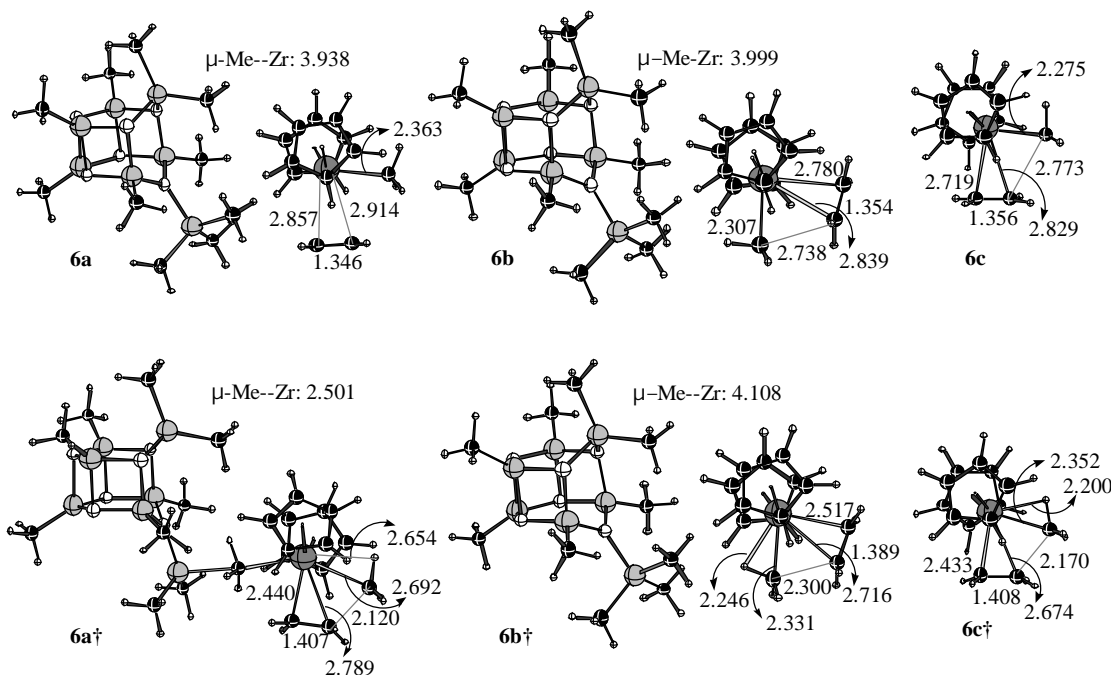
Figure 5.6: -complexes and Insertion Transition States with the Proposed Active

Species

For the *cis* approach we only show the transition state obtained when the olefin approached from below the cation. When the olefin approached from above, the Cp rings rotated into the plane, giving a transition state similar in geometry to **6a†** but 2.04

kcal/mol higher in energy (gas phase). We have not tried to optimize the geometry of a -complex with any other orientation than that shown.

The *cis* -complex (**6a**) has a large ion-pair separation: the μ-Me—Zr bond has elongated by 1.620 Å. The olefin-metal interactions are weaker than for the naked cation, or for the *trans* approach. This can be seen by the somewhat larger $C_{ethylene}$-Zr and the somewhat smaller $C_{ethylene}$- $C_{ethylene}$ distances found in **6a** as compared with **6b** or **6c**.

Using the aforementioned reaction coordinate, we have only been able to find an associative transition state, **6a†**. In going from **1** to **6a†** the μ-Me—Zr bond changed by only 0.084 Å while the Me-Zr bond elongated by 0.374 Å. The incoming olefin donates electron density to the metal center, weakening the interactions of the Zr with the other species found in the equatorial plane. Since the anion-cation interaction is stronger than that of the Me-Zr, the latter bond undergoes a greater amount of elongation. The increased length of the Me-Zr bond results in the absence of any agostic interactions: the H -Zr distance is 2.654 Å. The structural similarities between **6a†** and **6c†,** the insertion transition state for the free cation, include the C -$C_{ethylene}$ distance and the length of the complexed olefin. For the free cation, the Zr-Me bond is stronger, and an -agostic interaction is present.

The insertion barrier of 18.51 and 19.04 kcal/mol (gas phase and toluene) is somewhat higher than experimental estimates for the activation energy of propagation, which was determined as being (14.6 ± 1) kcal/mol on the basis of corrected reaction rates.[3g] However, it is known that the barrier to the first insertion is higher than for subsequent insertions. In this system the inclusion of solvation increases the insertion barrier by 0.53 kcal/mol. This can be explained by examining how the charge on the anion, *x* for $[AlMe_3Me(AlOMe)_6]^x$, changes during the insertion. Due to the fact that the metal is bound to both the olefin and anion at the transition state, it must back donate electron density to the anion in order to accept it from the olefin. Thus, the charge on the anion changes from -0.536 to -0.485 in going from **1** to **6a†**. Since the charge difference is smaller at the transition state, we expect inclusion of solvation effects to somewhat increase the insertion barrier.

We will use the term internal barrier to mean the energy difference between the insertion transition state and the -complex. The gas-phase internal barrier of 1.66 kcal/mol is similar to that for the naked cation, 1.57 kcal/mol. When solvation is taken into account the internal barrier changes drastically to 6.05 kcal/mol, since solvation stabilizes the dissociated -complex and destabilizes the associated transition state. For the naked cation the barrier changes to 1.90 kcal/mol in toluene solution.

Table 5.2: Energies of -complexes and Insertion Barriers for the Proposed Active Species, First Insertion[a]

	Cis, (-complex)	Cis, (TS)	Trans, (-complex)	Trans, (TS)	Cation, (-complex)	Cation, (TS)
Structure Label	6a	6a†	6b	6b†	6c	6c†
E_{gas}	16.85	18.51	22.61	23.75	-16.47	-14.90
$E_{toluene}$	12.99	19.04	16.90	17.68	-13.07	-11.17

[a]All Energies given in kcal/mol

The -complex for the *trans* approach, **6b,** is geometrically similar to that for the free cation, **6c**. However, in this case we find the energy of complexation as being endothermic by 22.61 and 16.90 kcal/mol in gas phase and toluene solution. In going from the ion-pair to the -complex a large degree of dissociation has occurred: the μ-Me—Zr bond is elongated by 1.582 Å. For this mode of approach, we could only find a dissociative transition state shown in **6b†**. In going from **1**, the μ-Me—Zr bond has elongated by 1.691 Å while the Me-Zr bond has changed by 0.013 Å resulting in an -agostic bond measuring 2.246 Å. The C -Zr and H -Zr distances are similar to those of **6c†**. The cation approaches the anion (by a very small amount, 0.109 Å) during insertion. The internal barrier of 0.78 kcal/mol is slightly smaller than that of the naked cation. The charge on the anion at the transition state, -0.836, arises from the large separation between anion and cation. In this case solvation lowers the insertion barrier from 23.75 to 17.68 kcal/mol.

In gas phase, the *cis* approach has a lower insertion barrier, however in toluene the *trans* approach is preferable. It is likely that different solvents will influence the ratio of *trans* to *cis* insertions, with more polar solvents favoring a *trans* approach. The reaction of $[Cp_2ZrMe]^+[AlMe_3Me(AlOMe)_6]^-$ with C_2H_4 to form $[Cp_2ZrProp]^+[AlMe_3Me(AlOMe)_6]^-$ was found to be exothermic by 18.75 and 17.16 kcal/mol in gas phase and toluene solution.

Ion-Pair Recombination

A large degree of ion-pair dissociation is found for **6b†**. After the olefin has inserted into the μ-Me—Zr bond it is feasible that $[AlMe_3Me(AlOMe)_6]^-$ and $[Cp_2ZrProp]^+$ may remain dissociated as subsequent insertions occur. In this case, it would not be necessary to overcome the energy barrier needed to form the separated ion-pair. Another possibility is that the μ-Me—Zr bond reforms after each insertion. In this case, energy would be given off as the cation and anion associate, however it would also be necessary to overcome this same energy barrier for the polymer chain to grow. In order to determine if the cation and anion remain dissociated, we performed a constraint-free geometry optimization, using **6b†** for our starting structure. During the optimization, the μ-Me—Zr bond reformed, indicating that ion-pair association occurs between subsequent insertions.

5.2.3 Second Insertion of Ethylene with the Model Active Species
The Resting State

Within this section we will examine the mechanism for the second insertion, using **1** as the model active species. We will assume that the preferred conformation of $Cp_2ZrProp^+$ relative to $[AlMe_3Me(AlOMe)_6]^-$ is the same as shown in **5**. In order to minimize steric interactions with the Cp rings, the propyl chain may point either away from, or towards the anion as shown in Figure 7. The energy difference between the two possibilities is minimal: **7a** is lower in energy than **7b** by 0.08 kcal/mol (gas phase) and 0.06 kcal/mol (toluene). We have not calculated the rotation barrier of the propyl chain,

but expect it to be small. The μ-Me—Zr distances are also almost identical: 2.437 Å for **7a** versus 2.442 Å for **7b**.

μ-Me--Zr: 2.437   **7a**   μ-Me--Zr: 2.442   **7b**
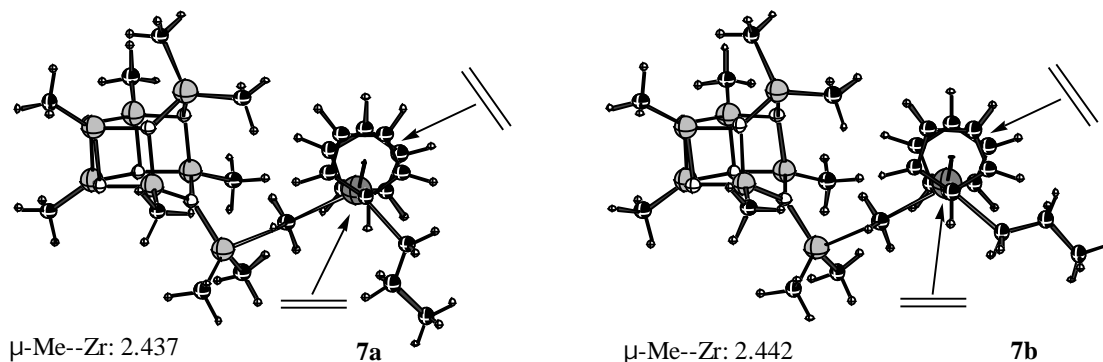
Figure 5.7: Resting States of the $[Cp_2ZrMe]^+$ $[AlMe_3Prop(AlOMe)_6]^-$ Ion-Pair

The olefin may approach either *cis* or *trans* to the μ-Me—Zr bond, and the resulting -complexes may conceivably have no agostic, -agostic or -agostic interactions leading to a total of twelve possible -complexes to consider.

π-*Complexes with No Agostic Interactions*

We have optimized the geometries of four possible -complexes with no agostic interactions. They are shown in Figure 5.8, and their energies relative to **7a** and free ethylene are given in Table 5.3. The hydrogen atoms on C can be either facing towards (front approach: **8a**, **8c**) or away from (back approach: **8b**, **8d**) the incoming olefin.

Table 5.3: Energies of -complexes without Agostic Interactions

Structure Label	E_{gas}	$E_{toluene}$
8a	17.08	12.41
8b	22.03	17.21
8c	22.10	14.17
8d	22.86	14.11

[a]All Energies given in kcal/mol

μ-Me--Zr: 4.169

2.970

3.195

1.344

2.946

8a

μ-Me--Zr: 4.344

3.622

3.121

1.345   2.780

8b

μ-Me--Zr: 4.532

2.890

1.348

2.838

3.391

8c

μ-Me--Zr: 4.391

2.989

1.344

2.847

4.053

8d
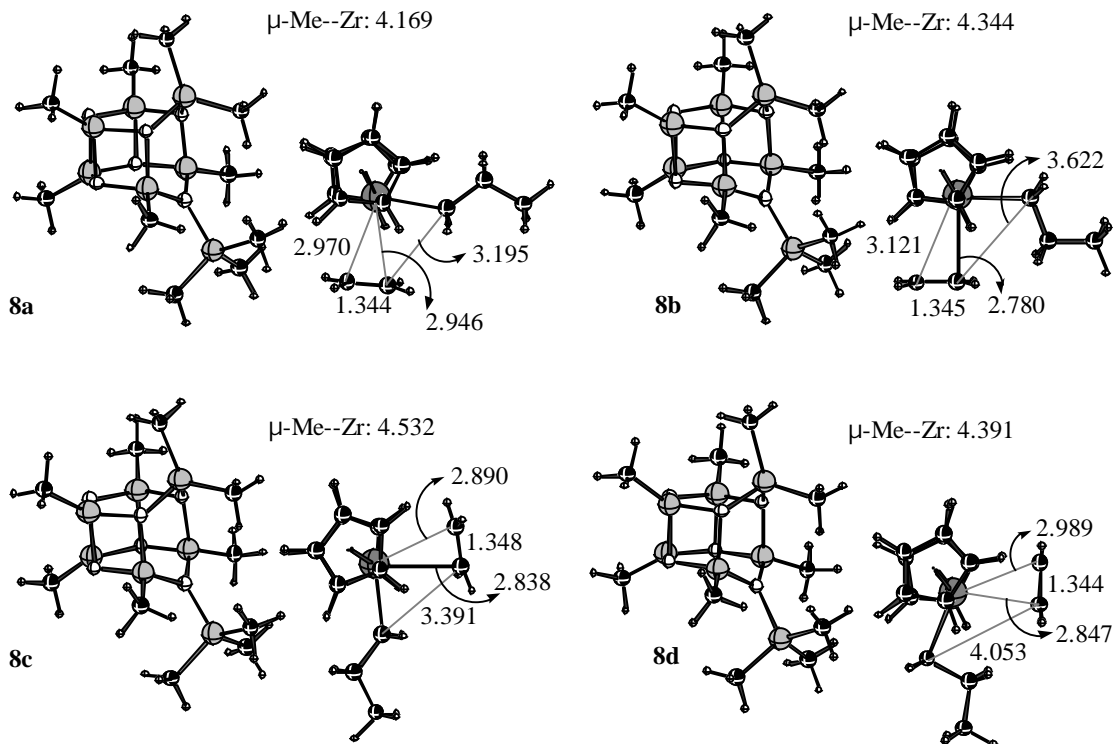
Figure 5.8: Geometries of -complexes without Agostic interactions

In order for insertion to occur from a front -complex, the propyl chain must first of all rotate about the C , resulting in the formation of a back -complex.

In all of the cases, the ion-pairs have undergone a large degree of dissociation in forming the olefin complex. The elongation of the μ-Me—Zr bond is greater for the *trans* approach due to the fact that the olefin is competing for the same metal orbital as the anion. As expected, inclusion of solvation becomes increasingly important the larger the charge separation. The energies of all of these species is quite high implying that they are unlikely to be global minima on the calculated potential energy surface and hence that they are probably not real olefin complexes.

π-*Complexes with* α-*Agostic Interactions*

The optimized geometries of four possible -complexes with -agostic interactions are shown in Figure 5.9, and their energies relative to **7a** and ethylene are

given in Table 5.4. Again, the ion-pair separation is quite large for all of the species, but somewhat smaller than in the case of **8a**-**8d**. The -agostic interactions are seen to be stabilizing resulting in energies somewhat lower than for **8a**-**8d**, implying that these species may be real olefin complexes. In **9b** the C -Zr and $C_{ethylene}$-Zr bonds are somewhat

Table 5.4: Energies of -complexes with -Agostic Interactions

Structure Label	E_{gas}	$E_{toluene}$
9a	18.96	13.29
9b	15.03	12.18
9c	20.38	12.30
9d	18.44	11.62

[a]All Energies given in kcal/mol

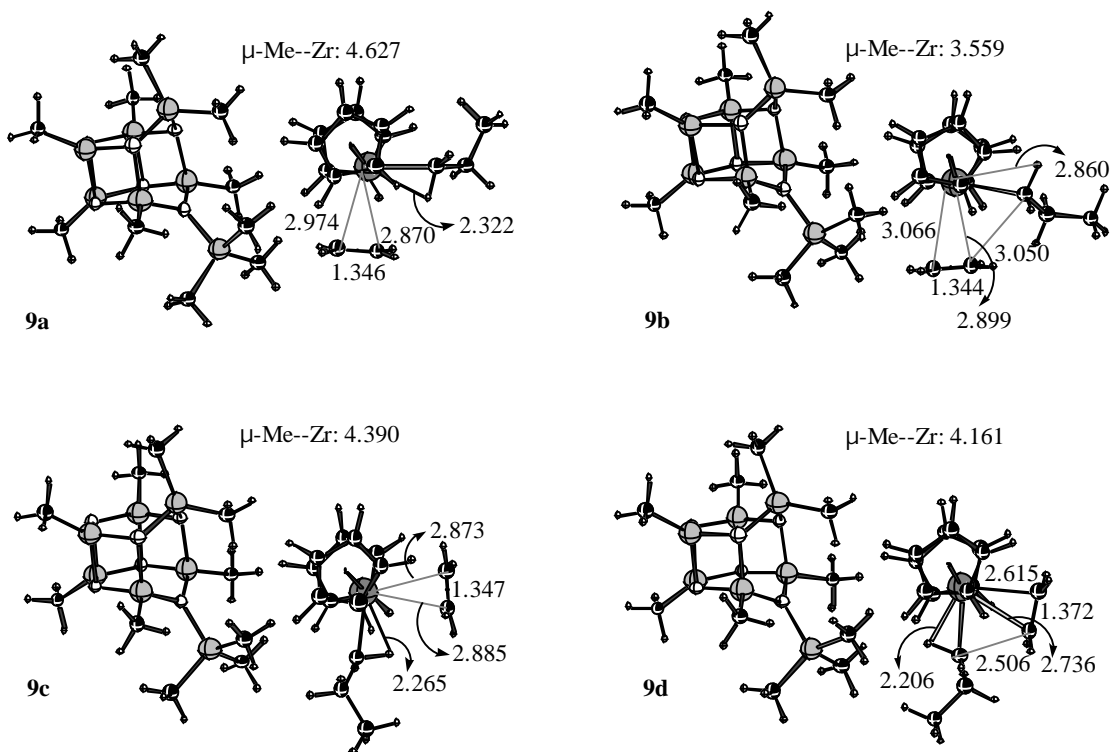**Figure 5.9:** Geometries of -complexes with -Agostic interactions

longer than expected due to the comparatively small μ-Me—Zr. The short $C_{ethylene}$-Zr bond and long $C_{ethylene}$-$C_{ethylene}$ bond of **9d** are reminiscent of a structure somewhere in between that of a -complex and an insertion transition state. We will comment on this later in more detail, showing that **9d** is not a real -complex.

π-*Complexes with* β-*Agostic Interactions*

The optimized geometries of four possible -complexes with -agostic interactions are shown in Figure 5.10, and their energies relative to **7a** and ethylene are listed in Table 5.5. The ion-pairs have undergone a large degree of dissociation in forming the olefin complex; in fact the μ-Me—Zr bond is even larger than for **8a**-**8d** or **9a**-**9d**. The amount of dissociation is greater for the *cis* than the *trans* approach, in contrast with the trend noted previously. The strong -agostic bond is now competing for the same metal orbital as the anion when the olefin is oriented *cis* to the μ-Me bond. The olefin is more strongly bound to the metal center in the back approach, as can be seen by the shorter $C_{ethylene}$-Zr bond lengths. Also, the back approach yields somewhat more stable complexes as compared to the front approach. These four structures are substantially lower in energy than those with no agositc or -agostic interactions indicating that they are the most likely alternatives for -complexes.

Table 5.5: Energies of -complexes with -Agostic Interactions

Structure Label	E_{gas}	$E_{toluene}$
10a	14.96	7.66
10b	14.63	7.23
10c	17.26	8.85
10d	14.03	7.06

[a]All Energies given in kcal/mol
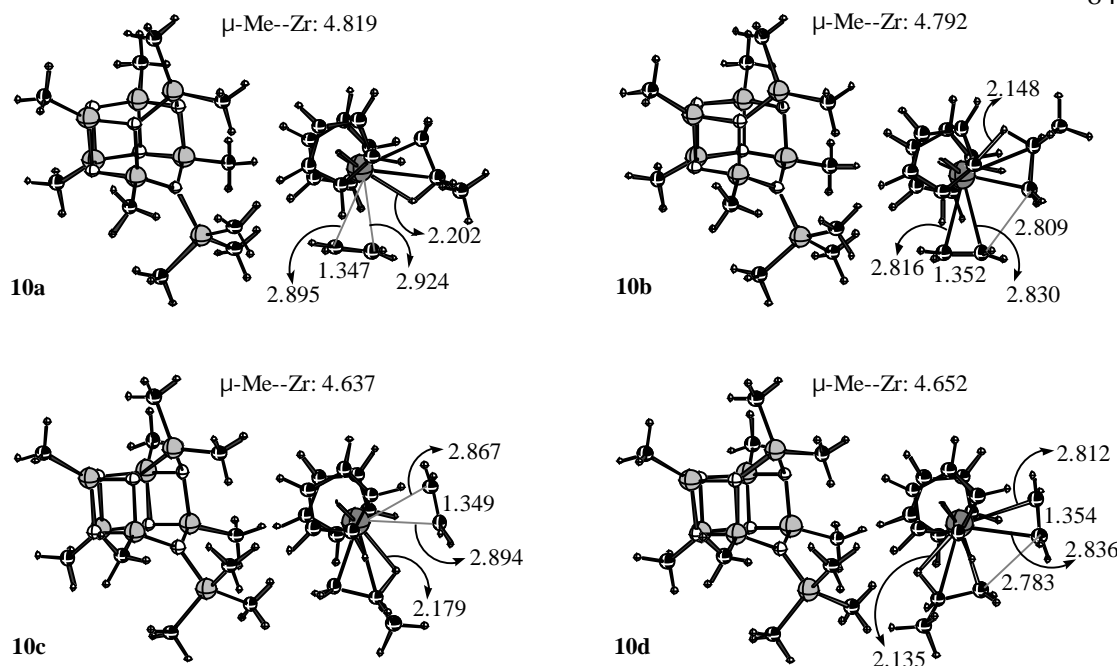
Figure 5.10: Geometries of -complexes with -Agostic interactions

Associated Transition States

We were able to locate one associated transition state for each of the *cis* and *trans* modes of approach. The geometries of these structures and their energies, with respect to **7a** and ethylene are shown in Figure 11. A comparison of **7a** and **11a**† shows that in the latter, the μ-Me—Zr and C -Zr bonds are longer by 0.066Å and 0.383Å. For **11b**†, these numbers change slightly to 0.080Å and 0.435Å. There are no agostic bonds present in either transition state due to the lengthening of the C -Zr bond.

Inclusion of solvation increases the insertion barrier by 1.86 and 1.82 kcal/mol for the *cis* and *trans* approaches. The charge on the anion decreases slightly from -0.527 for the ion-pair to -0.478 and -0.496 for **11a**† and **11b**†. As in the *cis* attack for the first insertion, since there is little change in the μ-Me—Zr bond distance, the metal must back donate electron density to the anion in order to accept it from the olefin. Thus, inclusion of solvation somewhat increases the insertion barrier.

 The calculated barrier for the associated transition state where the olefin is oriented *trans* to the bridging methyl group is too high in order for this to be a viable mechanism. The *cis* barrier is somewhat lower and not unreasonable, indicating that this

is a possible insertion transition state. However, in the next section we will show that dissociated transition states have an even lower barrier, ruling out the possibility of an associated mechanism.

E$_{(gas)}$ = 15.65 kcal/mol
E$_{(toluene)}$= 16.18 kcal/mol

E$_{(gas)}$ = 21.55 kcal/mol
E$_{(toluene)}$= 22.04 kcal/mol

11a†

11b†
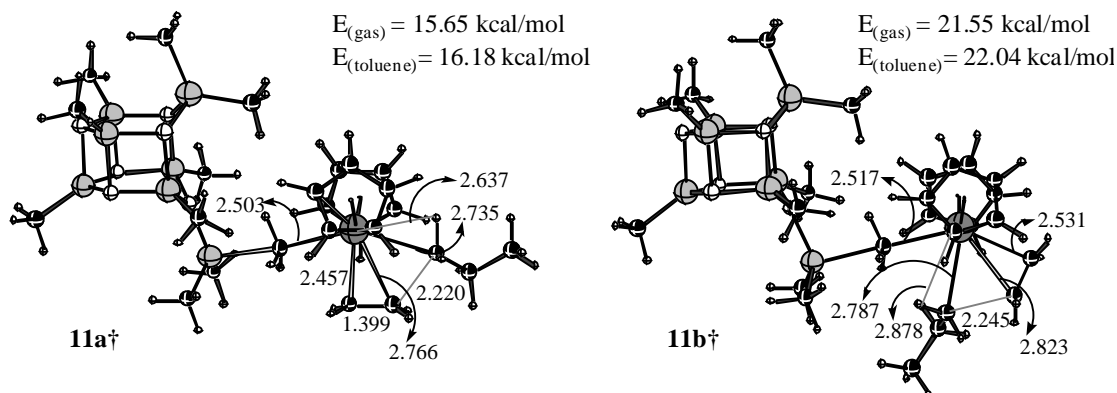
Figure 5.11: Transition States for the Second Insertion, Associated Mechanism

Dissociated Transition States: α*-agostic Interactions*

The insertion transition state for the *cis* attack and its energy relative to **7a** and ethylene is shown in Figure 5.12. In going from the -complex, **9b** to **12†**, the cation-anion distance increases by 0.530 Å. The internal barrier for the process is small, 0.65 kcal/mol (toluene), giving a total barrier of 12.83 kcal/mol. This barrier is substantially smaller than for **11†**, showing that a dissociated transition state is more likely to occur.

E$_{(gas)}$ = 19.31 kcal/mol
E$_{(toluene)}$= 12.83 kcal/mol

μ-Me--Zr: 4.089

12†
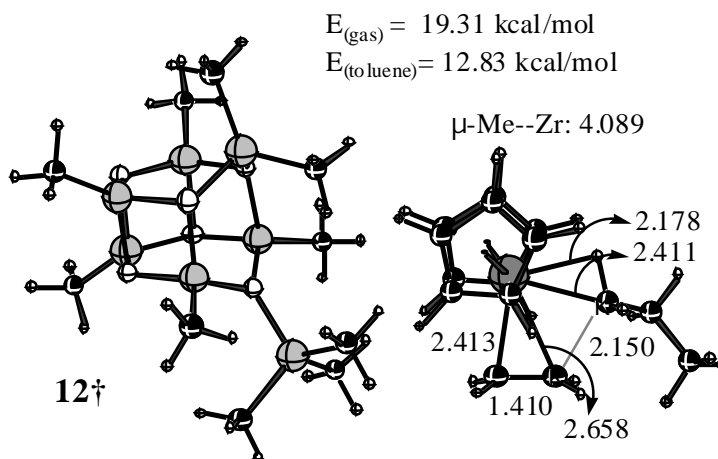
Figure 5.12: Transition State with an   -Agostic Interaction for the Second Insertion
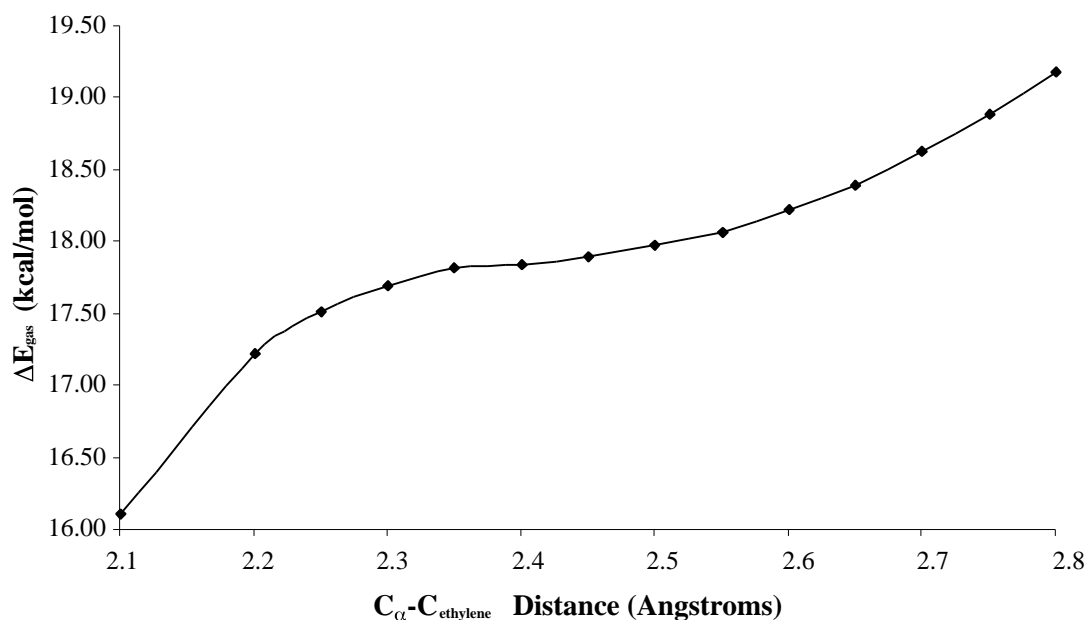
Figure 5.13: Gas Phase Reaction Profile for the *Trans* Attack; -agostic Interaction

Starting from **9d** we optimized a number of structures with fixed $C_{ethylene}$-Zr bond lengths in order to find the insertion transition state for the *trans* approach. From the gas phase reaction profile shown in Figure 5.13 it is evident that there is no barrier to insertion, which should occur at a $C_{ethylene}$-Zr distance of 2.1-2.3 Å. This also implies that **9d** is not a real -complex since it is not a minimum on the calculated potential energy surface. Moreover, if we do not consider other mechanisms (such as frontside insertion), then the propagation barrier will be equivalent to that of olefin uptake.

Dissociated Transition States: β*-agostic Interactions*

The insertion transition states with -agostic interactions for the *cis* (**14a†**) and *trans* (**14b†**) approaches along with their energies relative to **7a** and ethylene are shown in Figure 5.14. We obtained **14a†** by performing a linear transit using **10d** as the starting geometry. During the optimization the cation rotated about the anion so that the olefin's orientation changed from *cis* to *trans* and the Cp rings changed from being out of plane

to an orientation intermediate between an in plane and out of plane. The large ion-pair distance implies that a rotation of the Cp rings will not cause steric congestion and increase the energy of the structure.

Both transition states have large ion-pair separations: as compared to **7a**, the μ-Me—Zr bond is longer by 2.483 Å and 2.346 Å for **14a†** and **14b†**, suggesting that the anion will have little influence on the cation-olefin complex. This can be seen in the nearly equivalent energies of the two transition states and the very comparable geometries of the cation-olefin complexes, whose bond lengths differ by up to 0.020 Å.
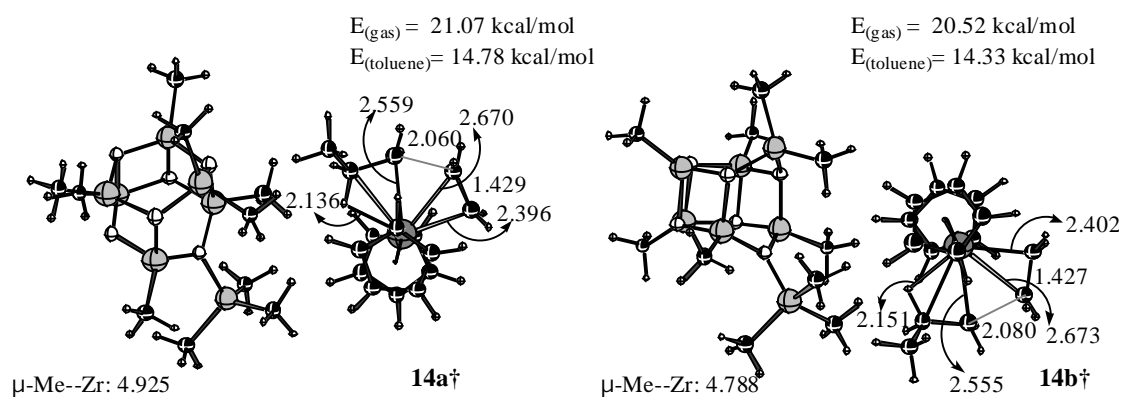
Figure 5.14: Transition States with -Agostic Interactions for the Second Insertion

The insertion barriers are somewhat higher than those obtained when structures with -agostic interactions were considered, but not unreasonable, indicating that olefin insertion may occur via these transition states.

Backside Insertion and Comparison with Naked Cation

Combining the aforementioned results gives us the following profile of the backside insertion mechanism. It begins with the olefin approaching *trans* to the bridging methyl group of **7a** or *cis* to the bridging methyl group of **7b**. A -agostic -complex is formed, **10b** for the *cis* case and **10d** for the *trans*. Next, the olefin approaches the C resulting in the formation of a five-membered insertion transition state, **14a†** for the *cis* approach and **14b†** for the *trans*. After insertion, the cation and anion associate and

energy must be put into dissociation of the ion-pair in order for the third insertion to begin.

We will now compare the geometries and energy barriers in solution for the above process with that for the naked cation. In the case of the latter, complexation of the olefin is exothermic by 11.82 kcal/mol, whereas it is endothermic by 7.23 kcal/mol and 7.06 kcal/mol for the *cis* and *trans* approaches. Table 5.6 compares the internal barriers and geometries of the insertion transition states, showing that they are all nearly identical. The bond lengths differ by up to 0.030 Å and the internal barriers for the *cis* and *trans* approaches are 0.22 kcal/mol higher and 0.06 kcal/mol lower, respectively, when compared to the naked cation. The large ion-pair separation prevents the anion from having any bonding or many steric interactions with the cation; the interactions are primarily electrostatic. Hence, the anion exerts very little influence on the geometry and energy of the anion, explaining the similarities. This data suggests that the main difference between the backside insertion mechanism with the naked cation as opposed to that of the ion-pair, is that in the former the binding of the olefin to the cation provides an overall stabilizing effect, whereas for the latter it is overall destabilizing.

Table 5.6: Comparison of the Geometries and Internal Barriers (IBs) for the *Cis* and *Trans* Backside Attacks with the Naked Cation[a]

	C -$C_{ethylene}$	Zr-H	Zr-C	$C_{ethylene}$-$C_{ethylene}$	IB (toluene)
Cis	2.060	2.136	2.559	1.429	7.55
Trans	2.080	2.151	2.555	1.427	7.27
Cation	2.050	2.147	2.556	1.431	7.33

[a]All Energies given in kcal/mol; all distances in Angstroms

The geometrical destabilization of **14b†** with respect to the contact ion-pair is 33.33 kcal/mol. Addition of the ethylene provides a stabilizing effect of 19.00 kcal/mol, resulting in an overall barrier of 14.33 kcal/mol. The transition state of the naked cation is geometrically destabilized by 14.88 kcal/mol. Bonding with the olefin provides a stabilization of 19.37 kcal/mol. This number is remarkably similar to that for the ion-pair,

which furthermore implies that the anion has very little influence on the cation at such a large separation. Since the geometry of the naked cation at the transition state is very similar to that of **14b**†, subtracting the two values for the geometrical destabilization should give us the amount of energy necessary to elongate the μ-Me—Zr bond. Our calculations show that this number is 18.45 kcal/mol.

Frontside Insertion

Combining the aforementioned results gives us the following profile of the frontside insertion mechanism. It begins with the olefin approaching *cis* to the bridging methyl group of **7a** or *trans* to the bridging methyl group of **7b**. A -agostic -complex results, **10a** for the *cis* case and **10c** for the *trans*. Next, the propyl chain rotates about the Zr – C bond resulting in the formation of an   -agostic bond. In the case of the *trans* attack the olefin spontaneously inserts since there is no barrier to olefin insertion. In the case of the *cis* attack a   -complex and five-membered insertion transition state are formed prior to insertion. After insertion, the cation and anion associate and energy must be put into dissociation of the ion-pair in order for the third insertion to begin.

5.3 Conclusions

The first goal of this chapter was to show that **1** is an active species in olefin polymerization whereas **2** is dormant. The high insertion barrier (29.26 kcal/mol for the *trans* approach and 35.55 kcal/mol for the *cis* approach) indicates that **2** is indeed a dormant species due to the strength of the Zr – O bond. For the first insertion into the Me – Zr bond of **1** the barrier was found as being 19.04 kcal/mol for the *cis* approach and 17.68 kcal/mol for the *trans* approach, showing that this may be an active species. For the second insertion, barriers ranging between approximately 12 - 15 kcal/mol were computed, further supporting that **1** is an active species.

We have further looked at the mechanism of polymerization with the proposed active species. For the first insertion, when the $C_{ethylene}$ – C distance was used as a reaction coordinate, a dissociated transition state was found for the *trans* approach, while an associated transition state was found for the *cis* approach. Both barriers are somewhat

higher than experimental estimate for the activation energy of propagation, which was measured to be (14.6 ± 1) kcal/mol. The experimental value corresponds to an average between the first and subsequent insertions. Our results indicate that after insertion occurs, the ion-pairs will associate prior to the second insertion.

For the second insertion with the active species many different possible mechanisms have been considered. Associated transition states were found to be higher in energy than dissociated transition states, though the insertion barrier for the associated transition state, *cis* approach is still low enough (16.18 kcal/mol) for this to be a possible, however unlikely route.

A more likely mechanism is that of backside insertion. A -complex such as **10b** or **10d** is formed and the olefin approaches the C resulting in the formation of an insertion transition state. The insertion barriers were calculated as being 14.78 kcal/mol and 14.33 kcal/mol for the *cis* and *trans* approaches. A comparison between these two modes of approach and the profile obtained for the naked cation showed that the internal barriers and geometries at the transition states in all cases were very similar. Due to the large ion-pair separation the anion has very little influence on the cation. The primary difference is that for the ion-pair, complexation of the olefin provides an overall destabilizing effect whereas it stabilizes the naked cation.

Another likely mechanism is that of frontside insertion. It begins with the formation of the -complexes **10a** and **10c**. The propyl chain rotates about the Zr – C bond and in the case of the *trans* approach there is no barrier to insertion. For the *cis* approach a -complex (**9b**), which is 12.18 kcal/mol higher in energy than the ion-pair and ethylene, is formed. The internal barrier to insertion is only 0.65 kcal/mol. In this case it is clear that the orientation of the olefin with respect to the μ-Me — Zr bond has an effect on the overall mechanism. The ion-pair separation is somewhat smaller for the -agostic species than for those with -agostic bonds and the anion likely has somewhat of an influence on the geometry and energy of the cation. The results obtained indicate that frontside insertion, *trans* approach has the lowest total barrier which will be equivalent to the barrier of rotation of the propyl chain.

Chapter 6

Summary and Future Prospects

The primary objective of this thesis was to computationally study the mechanism of MAO-activated, dimethylzirconocene-catalyzed ethylene polymerization and compare it to results obtained with the naked cation. Such an investigation would then allow us to elucidate the role of MAO as activator. However, first of all it was necessary to develop a model of the active species in polymerization and in order to do this a model for MAO itself.

To this end in the second chapter we proposed a model for MAO with the general formula $(AlOMe)_n$, otherwise known as 'pure' MAO. We found that 'pure' MAO consists of three-dimensional cage structures with three-coordinate oxygen and four-coordinate aluminum atoms. A formula showing that the number of square faces in such a structure is equal to the number of octagonal faces plus six was derived. Since square faces exhibit high ring strain destabilizing the MAO cages, the structures without octagonal faces were found to be the most stable for a given n. The presence of square-square bonds was also found to destabilize the MAO cages. Based on the Gibbs free energies, it was possible to calculate the percent abundance of different oligomers. The most abundant structure within the temperature range of 198.15K - 598.15K was determined to be $(AlOMe)_{12}$, a highly symmetric cage consisting of atoms in 2H+S environments with square-hexagonal and hexagonal-hexagonal bonds. From the percent abundance we were able to determine that the average 'pure' MAO oligomer has the unit formula $(AlOMe)_{17.23}$ at 298.15K.

In the third chapter we proposed a model for 'real' or TMA-containing MAO. The results indicated that TMA reacts with MAO cages containing strained bonds. In all but one case, the most acidic site for a given structure consisted of a square-square bond. TMA was found to react minimally with 'pure' MAO cages since the most stable and therefore most abundant MAO oligomers contain few, if any, acidic bonds. Using the calculated Gibbs free energies we were able to find an average unit formula of $\sim(AlOMe)_{17.04} \bullet (TMA)_{0.11}$ for 'real' MAO at 298.15K. The calculated Me/Al ratio of 1.01 was found to differ from experimental estimates[14c,14d] of 1.4-1.5. However our results

suggested that one of the experimental procedures[14c] would change the equilibrium present in 'real' MAO and inflate the amount of TMA coordinated to the MAO cages.

In the fourth chapter we considered a 'real' MAO solution to which dimethylzirconocene had been added. We used $(AlOMe)_6$ as a model for the reactive MAO cages in order to determine the structure of the weakly bound, dormant and active species in a MAO/Cp_2ZrMe_2 solution. This was done via calculation of relative energies and comparison of experimental and calculated NMR chemical shifts. The weakly bound species was identified as being one where Cp_2ZrMe_2 coordinated to an aluminum atom of an acidic MAO bond via a bridging methyl group. In the process, the acidic bond was broken. The dormant species was identified as being one where Cp_2ZrMe^+ bonded to an oxygen atom and Me^- to an aluminum atom of an acidic MAO bond, which was then broken. The active species was identified as being one where Cp_2ZrMe_2 coordinated to MAO•TMA via a single bridging methyl group.

In the fifth chapter we verified the dormancy of the proposed dormant species by calculating the barrier to olefin insertion. We found this barrier to be 35.55 kcal/mol and 29.26 kcal/mol for the *cis* and *trans* attacks, which is more than double the experimental estimate[3g] for the activation energy of propagation. Further evidence supporting the structure of the active species was also gained. For the first insertion, the *trans* approach had the lowest barrier of 17.68 kcal/mol. For the second insertion the frontside insertion mechanism where the olefin is *trans* to the μ-Me — Zr bond was found to have no barrier to insertion after the propyl chain had rotated about the Zr-C bond. Dissociated transition states were found to be lower in energy than associated transition states and hence the preferred mechanisms. For the dissociated mechanism, the barrier for the second insertion ranged between approximately 12 – 15 kcal/mol.

The proposed model for MAO explains the high Al/catalyst ratio ($\sim 10^3$–10^4) necessary in order for polymerization to occur. The most stable and therefore most abundant MAO cages do not react with TMA. However, the active species is formed when catalyst coordinates to MAO•TMA via a single bridging methyl group. Thus the formation of active species requires the presence of:

- a large excess of MAO in order to increase the amount of potentially active cage structures

- an excess of free TMA in order to slightly shift the equilibrium towards the formation of MAO•TMA (note that this equilibrium does not change much, since the reaction between MAO and TMA is minimal).

In short, the large Al/catalyst ratio is necessary in order to ensure that the concentration of active species is approximately equivalent to the concentration of catalyst in solution.

We will now comment on possible future projects which would build upon the results we have already obtained. The -agostic and -agostic front and back -complexes are all linked via a rotation of the propyl chain about the Zr – C bond. A linear transit using the C -C -Zr-olefin midpoint torsional angle ( ) as a constraint could be performed to find the rotation barrier between these -complexes. This could also be compared to the rotation barrier found with the naked cation. Knowing these rotation barriers would then give a more detailed picture of the frontside insertion mechanism.

Previously we have mentioned that in going from the -complex to the insertion transition state, the orientation of the olefin changed from *cis* to *trans* (see **14a†**). This information, coupled with the similarities between the geometries and energies of the backside transition states, implies that the interactions between the cation and anion are primarily steric and electrostatic in nature, at least for complexes with -agostic interactions (the complexes with -agostic interactions have a somewhat smaller ion-pair separation and as we have seen, the insertion barrier is dependent upon the position of the olefin relative to the bridging methyl group). This insinuates that rotation of the cation about the anion should be facile which would further imply that the distinction between the *cis* and *trans* approach is meaningless. This assertion could be tested by performing a linear transit using the $C_{ethylene}$-Zr-μ-Me bond angle as the reaction coordinate.

In view of computational expediency, within this study we assumed that all of the reactive MAO cages could be modeled appropriately with $(AlOMe)_6$. Further studies could test this assertion by computing the NMR chemical shifts of the proposed dormant and active species or looking at the olefin uptake and insertion mechanism using a more

realistic MAO model (for example $(AlOMe)_9$). Other possible projects could include a mechanistic study of:

- the olefin uptake barrier for the proposed active species
- the termination mechanism
- chain transfer to aluminum.
- the interconversion of different MAO oligomers using molecular dynamics simulations.

Alternatively, one could expand upon the proposed MAO model to gain insight into related systems such as:

- higher alkylaluminoxanes also known as substituted or modified MAO's (for example ethylaluminoxane, isobutylaluminoxane or a mixture of the two). Such mixtures are typically not as active as MAO, but are easier to store.[1c]
- pentafluorophenyl substituted MAO which is made by mixing $B(C_6F_5)_3$ or $Al(C_6F_5)_3$ with dried, solid MAO. It has been shown that this is a better activator than MAO under certain conditions.[1c]
- MAO's supported on porous inorganic oxides such as alumina, silica and $MgCl_2$. Although these cocatalysts yield polymers with similar properties to those obtained with MAO, the Al/catalyst ratio can be reduced significantly (~100-500). This difference is currently not understood.[1c]

References

(1)   For example, see:

(1a)   Angermund, K.; Fink, G.; Jensen, V.R.; Kleinschmidt, R. *Chem. Rev.* **2000**, *100*, 1457.

(1b)   Coates, G.W. *Chem. Rev.* **2000**, *100*, 1223.

(1c)   Chen, E.Y.X.; Marks, T.J. *Chem. Rev.* **2000**, *100*, 1391.

(1d)   Rappé, A.K.; Skiff, W.M.; Casewit, C.J. *Chem. Rev.* **2000**, *100*, 1435.

(2a)   Cossée, P.; *J. Catal.* **1964**, *3*, 80.

(2b)   Arlman, E.J.; *J. Catal.* **1964**, *3*, 89.

(2c)   Arlman, E.J., Cossée, P.; *J. Catal.* **1964**, *3*, 99.

(3a)   Woo, T.K.; Fan.L.; Ziegler, T. *Organometallics*, **1994**, *13*, 2252.

(3b)   Margl, P.; Lohrenz, J.C.W.; Ziegler, T.; Blöchl, P.E. *J. Am. Chem. Soc.* **1996**, *118*, 4434.

(3c)   Lohrenz, J.C.W; Woo, T.K.; Ziegler, T. *J. Am. Chem. Soc.* **1995**, *117*, 12793.

(3d)   Lohrenz, J.C.W.; Woo, T.K.; Fan.L.; Ziegler, T. *J. Organometallic Chem.*, **1995**, *497*, 91.

(3e)   Petitjean, L.; Pattou, D.; Ruiz-López, M.F. *J. Phys. Chem. B.*, **1999**, *103*, 27.

(3f)   Lanza, G.; Fragalà, I.L.; Marks, T.J.; *Organometallics*, **2001**, *20*, 4006.

(3g)   Thorshaug, K.; Støvneng, J.A.; Rytter, E.; Ystenes, M.; *Macromolecules*, **1998**, *31*, 7149.

(4a)   Vanka, K.; Chan, M.S.W.; Pye. C.C.; Ziegler. T. *Organometallics,* **2000**, *19*, 1841.

(4b)   Lanza, G.; Fragalà, I.L.; Marks, T.J. *J. Am. Chem. Soc.* **2000**, *122*, 12764.

(4c)   Fusco, R.; Longo, L.; Proto, A.; Masi, F.; Garbassi, F. *Macromolecules,* **1997**, *30*, 7673.

(4d)   Xu, Z.; Vanka, K.; Firman, T.; Michalak, A.; Zurek, E.; Zhu, C.; Ziegler, T. *Organometallics*, **2002**, *21*, 2444.

(4e)   Vanka, K.; Ziegler. T. *Organometallics*, **2001**, *21*, 83.

(5a)   Lanza, G.; Fragalà, I.L.; Marks, T.J. *J. Am. Chem. Soc.* **1998**, *120*, 8257.

(5b)   Fusco, R.; Longo, L.; Proto, A.; Masi, F.; Garbassi, F. *Macromol. Rapid. Commun.* **1998**, *19*, 257.

(5c)   Bernardi, F.; Bottoni, Z.; Miscione, G.P. *Organometallics,* **1998**, *17*, 16.

(5d)   Chan, M.S.W.; Vanka, K.; Pye. C.C.; Ziegler. T. *Organometallics,* **1999**, *18*, 4624.

(5e)   Chan, M.S.W.; Ziegler, T. *Organometallics*, **2000**, *19*, 5182.

(5f)   Nifant'ev, I.E.; Ustynyuk, L.Y.; Laikov, D.N.; *Organometallics*, **2001**, *20*, 5375.

(5g)   Schaper, F.; Geyer, A.; Brintzinger, H. H. *Organometallics,* **2002**, *21*, 473.

(6)   Sinn, H.; Kaminsky, W.; Vollmer, H.J.; Woldt, R.; *Angew. Chem.* **1980**, *92*, 396.

(7)   Pasynkiewicz, S.; *Polyhedron*, **1990**, *9*, 429.

(8)   Atwood, J.L.; Hrncir, D.C.; Priester, R.D.; Rogers, R.D.; *Organometallics* **1983**, *2*, 985.

(9)   Mason, M.R.; Smith, J.M.; Bott, S.G.; Barron, A.R.; *J. Am. Chem. Soc.* **1993**, *115*, 4971.

(10)   Harlan, C.F.; Mason, M.R.; Barron, A.R.; *Organometallics* **1994**, *13*, 2957.

(11)   Harlan, C.J.; Bott, S.G.; Barron, A.R.; *J. Am. Chem. Soc.* **1995**, *117*, 6465.

(12)   Koide. Y.; Bott, S.G.; Barron, A.R.; *Organometallics* **1996**, *15*, 5514.

(13a)   Babushkin, D.E.; Semikolenova, N.V.; Panchenko, V.N.; Sobolev, A.P.; Zakharov, V.A.; Talsi, E.P.; *Macromol. Chem. Phys.* **1997**, *198*, 3845.

(13b)   Talsi, E.P.; Semikolenova, N,V.; Panchenko, V.N.; Sobolev, A.P.; Babushkin, D.E.; Shubin, A.A.; Zakharov, V.Z.; *J. Molecular Catalysis A: Chemical, 1999*, *139*, 131.

(14a)   Tritto, I.; Sacchi, M.C.; Locatelli, P. *Macromol. Chem. Phys.* **1996**, *197*, 1537.

(14b)   Barron, A.R. *Organometallics* **1995**, *14*, 3581.

(14c)   Imhoff, D.W.; Simeral, L.S.; Samngokoys, S.Z.; Peel, J.H.; *Organometallics* **1998**, *17*, 1941.

(14d)   Sinn, H. *Macromol. Symp.* **1995**, *97*, 27.

(15a)   Tritto, I.; Mealares, C.; Sacchi, M.; Locatelli, P. *Macromol. Chem. Phys.* **1997**, *198*, 3963.

(15b)   Eilertsen, J.L.; Rytter, E.; Ystenes, M.; *Vibrational Spectroscopy* **2000**, *2*, 257.

(16)   Watanabi, M.; McMahon, N.; Harlan, C.J.; Barron, A. R. *Organometallics* **2001**, *20*, 460.

(17a)   Tritto, I.; Donetti, R.; Sacchi, M.C.; Locatelli, P.; Zannoni, G. *Macromol.* **1997**, *30*, 1247.

(17b)   Tritto, I.; Donetti, R.; Sacchi, M..C.; Locatelli, P.; Zannoni, G. *Macromol.* **1999**, *32*, 264.

(18)   Babushkin, D.E.; Semikolenova, N.V.; Zakharov, V.A.; Talsi, E.P. *Macromol. Chem. Phys.* **2000**, *201*, 558.

(19)   Siedle, A.R.; Lamanna, W. M.; Newmark, R.A.; Schroepfer, J.N. *J. Mol. Catal. A: Chem.* **1998**, *128*, 257.

(20)   Kaminsky, W. *Macromol. Chem. Phys.* **1996**, *197*, 3907.

(21)   Zakharov, I.I.; Zakharov, V.A.; Potapov, A.G.; Zhidomirov, G.M. *Macromol. Theory Simul.* **1999**, *8*, 272.

(22)   Zakharov, I.I.; Zakharov, V.A. *Macromol. Theory Simul.* **2002**, *11*, 352.

(23)   Luhtanen, T.N.P.; Linnolahti, M.; Pakkanen, T.A. *J. Organometallic Chem.* **2002**, *648*, 49.

(24)   Ystenes, M.; Eilertsen, J.L.; Liu, J.K.; Ott, M.; Rytter, E.; Stovneng, J.A. *J. Polym. Sci. Pol. Chem.* **2000***, 38,* 3106.

(25)   Bryant, P.L.; Harwell, C.R.; Mrse, A.A.; Emery, E.F.; Gan, Z.; Caldwell, T.; Reyes, A.P.; Kuhns, P.; Hoyt, D.W.; Simeral, L.S.; Hall, R.W.; Butler, L.G. *J. Am. Chem. Soc.* **2001**, *123*, 12009.

(26)   te Velde, G.; Bickelhaupt, F.M.; Baerends, E.J.; Fonseca Guerra, C.; van Gisbergen, S.J.A.; Snijders, J.G.; Ziegler, T. J. Comp. Chem. **2001**, *22*, 931.

(27a)   Baerends, E.J.; Ellis, D.E.; Ros, P. *Chem. Phys.* **1973**, *2*, 41.

(27b)   Baerends, E.J.; Ros, P. *Chem. Phys.* **1973**, *2*, 52.

(28)   Ravenek, W. Algorithms and Applications on Vector and Parallel Computers; te Riele, H.J.J.; Dekker, T.J.; vand de Horst, H.A.; Eds. Elservier: Amsterdam, The Netherlands, 1987.

(29a)   te Velde, G.; Baerends, E.J. *Comput. Chem.* **1992**, *99*, 84.

(29b)   Boerringter, P.M,; te Velde, G.; Baerends, E.J. *Int. J. Quantum Chem..* **1998**, *33*, 87.

(30)   Versluis, L.; Ziegler, T. *J. Chem. Phys.* **1988**, *88*, 322.

(31)   Becke, A.D. *Phys. Rev. A.* **1988**, *38*, 3098.

(32)   Perdew, J.P. *Phys. Rev. B.* **1986**, *33*, 8822.

(33)   Vosko, S.H.; Wilk, L.; Nusair, M. *Can. J. Phys.* **1980**, *58*, 1200.

(34)   Krijn, J.; Baerends, E.J.; Fit Functions in the HFS-Method; Free University of Amsterdam, 1984.

(35a)   Casewit, A.K.; Colwell, K.S.; Rappé, A.K.; *J. Am. Chem. Soc.* **1992**, *114*, 10046.

(35b)   Casewit, C.J.; Colsell, K.S.; Rappé, A.K.; *J. Am. Chem. Soc.* **1992**, *114*, 10035.

(36a)   Klamt, A.; Schüürmann, G. *J. Chem. Soc. Perkin. Trans. 2.* **1993**, 799.

(36b)   Pye, C.C.; Ziegler, T.; *Theor. Chem. Acc.* **1999**, *101*, 396.

(37a)   Schreckenbach, G.; Ziegler, T. *J. Phys. Chem.* **1995**, *99*, 606.

(37b)   Schreckenbach, G.; Ziegler, T. *Int. J. Quantum Chem.* **1997**, *61*, 899.

(37c)   Wolff, S.K.; Ziegler, T. *J. Chem. Phys.* **1998**, *109*, 895.

(37d)   Wolff, S.K.; Ziegler, T.; van Lenthe, E.; Baerends, B.J, *J. Chem.Phys.* **1999**, *110*, 7689.

(38a)   Mulliken, R. *J. Chem. Phys.* **1955**, *23*, 1833.

(38b)   Mulliken, R. *J. Chem. Phys.* **1955**, *23*, 2343.

(39)   Coxeter, H.S.M.; *Regular Polytopes*, 2nd ed., Macmillian Company, 1963, New York.

(40)   Hehre, W.J.; Radom, L.; Schleyer, P.V.R.; Pople, J.A.; *Ab Initio Molecular Orbital Theory*, John Wiley & Sons, 1986, pp. 251, 259., New York.

(41)   Smith, M.B. *J. Organometallic Chem.* **1972**, *46*, 31.

(42)   Tritto, I.; Sacchi, M.C.; Locatelli, P.; Xi Li, S. *Macromol. Chem. Phys.* **1996**, *197*, 1537.